

3-D STABILITY ANALYSIS OF ABUTMENT SLOPES OF SRINAGAR DAM

A DISSERTATION

*submitted in partial fulfilment of the
requirements for the award of the degree*

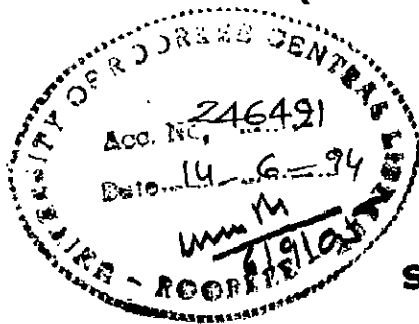
of

MASTER OF ENGINEERING

in

CIVIL ENGINEERING

**Specialization in Geotechnical Engineering
(Diversification in Rock Mechanics)**



By

SHEORAJ SINGH



**DEPARTMENT OF CIVIL ENGINEERING
UNIVERSITY OF ROORKEE
ROORKEE-247 667 (INDIA)**

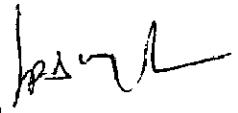
FEBRUARY, 1994

CANDIDATE'S DECLARATION

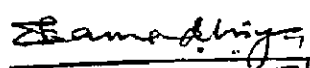
I hereby certify that the dissertation entitled "3-D STABILITY ANALYSIS OF ABUTMENT SLOPES OF SRINAGAR DAM" in partial fulfilment of the requirements for the award of the Degree of Master of Engineering, submitted in the Department of Civil Engineering of the university is an authentic record of my own work carried out since October, 1993 under the supervision of Dr. Bhawani Singh, Professor of Civil Engineering and Mr. N.K. Samadhiya, Lecturer in Civil Engineering, University of Roorkee, Roorkee, India.


The matter submitted in this thesis has not been submitted by me for the award of any other degree.

Dated : February 7 , 1994


(Sheoraj Singh)

This is to certify that the above statement made by the candidate is correct to the best of our knowledge.


(N. K. Samadhiya) 7/2
Lecturer
Civil Engineering Deptt.
University of Roorkee
Roorkee

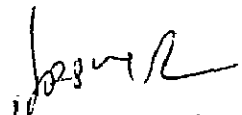

(Dr. Bhawani Singh)
Professor
Civil Engineering Deptt.
University of Roorkee
Roorkee

ACKNOWLEDGEMENT

I express my deep and sincere thanks to Dr. Bhawani Singh and Mr. N.K. Samadhiya for their continuous guidance and invaluable suggestions during the course of this study.

I also express my deep sense of gratitude to Dr. R. Anbalagan, Lecturer in Deptt. of Earth Sciences, U.O.R., Roorkee and Mr. S. C. Giri, Executive Engineer, I.D.O., Roorkee for their active cooperation and inspiration in preparing the dissertation.

Thanks are also due to my seniors and colleagues in my organisation for their encouragement and inspiration.


(Shebraj Singh)

ABSTRACT

A 90 m high concrete gravity dam has been proposed across the river Alaknanda at Srinagar in District Tehri/Pauri Garhwal of Uttar Pradesh. The proposed dam axis is aligned in N 31°-14'-26" E or S 31°-14'-26" W direction in narrow gorge of river having a cord-height ratio of 3.52.

Geotechnical investigations revealed that the proposed dam is located within a complexly folded, sheared and fractured sequence of quartzite and metabasic rocks. The foundation rock of the proposed dam is quartzite and the metabasic rock is exposed in at higher levels on both the abutments.

Study of rock slopes has been carried out in both the static and dynamic conditions in order to assess the stability of abutment slopes. Study shows that the overall slope of left abutment is stable while the overall slope of right abutment is unstable in both normal and dynamic conditions.

Provision of cable anchors has been suggested to increase factor of safety to 1.5 in static condition and 1.0 in dynamic condition. The required capacity of anchors for unstable wedges has been worked out.

TABLE OF CONTENTS

| CHAPTER NO. | TITLE | PAGE NO. |
|-------------|---|----------|
| | CANDIDATE'S DECLARATION | (i) |
| | ACKNOWLEDGEMENT | (ii) |
| | ABSTRACT | (iii) |
| | TABLE OF CONTENTS | (iv) |
| | LIST OF FIGURES | (vi) |
| | LIST OF TABLES | (ix) |
| I | INTRODUCTION | |
| | 1.1 GENERAL | 1 |
| | 1.2 SALIENT FEATURES | 2 |
| II | REVIEW OF LITERATURE AND GRAPHICAL TECHNIQUE OF ANALYSIS | |
| | 2.1 GENERAL | 3 |
| | 2.2 GRAPHICAL TECHNIQUE FOR PRESENTATION OF GEOLOGICAL DATA | 4 |
| | 2.3 SAMPLE SIZE OPTIMIZATION | 5 |
| | 2.4 CONTOUR DIAGRAM | 6 |
| | 2.5 MODES OF SLOPE FAILURE | 7 |
| | 2.6 EVALUATION OF FAILURE MODE | 8 |
| | 2.7 FRICTION CONE CONCEPT TO STABILITY ANALYSIS | 11 |
| | 2.7.1 General | 11 |
| | 2.7.2 Extension of friction cone concept to include cohesion | 11 |
| | 2.7.3 Influence of an external force | 12 |

LIST OF FIGURES

| FIG. NO. | DESCRIPTION | PAGE NO. |
|----------|--|----------|
| 1. | Layout of Srinagar Hydroelectric Project | 40 |
| 2. | Definition of Geological terms | 41 |
| 3. | Technique of Equal Angle Projection | 42 |
| 4. | Technique of Equal Area Projection | 42 |
| 5. | Plane Failure | 43 |
| 6. | Wedge Failure | 43 |
| 7. | Circular Failure | 43 |
| 8. | Toppling Failure | 43 |
| 9. | Main types of slope failure and stereoplots of structural conditions likely to give rise to these failures | 44 |
| 10. | Various conditions of rock slope failure | 45 |
| 11. | Various conditions for sliding failure of a wedge on a rock slope | 46 |
| 12. | Block sliding down a plane under its own weight | 47 |
| 13. | Pictorial representation of the Friction Cone Concept on the lower hemisphere. | 47 |
| 14. | Representation of the Friction Cone Concept on a stereoplot | 47 |
| 15. | Construction of Friction Cone Projection | 48 |
| 16. | Apparent Friction Angle obtained for Resistance due to both friction and cohesion | 49 |
| 17. | Influence of an external force T upon the | 49 |

stability of a block sliding on an inclined plane

| | | |
|-----|---|----|
| 18. | Pictorial and graphical representation of friction cone concept applied to sliding on two intersecting planes | 50 |
| 19. | Plan showing geology of dam area | 51 |
| 20. | Geological map showing surface geology in dam area | 52 |
| 21. | Geological section along dam axis | 53 |
| 22. | Cross-Section of the deepest block showing foundation geology in Srinagar dam | 54 |
| 23. | 3-D geological log of drift L-3 | 55 |
| 24. | 3-D geological log of drift L-4 | 56 |
| 25. | 3-D Geological log of drift R-5 | 57 |
| 26. | 3-D Geological log of drift R-6 | 58 |
| 27. | Schmidt Net | 59 |
| 28. | Floating circle counting net | 60 |
| 29. | Plot of poles representing geological discontinuity planes in drifts, L-3 & L-4 | 61 |
| 30. | Stereoplot depicting the various geological discontinuity planes in drifts L-3 & L-4 | 62 |
| 31. | Plot of poles representing geological discontinuity planes in drift R-5 | 63 |
| 32. | Stereoplot depicting the various geological discontinuity planes in drift R-5 | 64 |
| 33. | Combined stereoplot of discontinuity planes (Table - 1) for right abutment | 65 |

| | | |
|-----|--|----|
| 34. | Combined stereoplot of discontinuity planes (Table - 2) for right abutment | 66 |
| 35. | F.O.S. for friction (ϕ) only condition | 67 |
| 36. | Pictorial view of wedge no. 1 (Right abutment) | 68 |
| 37. | Stereoplot for wedge no. 1 (Right abutment) | 69 |
| 38. | Stereoplot for uplift forces (Wedge No. 1, Right abutment) | 70 |
| 39. | Stereoplot for effective weight vector (Wedge No. 1, Right abutment) | 71 |
| 40. | F.O.S. for saturated condition (Wedge No. -1, Right abutment) | 72 |
| 41. | F.O.S. for dynamic condition in dry rockmass (Wedge No. 1, right abutment) | 73 |
| 42. | F.O.S. for dynamic condition in saturated rockmass (Wedge No. 1, right abutment) | 74 |
| 43. | Combined stereoplot of discontinuity planes (Table - 3) for right abutment | 75 |
| 44. | Determination of cable anchor tension (T) for F=1.5 (Wedge No. 1, Right abutment) | 76 |
| 45. | Determination of cable anchor tension (T) for F=1.0 (Wedge No. -1, Right abutment) | 77 |
| 46. | Optimum cable anchor direction for reinforcing a wedge | 78 |
| 47. | Provision of cable anchors to form reinforced rock breast wall to stabilize the right abutment slope | 78 |

| | | |
|-----|---|----|
| | 2.7.4 Graphical determination of the factor of safety | 13 |
| | 2.8 EXTENSION OF FRICTION CONE CONCEPT TO THE CASE OF TWO INTERSECTING PLANES | 13 |
| III | GEOLOGICAL FEATURES AND GEOLOGICAL PARAMETERS | |
| | 3.1 GEOLOGICAL FEATURES | 15 |
| | 3.2 EVALUATION OF GEOLOGICAL DISCONTINUITIES | 16 |
| | 3.3 GEOTECHNICAL PARAMETERS | 18 |
| IV | STABILITY ANALYSIS | |
| | 4.1 GENERAL | 20 |
| | 4.2 STABILITY ANALYSIS OF LEFT ABUTMENT SLOPE | 20 |
| | 4.3 STABILITY ANALYSIS OF RIGHT ABUTMENT SLOPE | 20 |
| | 4.4 STABILITY ANALYSIS AS PER DISCONTINUITIES PLANES PRESENTED IN TABLE - 3. | 29 |
| | 4.5 PROTECTIVE MEASURES | 31 |
| V | DISCUSSION OF RESULTS | |
| | 5.1 LEFT ABUTMENT SLOPE | 35 |
| | 5.2 RIGHT ABUTMENT SLOPE | 35 |
| VI | CONCLUSIONS | 37 |
| | REFERENCES | 38 |
| | FIGURES | 40 |

LIST OF FIGURES

| FIG. NO. | DESCRIPTION | PAGE NO. |
|----------|--|----------|
| 1. | Layout of Srinagar Hydroelectric Project | 40 |
| 2. | Definition of Geological terms | 41 |
| 3. | Technique of Equal Angle Projection | 42 |
| 4. | Technique of Equal Area Projection | 42 |
| 5. | Plane Failure | 43 |
| 6. | Wedge Failure | 43 |
| 7. | Circular Failure | 43 |
| 8. | Toppling Failure | 43 |
| 9. | Main types of slope failure and stereoplots of structural conditions likely to give rise to these failures | 44 |
| 10. | Various conditions of rock slope failure | 45 |
| 11. | Various conditions for sliding failure of a wedge on a rock slope | 46 |
| 12. | Block sliding down a plane under its own weight | 47 |
| 13. | Pictorial representation of the Friction Cone Concept on the lower hemisphere. | 47 |
| 14. | Representation of the Friction Cone Concept on a stereoplot | 47 |
| 15. | Construction of Friction Cone Projection | 48 |
| 16. | Apparent Friction Angle obtained for Resistance due to both friction and cohesion | 49 |
| 17. | Influence of an external force T upon the | 49 |

LIST OF TABLES

| TABLE NO. | DESCRIPTION | PAGE NO. |
|-----------|---|----------|
| 1. | Attitude of Geological Discontinuities obtained from Drifts, L-3 and L-4 | 17 |
| 2. | Attitude of Geological Discontinuities obtained from Drift R-5 | 17 |
| 3. | Attitude of Geological Discontinuities obtained from Drift R-6 | 18 |
| 4. | Attitude of Slope face and Upper Slope Face | 18 |
| 5. | Shear Parameters for Rockmass | 18 |
| 6. | Unit Weight of Rockmass | 19 |
| 7. | Shear Parameters of Filled Material | 19 |

CHAPTER I INTRODUCTION

1.1 GENERAL

Srinagar Hydroelectric Project is located on river Alaknanda near Srinagar town in U.P.. This project envisages the utilization of 70 m of water drop available in river Alaknanda between tail water level of proposed Utyasu dam on upstream side and head water level of Kotli-Bhel dam reservoir on downstream side.

Srinagar dam axis is aligned in the $N31^{\circ}-14'-26''E$ direction on river Alaknanda. The dam is proposed in a narrow reach of river. The width of the valley at the proposed dam height is about 232 m and the cord-height ratio is 3.52. The Alaknanda river at the proposed dam site flows in general from east to west direction.

This project comprises of various structures such as a concrete gravity dam, spillway, intake, sedimentation tank, power channel, forebay, penstocks and a power house. Layout plan is shown in Fig. 1.

The spillway has been accomodated in the dam body itself due to non availability of sufficient suitable space on the left bank of river Alaknanda. The intake and sedimentation tank have been provided on the left bank of river. The water from sedimentation tank would be led through a 4.3 km long open power channel on right bank crossing the river through a 180m long aqueduct. Other structures such as forebay, penstocks, power house, tail race channel etc have been proposed on right bank of river.

This project lies within the Chandpur (Dudatoli) and Garhwal groups of rocks which are separated by the Srinagar thrust.

The dam, intake and sedimentation tank have been proposed in Garhwal group of rocks and major portion of power channel and the power house have been proposed in the Dudatoli group of rocks.

1.2 SALIENT FEATURES

Some salient features are as follows :

| | |
|--|-----------------------------------|
| (i) Total Catchment Area | 10,215 Sq. km. |
| (ii) Snow bound catchment area | 6,100 Sq. Km. |
| (iii) Top Elevation of dam | 611.00 m |
| (iv) Expected deepest foundation level | 521.00 m |
| (v) Reservoir Level (F.R.L.) | 605.50 m |
| (vi) Dead Storage Level | 577.50 m |
| (vii) R.L. of river bed at dam axis | 545.00 m |
| (viii) Installed capacity of power house | 330 MW (6 units of 55 MW each) |
| (ix) Type of power house | Surface |

CHAPTER II

REVIEW OF LITERATURE AND GRAPHICAL TECHNIQUE OF ANALYSIS

2.1 GENERAL

Rockmass contains a number of geological discontinuities such as joints, bedding planes, shear zones and faults etc. These geological discontinuities play a dominant role in the rock slope stability. The stability of individual slope is controlled by the local geological conditions, strength parameters, local ground water conditions, the shape of the overall hill slope in that area and by the excavation technique used. These controlling factors vary widely for different slope conditions. Hence it is impossible to generalize a slope, so that it should be stable in all conditions. Therefore critical slopes can only be defined if sufficient information is available for evaluating their stability.

The information regarding data collection must, therefore, be carried out in two stages-

- (i) First stage involves an examination of existing regional geological maps, air photographs, easily accessible outcrops and the core recovered during exploration drilling. A preliminary analysis of data will indicate slopes which are likely to prove critical and which require more detailed analysis.
- (ii) The second stage involves a much more detailed examination of the geological features of these critical regions and may require the drilling of special holes, examination of trial pits or adits and the detailed mapping and testing of discontinuities.

The geological data should be presented in such a form that it can be easily understood and interpreted by others, who may be involved in the stability analysis. Geological terms, which are generally used are given in Fig. 2.

2.2 GRAPHICAL TECHNIQUE FOR PRESENTATION OF GEOLOGICAL DATA

The presentation of geological data for rock slope analysis should be in such a way that it can easily be evaluated and incorporated into the stability analysis. Spherical projection method provides a convenient means for the presentation of geological data. The spherical projection method is a graphical method whereby geological data on the three dimensional orientation of geological features such as planer and linear features can be presented and analysed in two dimensions on a sheet of paper. The spherical projection methods used in geological or rock mechanics studies have been used by many authors notably Phillips(1971), Goodman(1976), Turner and Weiss(1963), Radgley, Hook and Bray(1981), Fried man and Ragon(1973).

The following two types of projections are frequently used by the geologists and rock engineers:

- (i) Equal angle projection
- (ii) Equal area projection

Equal Angle Projection

Equal angle projections are used to plot the geological data regarding orientation of some planes such as bedding, cleavage schistosity or fault surfaces. The principle of this projection is given in Fig. 3. The projection of point 'A' on spherical projecting surface can be obtained on plane of projection as C. The plane of projection is Equatorial plane.

Equal Area Projection

Equal area projection have the unique advantage of keeping the area proportionately equal on net as that on the hemisphere, i.e. areas are preserved. This ensures the intensity of poles on the net as well as on the hemisphere are equal. This feature is useful in the statistical analysis of geological data. The equal area projection is commonly used in geological data analysis. The method of plotting on an equal area net is illustrated in Fig. 4.

Projection of point 'A' on spherical projecting surface is

made on 'C' for marking an equal area projection. This can be explained by taking a distance between the point to be projected and bottom most point of the projecting sphere as arc and rotation around bottom most point is made to project it on a plane tangential to the same point. The arc distance is reduced by $(2)^{1/2}$ to equalize the radius of the projection plane and projecting sphere. The projections can be made using either upper or lower hemisphere. In engineering applications generally lower hemisphere is used for presentation of data and for its projection.

In dealing with the geological features, it is always convenient to plot poles of planes rather than planes. Because if we have to plot large number of planes it becomes a more time consuming process.

2.3 SAMPLE SIZE OPTIMIZATION

The collection of geological data is time consuming and expensive. Therefore, it is important that the amount of data collected should be minimum and fully sufficient to define the geometrical characteristics of the rockmass. The purpose of defining the rockmass geometry is to provide a basis for choosing the most appropriate mode of failure. This is the most important decision in the entire process of a slope stability investigation, since an incorrect choice of failure mechanism will invalidate the analysis.

A hard rockmass, in which two or three well developed discontinuity sets show up as dense pole concentrations on a stereoplot, will usually fail by sliding on one or two planes or by toppling. A single through going feature such as a fault can play a dominant role in a slope failure, so it is important that such failure should be identified separately in order that they are not lost in the averaging which occurs during the contouring of a pole plot. A soft rockmass such as coal deposit which may be horizontally bedded or vertically jointed or a hard rock in which joint orientations appear to be random may fail in a circular mode.

There are various factors in addition to the density of pole concentrations, which have to be taken into account for assessing the most likely failure mechanism in any given slope. They include the strength parameters of rockmass and the ground water conditions in the slope. These factors assist the geologist in deciding how much structural geology data is required in order to take realistic decision on the slope failure mechanism.

The following guide lines on pole plots may be adopted from a paper by Stauffer(1966):

1. First plot and contour 100 poles
2. If no preferred orientation is apparent, plot an additional 300 poles and contour all 400 poles. If the diagram still shows no preferred orientation, it is probably a random distribution.
3. If step 1 yields a single pole concentration with a value of 20% or higher, the structure is probably truly representative and little could be gained by plotting more data.
4. If step-1, results in a single pole concentration with a contour value of less than 20%, the following total numbers of poles should be contoured.
12-20% add 100 poles and contour all 200.
4-8 % add 500 to 900 poles and contours all 600 to 1000.
<4% at least 1000 poles should be contoured.
5. If step-1, yield a contour diagram with several pole concentrations, it is usually best to plot at least another 100 poles and contour all 200 before attempting to determine the optimum sample size.

More detailed study may be carried out as suggested the paper by Stauffer (1966).

2.4 CONTOUR DIAGRAM

After plotting the poles of geological features on an equal area net, contouring is done. While plotting the geological features, different type of symbols should be used to represent the poles of different types of geological features. The

interpretation of a pole plot for the purpose of stability analysis is simplified if different types of geological features can easily be identified.

There could be any number of concentration areas on poles plot. The contouring of pole plot is carried out according to density of poles per unit area of the equal area projection. Product of this process results as contour diagrams.

Several techniques of contouring pole plots have been suggested on the basis of numerous trials in which speed, convenience and accuracy of different contouring methods were evaluated.

Denness curvilinear cell counting method and Floating circle counting methods are generally used. These methods are given in text books. In this analysis floating circle counting method has been used.

2.5 MODES OF SLOPE FAILURE

The failure of slope is mainly governed by the nature and orientation of discontinuities present in the rockmass. Following types of failures usually occur in the rock mass.

- (i) Plane failure
- (ii) Wedge failure
- (iii) Circular failure
- (iv) Toppling failure

Plane Failure:

When a geological discontinuity such as a bedding plane strike nearly parallel ($\pm 20^\circ$) to the slope face and dips into the excavation at an angle greater than the angle of internal friction (ϕ), plane failure takes place as shown in Fig. 5.

Wedge Failure

When two geological discontinuities strike obliquely across the slope face and their line of intersection day-lights in the slope face, the wedge resting on these discontinuities will slide down along the line of intersection provided that the inclination of this line is significantly greater than the angle of friction. This type of failure is shown in Fig. 6.

Circular Failure

When the material is very weak as in soil slope, or when the rockmass is very heavily jointed or fractured as in a waste rock dump, the failure will be defined by a single discontinuity surface but will tend to follow a circular failure path as shown in Fig. 7.

Toppling Failure:

Toppling failure involves rotation of steeply dipping thin columns or blocks of rocks about some fixed base as shown in Fig.8 and the simple geometrical condition governing the toppling of a single block on an inclined surface is that the block is tall and slender. The weight vector falls outside the base, i.e. the block will rotate about its lowest contact edge.

All the types of failure are shown in Fig. 9. This figure shows typical pole plots of geological conditions likely to lead such failure. The cut face of the slope also included in the equal area plot to assess the stability of the slope, because sliding can only taken place as a result of movement of rockmass towards the free face created by the cut. The diagram given in Fig.9. have been simplified for the sake of clarity. In an actual rock slope, combination of general types of geological structures may be present and gives rise to additional type of failure. For example, presence of discontinuities which can lead to toppling as well as planes upon which wedge sliding can occur could lead to the sliding of a wedge which is separated from the rock mass by a tension crack.

2.6 EVALUATION OF FAILURE MODE

In a typical field study in which structural data has been plotted on stereonet, a number of significant pole concentrations may be present. It is useful to identify those which represent potential failure planes and to eliminate those which represent structures which are unlikely to be involved in slope failures. Various methods for identifying the important pole concentrations have been discussed by John(1969), Panet and McMahon(1974), but the method developed by Markland(1972) is preferred by the

authors.

Markland's test is designed to establish the possibility of a wedge failure in which sliding takes place along the line of intersection of two planar discontinuities as shown in Fig. 9. Plane failure shown in Fig 9(b), is also covered by this test, since it is a special case of wedge failure. If contact of wedge is maintained on both the planes, sliding can only occur along the line of intersection and hence this line of intersection must day-light in the slope face i.e., the plunge of line of intersection must be less than the dip of the slope face, measured in the direction of the line of intersection as shown in Fig. 10. The factor of safety of the slope in case of wedge failure depends upon the plunge of line of intersection, the shear strength of the discontinuity surfaces and the geometry of the wedge. The limiting case occurs when the wedge degenerates to a plane i.e. dips and dip-directions of the two planes are same and when the shear strength of this plane is due to friction only. Sliding under these conditions takes place when the dip of the plane is greater than the angle of friction (ϕ). The slope is potentially unstable when the point defining the line of intersection of the two planes falls within the area included between the great circle defining the slope face and the circle defined by the angle of friction (ϕ) as shown in Fig. 10(b).

Markland's test is designed to identify the critical discontinuities for detailed analysis in order to work out the factor of safety of the slope.

REFINEMENT OF MARKLAND'S TEST

A refinement to Markland's test has been discussed by Hocking(1976) to permit the users to differentiate between sliding of a wedge along the line of intersection or along one of the planes forming the base of the wedge. If the conditions for the Markland's test are satisfied i.e. the line of intersection of two planes falls within the shaded crescent as shown in Fig. 11 and if the dip direction of either of the plane falls between the dip direction of the slope face and the trend of the line of

intersection, the sliding will occur on the steeper of the two planes rather than along the line of intersections as shown in Fig. 11(b).

Figs. 10(a) and 10(b) show the discontinuity planes which are represented by great circles and in Fig. 10(c) the two discontinuity planes are represented by their poles. Tracing on which the poles are plotted is rotated until both poles lie on the same great circle. The pole of this great circle defines the line of intersection of the two planes.

For an example, the use of Markland's test is illustrated in Fig. 10(d) in which contoured stereoplot of poles is shown. It is required to examine the stability of a slope face with a dip of 50° and dip direction of 120° . A friction angle of 30° is assumed for this analysis. In this analysis an overlay is prepared on which the following information is included :

- a. The great circle representing the slope face.
- b. The pole representing the slope face.
- c. The friction circle

This overlay is placed over the contoured stereoplot and this overlay with contoured stereoplot is rotated over the stereonet to find great circles passing through the pole concentrations. The lines of intersection are defined by the poles of these great circles as shown in Fig. 10(d). From this figure it will be seen that the most dangerous combination of discontinuities are those represented by the pole concentrations as numbered 1, 2 and 3. The intersection I_{13} lies outside the critical area and unlikely to give rise to instability. The pole concentration numbered 4 will not be involved in sliding but it could give rise to toppling or the opening of tension cracks. The poles of planes 1 and 2 lie outside the angle included between the dip direction of the slope face and the line of intersection I_{12} and hence the failure of this wedge will be by sliding along the line of intersection, I_{12} . However, in the case of planes 2 and 3, the pole representing plane 2 falls within the angle between the dip direction of the slope face and the line of intersection I_{23} and hence the failure of wedge will be by sliding on plane 2. This is the most critical

unstability condition which will control the behaviour of the slope.

2.7 FRICTION CONE CONCEPT TO STABILITY ANALYSIS

2.7.1 GENERAL

It can be explained by considering a block of weight 'W' resting on an inclined plane with horizontal at an angle ψ_p as shown in Fig. 12. The disturbing force S, which is acting down the plane, is given by $S=W.\sin \psi_p$ and the normal force N acting across the plane is given by, $N= W \cos \psi_p$. If the shear strength of the surface between the block and the inclined plane is purely frictional i.e., the cohesive strength is zero, then the force R_f which resists the sliding is given by

$R_f = N. \tan\phi = W. \cos\psi_p . \tan\phi$, where ϕ is the angle of friction of the surfaces.

Sliding of block will occur if the disturbing force S is greater than the resisting force R_f i.e.

$$W.\sin \psi_p > W.\cos \psi_p \tan\phi$$

This shows that sliding of block takes place when $\psi_p > \phi$.

This resisting force R_f acts uniformly on the surface between the block and the plane (assuming that the frictional strength of the surfaces is the same in all directions in the plane). One can imagine a 'friction cone' surrounding the normal force N as shown in Fig. 12. This cone has a base circle radius R_f , a vertical height N and a semiapical angle. Condition of sliding ($\psi_p > \phi$) is satisfied if the weight vector W falls outside the friction cone as shown in Fig. 12.

The graphical representation of friction cone is shown in Fig. 13 and Fig. 14.

The method of constructing the projection of cone on the stereonet for $\phi=30^\circ$ is shown in Fig. 15.

2.7.2 EXTENSION OF FRICTION CONE CONCEPT TO INCLUDE COHESION

The cohesive force resisting the sliding of a block or a wedge on a plane is given by $R_c = C.A.$, where, C is the cohesive strength of the surface and A is the base area of the block or wedge. This force R_c acts uniformly in the plane of sliding,

assuming the cohesive strength to be uniform in all directions in the plane. This cone has a base circle radius of $R_f + R_c$, a vertical height N and a semi-apical angle of ϕ_a . This apparent friction angle ϕ_a can be determined from the following relationship

$$\tan \phi_a = \frac{R_f + R_c}{N} = \tan \phi + \frac{C \cdot A}{W \cdot \cos \psi_p}$$

After determining the apparent friction angle ϕ_a , the graphical representation of the apparent friction cone is constructed. Sliding will occur if S exceeds $R_f + R_c$ or if $\psi_p > \phi$. This indicates that sliding will occur if the weight vector, W represented by the centre of the stereonet, falls outside the projection of the friction cone.

If the weight vector W falls inside the friction cone as shown in Fig. 16 then the slope will be stable.

2.7.3 INFLUENCE OF AN EXTERNAL FORCE

If the block of weight W is acted upon by an external force T as shown in Fig. 17 the condition for instability discussed in previous cases will no longer apply. This external force may be due to water pressure or to a force exerted by cable anchor or a rockbolt system. One of the most convenient ways of dealing with this problem is to consider the resultant of the block weight W and external force T as an effective weight vector W_e as shown in Fig. 17. The dip and dip direction of this resultant can be determined from a stereonet. The dip and dip direction of this effective weight vector is no longer vertical, will determine whether it falls outside the friction cone and hence whether the block is unstable. In this case shear force S and normal force N are the components of the effective weight vector W_e and that the apparent friction angle ϕ_a is calculated on the basis of W_e .

2.7.4 GRAPHICAL DETERMINATION OF THE FACTOR OF SAFETY

The factor of safety of the block on the inclined plane is calculated as follows :

$$F = \frac{R}{S_e} = \frac{W_e \cos \eta \cdot \tan \phi_a}{W_e \cdot \sin \eta}$$
$$= \frac{\tan \phi_a}{\tan \eta}$$

These angles ϕ_a and η are calculated from relationships which incorporate friction, cohesion, the self weight of the block and the influence of external forces including water pressure, this relationship is valid for the most general case of slope stability.

2.8.0 EXTENSION OF FRICTION CONE CONCEPT TO THE CASE OF TWO INTERSECTING PLANES

Considering planes A and B which intersect as shown in pictorial view in Fig. 18 sliding of a wedge of rock resting on two planes takes place along the line of intersection, if it is remain in contact with both planes during sliding. In order to assess the stability of a wedge of rock, it is necessary to determine the apparant friction angle ϕ_i , which acts in a vertical plane parallel to the line of intersection.

As illustrated in Fig. 18 the resisting force vector Q_a in plane A is the resultant of normal force N_a and the resisting force R_a . This Q_a acts parallel to the line of intersection of the two planes. Similarly the resisting force vector in plane B is Q_b . If the force vectors Q_a and Q_b are summed to find their resultant in a plane parallel to the line of intersection, then this resultant Q_i must lie in the same plane as Q_a and Q_b . The plane Q_{alb} containing Q_a , Q_i and Q_b is shown in the pictorial view in Fig. 18 and is represented on a stereoplot by a great circle which passes through points a and b.

The point 'a' is found by rotating the tracing untill the pole of plane A, marked N_a lies on the same great circle as the

point I which defines the line of intersection of plane A and B. The great circle which passes through N_a and I shown dotted in the Fig. 18 defines a plane which is parallel to the line of intersection. The point 'a' is given by the intersection of this great circle and the friction cone surrounding the normal N_a . Similarly the point 'b' is found by the intersection of great circle passing through N_b and I, and the friction cone surrounding the normal N_b .

The tracing is now rotated until the points 'a' and 'b' lie on the same great circle which defines the plane Q_{alb} which contains the three force vectors Q_a , Q_i and Q_b . The intersection of this great circle with the line of intersection defines the point 'i'. A great circle passing through N_a and N_b defines the position of N_i on the line of intersection. The apparent friction angle ϕ_i , resulting from the combined resistance of planes A and B is measured between N_i and i.

The angle ' η ' between the resultant of normal force N_i and the weight vector (represented by the centre point of the stereonet) is measured as shown the tracing having been rotated until the $N_i I$ is coincident with the W-E axis of the stereonet.

The factor of safety for the case in which sliding of wedge is resisted by two intersecting discontinuity planes is computed as follows :

$$F = \frac{\text{Tan}\phi_i}{\text{Tan}\eta}$$

CHAPTER III
GEOLOGICAL FEATURES AND GEOLOGICAL PARAMETERS

3.1 GEOLOGICAL FEATURES

The proposed dam is located within a complexly folded, sheared and fractured sequence of quartzite and metabasic rocks. The local trend of the formation varies from $N40^{\circ}E - S40^{\circ}W$ to $N60^{\circ}E - S60^{\circ}W$ with moderate dips on either side. The generation of folding is identifiable in the field in both the rock units. Folds of both the generation are co-axial in nature and steeply plunging towards north direction. The trend of the fold axis near the proposed dam site is $N50^{\circ}E-S50^{\circ}W$ with $70^{\circ}-85^{\circ}$ plunges towards north direction.

The geology of the dam area is shown in Fig 19. The proposed dam axis is aligned in the $N31^{\circ}-14'-26''E$ or $S31^{\circ}-14'-26''W$ direction. The geological plan and section along the proposed dam axis are shown in Figs. 20 & 21. The profile of the section indicates that the slope on right side is moderate to steep and on the left side, the slope is low to moderate. The foundation rock is quartzite throughout the base width of the proposed dam as shown in Fig. 22. Metabasic rock is exposed at higher levels on both the abutments.

Sub-surface explorations were carried out by means of drilling and drifting in the dam area. The rectangular drift R-5 and R-6 were excavated in the right bank and two drifts L-3 and L-4 were excavated in the left bank as shown in Figs. 23, 24, 25 and 26. Details of observations on joints, minor shear zones are given in these figures. No major shear zone is observed in both the banks. Only localised minor shear zones are observed in both the banks. The opening of these joints/minor shear zones varies from 0.5 cm to 20 cm and filled with siliceous clay gouge with rock fragments/chips.

3.2 EVALUATION OF GEOLOGICAL DISCONTINUITIES

Since the left side drifts L-3 and L-4 have been excavated at El. 563.50 m and El. 578.34m and are existing in quartzite rock, hence structural geology data obtained from drifts L-3 and L-4 are plotted in the form of poles on equal area stereonet (Schmidt net Fig. 27) as shown in Fig. 29 The poles are contoured by using the floating circle counting net (Fig. 28) for deducing the preferred orientation of the geological discontinuities as shown in Fig. 30. The results obtained from this stereonet analysis are shown in Table 1.

Two nos. drifts R-5 and R-6 were excavated in right side bank at El. 564.00m and 599.08 m respectively. Out of these two drifts, Drift R-5 is existing in quartzite rock and drift R-6 is existing in metabasic rock. Observations of structural geology data obtained from drift R-5 are plotted separately in the form of poles on an equal area stereonet (Schmidt net) as shown in Fig. 31 . The poles are contoured by using the floating circle counting net for deducing the preferred orientation of geological discontinuities as shown in Fig. 32. The results obtained from stereonet analysis are shown in Table 2.

The drifts R-6 is existing in metabasic rock and details of prominent joint sets are available in G.S.I. report, Field season 1987-88 and 1988-89, as shown in Table - 3.

The attitudes of slope face and upper slope face of left and right side banks of proposed Srinagar dam are presented in Table 4.

Table 1: Attitude of Geological Discontinuities obtained from Drifts L-3 and L-4

| Discontinuity Planes | Value of maxima pole concentration (%) | Strike | Dip Direction (α) | Dip (ψ) |
|-------------------------|--|--------|----------------------------------|-------------------|
| J ₁ | 7 | N60° W | 210° | 70° |
| J ₂ | 5 | N80° E | 170° | 70° |
| J ₃ | 5 | N24° E | 114° | 78° |
| J ₄ | 5 | N60° E | 150° | 69° |
| J ₅ | 4 | N67° W | 23° | 80° |
| J ₆ | 2 | N26° W | 244° | 43° |
| J ₇ | 2 | N32° E | 302° | 30° |
| J ₈ | 2 | N61° W | 209° | 34° |

Table 2: Attitude of Geological Discontinuities obtained from Drifts R-5

| Discontinuity Planes | Value of maxima pole concentration (%) | Strike | Dip Direction (α) | Dip (ψ) |
|-------------------------|--|--------|----------------------------------|-------------------|
| J ₁ | 12 | N60° W | 210° | 70° |
| J ₂ | 8 | N16° W | 74° | 55° |
| J ₃ | 4 | N40° E | 130° | 85° |
| J ₄ | 4 | N45° E | 315° | 85° |
| J ₅ | 4 | N77° W | 13° | 47° |
| J ₆ | 4 | N23° W | 247° | 75° |

Table 3: Attitude of Geological Discontinuities obtained from Drifts R-6*

| Discontinuity Planes | Strike | Dip Direction (α) | Dip (ψ) |
|-------------------------|--------|----------------------------------|-------------------|
| J ₁ | N35°E | 125° | 90° |
| J ₂ | N50°W | 220° | 50° |
| J ₃ | N80°W | 190° | 55° |
| J ₄ | N80°E | 170° | 60° |

* After Sharma and Tripathi (Field Seasons 1987-88 & 1988-89)

Table 4 : Attitude of Slope Face and Upper Slope Face

| Loaction | Strike | Dip Direction (α) | Dip (ψ) |
|-----------------------------|--------|-------------------------------|-------------------|
| Left side slope face | N59°W | 31° | 48° |
| Left side upper slope face | N59°W | 31° | 18° |
| Right side slope face | N59°W | 211° | 71° |
| Right side upper slope face | N59°W | 211° | 32° |

3.3 GEOTECHNICAL PARAMETERS

The shear parameters for rockmass based on field observations available from I.R.I. Roorkee are presented in Table 5.

Table 5 : Shear Parameters for Rockmass

| S.No. | Drift No. | Type of rock | Test condition | Shear Parameter | |
|-------|--------------|-----------------|-------------------|----------------------|-----------------|
| | | | | c(T/m ²) | ϕ (degree) |
| 1. | L-3 | Quartzite | Dry | 26.0 | 57° |
| 2. | L-4 | Quartzite | Dry | 37.5 | 60° |
| 3. | R-5 | Quartzite | Dry | 36.5 | 53° |
| 4. | R-6 | Metabasic | Dry | 20.0 | 58° |

Unit weight of rock mass are presented in Table 6

Table 6 : Unit Weight of Rock Mass

| S.No. | Rock Type | Unit Weight (T/m^3) |
|-------|-----------|-------------------------|
| 1. | Quartzite | 2.64 |
| 2. | Metabasic | 2.98 |

Shear Parameters of filled material in seams are presented in Table 7.

Table 7 : Shear Parameters of Filled Material*

| S.No. | Type of Material | Test condition | Shear Parameter | |
|-------|------------------|----------------|-----------------|-----------------------|
| | | | $c(T/m^2)$ | $\phi(\text{degree})$ |
| 1. | Clay | Peak | 0-18.00 | 12-18.5° |
| 2. | Clay | Residual | 0- 0.30 | 10.5-16° |

* After Skempton & Petley (1968)

Although the shear parameters obtained from the field tests (Table 5) suggest good condition of rockmass in which very high and steep slopes may be stable but due to possible clay infillings between joint surfaces shear parameters of clay have been used in the analysis (Table 7). $C=0$ and $\phi = 14^\circ$ (av.) have been used.

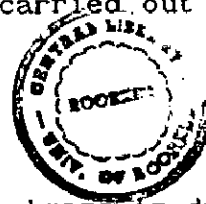
↳ no conservative values involved

CHAPTER IV STABILITY ANALYSIS

4.1 GENERAL

Stability analyses of abutments of proposed dam have been carried out taking into account the various parameters such as water pressure and dynamic forces acting on the planes of weakness present in the rockmass. However the chances of occurring heavy rainfall and earthquake simultaneously are very less during the construction period of dam. The effect of cohesion of infilling material in seams is not considered so as to be on the conservative side. The stability analysis is carried out for the following conditions :

- (a) Resistance due to friction (ϕ) only
- (b) Saturated condition
- (c) Effect of dynamic force, when the rockmass is dry
- (d) Effect of dynamic force, when the rockmass is saturated



4.2 STABILITY ANALYSIS OF LEFT ABUTMENT SLOPE

A combined stereonet for all discontinuity planes (Table 1) and slope face for left abutment (Table 4), is prepared as shown in Fig. 33. Equal area stereonet (Schmidt net) has been used in the analysis. The friction circle for $\phi = 14^\circ$ is also superimposed on the plot. As none of the lines of intersections falls within the region bounded by great circle of slope face and friction circle. This region is shown as hatched in Fig. 33. There is no possibility of wedge sliding. There is no possibility of failure by other modes. Slope is found STABLE.

4.3 STABILITY ANALYSIS OF RIGHT ABUTMENT SLOPE

Two types of rock are existing on the right bank side viz quartzite and metabasic rocks. Details of attitudes of discontinuity planes are given in Table 2 and Table 3. The stability analysis is carried out separately for both the rock types.

- (i) Stability analysis as per discontinuity planes presented in Table 2.

A combined stereoplot for the prominent discontinuity planes (Table 2) and slope face (Table 4) for right abutment is prepared as shown in Fig. 34. The friction circle for $\phi=14^\circ$ is also superimposed on the plot.

From combined stereoplot (Fig. 34), it is obvious that only three joint combinations can cause wedge failure as the lines of intersections of discontinuity planes forming the wedges lie within the hatched region (Fig. 34). These unstable wedges are marked as wedge Nos. 1, 2 & 3 as shown in the combined stereoplot. Remaining lines of intersections of discontinuity planes lie outside the hatched region, hence there is no possibility of wedge sliding along these lines of intersections. Stability analyses for these wedges Nos. 1, 2 & 3 is carried out. There is no possibility of failure by other modes.

Stability Analysis of Wedge No. 1

Details of discontinuity plane forming the wedge No. 1 is given in Table 8.

Table 8

| Plane | J ₃ | J ₆ | Slope face | Upper Slope face |
|----------------|----------------|----------------|---------------|---------------------|
| Dip | 85° | 75° | 71° | 32° |
| Dip Direction | 130° | 247° | 211° | 211° |
| Friction angle | 14" | 14" | - | - |

The height of slope to be excavated on right side bank is 108.50 m.

This slope stability analysis is carried out as follows.

(a) Factor of Safety for Friction (ϕ) Only

Various planes forming the wedge No. 1 are plotted as great circles on the stereonet using the equal area stereonet (Schmidt net) and poles of the planes are also marked on the stereoplot. The point of intersection of J₃ and J₆ is marked as I on the stereoplot as shown in Fig. 35. This point of intersection

represents the attitude of the line of intersection along which sliding of the wedge will take place. Friction circles are plotted about poles N_3 and N_6 respectively. To find the point 'a', the tracing is rotated over stereonet until N_3 and I lie on the same great circle, defines a plane parallel to the line of intersection, shown dotted in Fig. 35. The intersection point of this great circle with the friction cone surrounding the normal N_3 is marked as 'a'. Similarly the point 'b' lies on the great circle passes through N_6 and I. Intersection of this great circle and friction cone surrounding the normal N_6 defines the point 'b'.

The tracing is now rotated until the points 'a' and 'b' lie on the same great circle passing through a and b. The intersection of this great circle with the line of intersection defines the point 'i'. A great circle passing through N_3 and N_6 determines the position of N_1 on the line of intersection. The apparent friction angle (ϕ_a), resulting from the combined resistance of planes J_3 and J_6 , is the angle between N_1 and i. The angle η is the angle between the resultant normal force N_1 and the weight vector W (represented by centre on the stereonet). Both angles ϕ_a and η are measured by rotating the tracing until the line N_1I is coincident with the W-E axis of the stereonet. The angle ϕ_a and η are obtained as below :

$$\begin{aligned}\phi_a &= 24^\circ \\ \eta &= 72^\circ\end{aligned}$$

Factor of safety of slope for friction (ϕ) condition

$$F = \frac{\tan \phi_a}{\tan \eta} = \frac{\tan 24^\circ}{\tan 72^\circ} = 0.145$$

(b) Factor of Safety for Saturated Condition

The various planes which bound the wedge No. 1 as shown pictorially in Fig. 36 are plotted as great circles with the help of equal area stereonet (Schmidt net). The resulting tracing is reproduced as shown in Fig. 37. In this plot the point 'I' is the point of intersection of these two planes which indicates the attitude of the line of intersection along which sliding of wedge

will take place.

Area of planes and volume of the wedge are determined as follows :

From Fig. 37

| | |
|--------------------------------|--------------------------|
| Plunge of line 1 | $\psi_1 = 71^\circ$ |
| Plunge of line 2 | $\psi_2 = 71^\circ$ |
| Plunge of line of intersection | $\psi_5 = 70^\circ$ |
| Angle between line 1 and 5 | $\theta_{15} = 1^\circ$ |
| Angle between line 2 and 5 | $\theta_{25} = 2^\circ$ |
| Angle between line 1 and 2 | $\theta_{12} = 2^\circ$ |
| Angle between line 3 and 5 | $\theta_{35} = 40^\circ$ |
| Angle between line 4 and 5 | $\theta_{45} = 54^\circ$ |

Since the maximum height of slope to be excavated on right bank side is 108.50 m. Hence the vertical height (H) of the point 'A' above the toe of wedge i.e. the point 'O' is 108.50 m. The plunge of line 1 is measured as $\psi_1 = 71^\circ$, therefore the length of line 1 is found to be $108.50 \operatorname{cosec} 71^\circ$ i.e. $L_1 = 114.75$ m.

Similarly the plunge of line 2 is measured on $\psi_2 = 71^\circ$, hence $L_2 = 114.75$ m.

From pictorially view of wedge (Fig. 36) Angle between line 1 and 3.

$$\theta_{13} = 180^\circ - \theta_{15} - \theta_{35} = 180^\circ - 1^\circ - 40^\circ = 139^\circ$$

Similarly the angle between line 2 and 4

$$\theta_{24} = 180^\circ - \theta_{25} - \theta_{45} = 180^\circ - 2^\circ - 54^\circ = 124^\circ$$

From Fig. 36

Length of line 5 from triangle OAC

$$L_5 = L_1 \times \frac{\sin \theta_{13}}{\sin \theta_{35}} = 114.75 \times \frac{\sin 139^\circ}{\sin 40^\circ} = 117.12 \text{ m}$$

Length of line 5 from triangle OBC

$$L_5 = L_2 \times \frac{\sin \theta_{24}}{\sin \theta_{45}} = 114.75 \times \frac{\sin 124^\circ}{\sin 54^\circ} = 117.59 \text{ m}$$

Hence average length of line 5

$$L_5 = (117.12 + 117.59) / 2 = 117.355 \text{ m}$$

Area of triangle = one half product of adjacent sides X sin of the included angle

and volume = one sixth of the product of the three adjacent sides X K

$$\text{where, } K = (1 - \cos^2 \theta_{12} - \cos^2 \theta_{15} - \cos^2 \theta_{25} + 2 \cos \theta_{12} \cdot \cos \theta_{15} \cdot \cos \theta_{25})^{1/2}$$

substitution gives, $K = 5.933 \times 10^{-4}$

Area OAC on plane J_3

$$A_3 = \frac{1}{2} \times 114.75 \times 117.355 \times \sin 1^\circ = 117.51 \text{ m}^2$$

Area OBC on plane J_6

$$A_6 = \frac{1}{2} \times 114.75 \times 117.355 \times \sin 2^\circ = 234.99 \text{ m}^2$$

Volume of wedge OABC

$$V = \frac{1}{6} \times 114.75 \times 114.75 \times 117.355 \times 5.933 \times 10^{-4} \text{ m}^3 = 152.80 \text{ m}^3$$

Weight of wedge OABC

$$W = 152.80 \times 2.64 \text{ T} = 403.39 \text{ T}$$

Two uplift forces U_3 and U_6 also act on the wedge. These uplift forces are determined as follows :

Total vertical height wedge from bottom to top,

$$H_t = L_5 \cdot \sin \psi_5 = 117.355 \times \sin 70^\circ = 110.28 \text{ m}$$

The uplift force U_3 due to water pressure on area OAC

$$U_3 = \frac{1}{6} \times 1.0 \times 110.28 \times 117.51 \text{ T}$$

$$= 2159.83 \text{ T}$$

The uplift force U_6 due to water pressure on area OBC

$$U_6 = \frac{1}{6} \times 1.0 \times 110.28 \times 234.99 \text{ T}$$

$$= 4319.12 \text{ T}$$

The uplift forces U_3 and U_6 act in opposite direction to the normals N_3 and N_6 and are represented by points U_3 and U_6 on the stereoplot as shown in Fig. 38. The angle between U_3 and U_6 is 118° , obtained from Fig. 38 by measuring along the great circle passing through the points U_3 and U_6 . The resultant U is found as below

$$U = \left[(2159.83)^2 + (4319.12)^2 + 2 \times 2159.83 \times 4319.12 \cos 118^\circ \right]^{1/2}$$

$$= 3815.84 \text{ T}$$

$$\text{Angle of } U \text{ from } U_3 = \tan^{-1} \frac{4319.12 \sin 118^\circ}{2159.83 + 4319 \cos 118^\circ}$$

$$= 88^\circ$$

Finally, U and W are resolved to find out the magnitude and location of effective weight vector W_e . The angle between U and W is 73.5° , measured along the great circle passing through them. Since U is acting on the wedge in upward direction hence the angle between the U and W is $180^\circ - 73.5^\circ$ i.e. 106.5° , to find out the W_e .

$$\text{Now } W_e = \left[(3815.84)^2 + (403.39)^2 + 2 \times 3815.84 \times 403.39 \cos 106.5^\circ \right]^{1/2}$$

$$= 3721.43 \text{ T}$$

Angle of W_e from U

$$= \tan^{-1} \frac{403.39 \sin 106.5^\circ}{3815.84 + 403.39 \cos 106.5^\circ}$$

$$= 6^\circ$$

W_e is marked on the stereoplot as shown in Fig. 39.

From Fig. 40 the angle $\phi_a = 29^\circ$ and $\eta = 153^\circ$, are measured

along the great circle passing through N_i and W_e .

Hence factor of safety in saturated condition is computed as follows :

$$\begin{aligned}
 F &= \frac{\text{Tan } \phi_a}{\text{Tan } \eta} \\
 &= \frac{\text{Tan } 29^\circ}{\text{Tan } 153^\circ} \\
 &= -1.088 \text{ say } 0.000
 \end{aligned}$$

Negative value of factor of safety clearly indicates the lifting up of the wedge due to water pressure acting on the planes J_3 and J_6 .

(C) Effect of Dynamic Forces on the Stability of Rock Wedge, when the rock mass is dry

Since the Srinagar Hydroelectric Project is located in seismic zone IV according to seismic zoning map of India prepared by the Indian Standard Institution, hence coefficient of horizontal acceleration of 0.15 is taken.

Dynamic force on wedge

$$\begin{aligned}
 F_d &= 0.15 W \\
 &= 0.15 \times 403.39 \text{ T} \\
 &= 60.51 \text{ T}
 \end{aligned}$$

This force F_d is shown on the stereoplot with zero plunge and in the direction of line of intersection as shown in Fig. 41.

Finally F_d and W are resolved to find out the magnitude and location of the effective weight vector (W_{ed}). The angle between F_d and W is 90° , measured along the line of intersection.

$$\begin{aligned}
 \text{Now, } W_{ed} &= \left[(60.51)^2 + (403.39)^2 + 2 \times 60.51 \times 403.39 \cos 90^\circ \right]^{1/2} \\
 &= 407.90 \text{ T}
 \end{aligned}$$

$$\begin{aligned}
 \text{Angle of } W_{ed} \text{ from } W &= \tan^{-1} \frac{60.51 \sin 90^\circ}{403.39 + 60.51 \cos 90^\circ} \\
 &= 8.5^\circ
 \end{aligned}$$

The effective weight vector W_{ed} is marked on the stereoplot as shown in Fig. 41. The angle, $\phi_a = 24.5^\circ$ and $\eta = 83^\circ$ and measured along the line of intersection.

Factor of safety in dynamic condition for dry rockmass,

$$F = \frac{\tan 24.5^\circ}{\tan 83^\circ} = 0.056$$

(d) Effect of dynamic force when the rockmass is saturated

Dynamic force on the wedge

$$F_d' = 0.15 w_e$$

i.e. $F_d' = 0.15 \times 3721.43 \text{ T} = 558.21 \text{ T}$

This force F_d' is shown on the stereoplot with zero plunge and in the direction of line of intersection as shown in Fig. 42.

Finally F_d' and W_e are resolved to find out the magnitude and location of the effective weight vector (W_{ed}'). The angle between F_d' and W_e is 15.5° measured along the great circle passing through them.

$$\text{Now } W_{ed}' = \left[(558.21)^2 + (3721.43)^2 + 2 \times 558.21 \times 3721.43 \cos 15.5^\circ \right]^{1/2}$$

$$= 4261.95 \text{ T}$$

Angle of W_{ed}' from W_e

$$= \tan^{-1} \frac{558.21 \sin 15.5^\circ}{3721.43 + 558.21 \cos 15.5^\circ}$$

$$= 2^\circ$$

The effective weight vector W_{ed}' is marked on the stereoplot as shown in Fig. 42.

The angles $\phi_a = 28^\circ$ and $\eta = 154^\circ$ are measured along the great circle passing through them.

Factor of safety in dynamic condition for saturated rockmass

$$F = \frac{\tan 28^\circ}{\tan 154^\circ}$$

$$= -1.09 \text{ say } 0.000$$

Similar computations may also be done for the other two wedges. For the sake of comparison, stability analysis of all wedges have been done by using computer program SASW. The results of stereographic projection method and SASW are in close agreement.

Factor of safeties for other wedges have been calculated by computer program SASW for various conditions are as given below :

(i) Friction (f) only condition

| Wedge No. | Planes Forming the Wedge | F.O.S. | Remark |
|-----------|-----------------------------|--------|-------------------------|
| 1 | 3 & 6 | 0.1563 | Contact on both planes |
| 2 | 1 & 2 | 0.3990 | Contact on Plane 1 only |
| 3 | 1 & 6 | 0.3990 | Contact on Plane 1 only |

(ii) Saturated condition

| Wedge No. | Planes Forming the Wedge | F.O.S. | Remark |
|-----------|-----------------------------|--------|--------------------------------|
| 1 | 3 & 6 | 0.0000 | Contact is lost on both planes |
| 2 | 1 & 2 | 0.2610 | Contact on Plane 1 only |
| 3 | 1 & 6 | 0.2625 | Contact on Plane 1 only |

(iii) Dynamic condition when Rockmass is dry

| Wedge No. | Planes Forming the Wedge | F.O.S. | Remark |
|-----------|-----------------------------|--------|-------------------------|
| 1 | 3 & 6 | 0.0818 | Contact on both planes |
| 2 | 1 & 2 | 0.2906 | Contact on Plane 1 only |
| 3 | 1 & 6 | 0.2906 | Contact on Plane 1 only |

If the FOS is too low, nearly zero and the slope has already failed, it is true.

(iv) Dynamic condition when Rockmass is saturated

| Wedge No. | Planes Forming the Wedge | F.O.S. | Remark |
|-----------|-----------------------------|--------|-----------------------------------|
| 1 | 3 & 6 | 0.0000 | Contact is lost on both planes |
| 2 | 1 & 2 | 0.1753 | Contact on Plane 1 only |
| 3 | 1 & 6 | 0.1765 | Contact on Plane 1 only |

4.4 Stability Analysis as per Discontinuity Planes Presented in Table -3

A combined stereoplot for the prominent discontinuity planes (Table 3) in metabasic rock and slope face (Table 4) for right abutment is prepared as shown in Fig. 43 using equal area stereonet (Schmidt net). The friction circle for $\phi=14^\circ$ is also superimposed on the plot. Six joint combinations can cause wedge failure as the lines of intersections of discontinuity planes forming the wedges lie within the hatched region (Fig. 43). These unstable wedges are marked as wedge nos. 1 to 6, as shown on the stereoplot. Stability analyses for these wedges have been carried out.

The height of slope to be excavated in metabasic rock is 57.00 m. Factor of safeties for all wedges have been calculated by computer program SASW for various conditions are as given below :

(i) Friction (f) only condition

| Wedge No. | Planes Forming the Wedge | F.O.S. | Remark |
|-----------|-----------------------------|--------|----------------------------|
| 1 | 1 & 2 | 0.2245 | Contact on both planes |
| 2 | 1 & 3 | 0.2764 | Contact on both planes |
| 3 | 1 & 4 | 0.4152 | Contact on both planes |
| 4 | 2 & 3 | 0.2092 | Contact on plane 2 only |
| 5 | 2 & 4 | 0.2130 | Contact on both planes |
| 6 | 3 & 4 | 0.4896 | Contact on both planes |

(ii) Saturated condition

| Wedge No. | Planes Forming the Wedge | F.O.S. | Remark |
|-----------|-----------------------------|--------|-----------------------------------|
| 1 | 1 & 2 | 0.0000 | Contact is lost on both planes |
| 2 | 1 & 3 | 0.0608 | Contact on both planes |
| 3 | 1 & 4 | 0.1215 | Contact on both planes |
| 4 | 2 & 3 | 0.0616 | Contact on plane 2 only |
| 5 | 2&4 | 0.0656 | Contact on plane 2 only |
| 6 | 3 & 4 | 0.0209 | Contact on plane 3 only |

(iii) Dynamic condition when the rockmass is dry

| Wedge No. | Planes Forming the Wedge | F.O.S. | Remark |
|-----------|-----------------------------|--------|----------------------------|
| 1 | 1 & 2 | 0.1473 | Contact on both planes |
| 2 | 1 & 3 | 0.2067 | Contact on both planes |
| 3 | 1 & 4 | 0.3315 | Contact on both planes |
| 4 | 2 & 3 | 0.1520 | Contact on plane 2 only |
| 5 | 2&4 | 0.1527 | Contact on both planes |
| 6 | 3 & 4 | 0.4012 | Contact on both planes |

(iv) Dynamic condition when the rockmass is saturated

| Wedge No. | Planes Forming the Wedge | F.O.S. | Remark |
|-----------|-----------------------------|--------|-----------------------------------|
| 1 | 1 & 2 | 0.0000 | Contact is lost on both planes |
| 2 | 1 & 3 | 0.0032 | Contact on both planes |
| 3 | 1 & 4 | 0.0662 | Contact on both planes |
| 4 | 2 & 3 | 0.0130 | Contact on plane 2 only |
| 5 | 2 & 4 | 0.0167 | Contact on plane 2 only |
| 6 | 3 & 4 | 0.0258 | Contact on plane 3 only |

4.5 PROTECTIVE MEASURES

One of the following slope protection measures, if possible may be used :

- (i) Reduction of slope height
- (ii) Reduction of slope face inclination
- (iii) Drainage of slope
- (iv) Reinforcement of slope with cable anchors

As the factor of safety is minimum for wedge no. 1 as compared to all other wedges, it is found critical. Therefore, capacity of cable anchor has been worked out for this wedge in static as well as in dynamic condition.

(a) Determination of cable anchor tension (T) to increase the factor of safety of the slope to 1.5 in static condition.

- (i) Since the factor of safety for wedge No. 1 is very less for saturated condition as compared to dynamic condition, hence cable anchor tension 'T' is computed to increase the factor of safety of the slope to 1.5.
- (ii) The optimum plunge and trend of the cable anchor can be fixed from a thumb rule. The best direction in which the cable anchor should be installed to reinforce a wedge is along the line of intersection of the planes, viewed

from bottom of a slope and it should be inclined at the average friction angle to the line of intersection of the planes.

Optimum cable anchor direction

$$\alpha_t = \alpha_i = 205^\circ$$

Optimum plunge of cable anchor

$$\psi_t = \psi_i - \phi_{\text{average}}$$

$$= 70^\circ - 14^\circ$$

$$= 56^\circ$$

Since the computed value of $\psi_t = 56^\circ$ is very high, hence assuming the location of cable anchor at the location N_1 of resisting force i.e. the plunge of cable anchor is adopted as 18° .

(iii) The resultant W_t of W_e and T lies along the great circle passing through these two points on the stereonet as shown in Fig. 44. The location of point W_t is determined by the intersection of the locus $F=1.5$ with the great circle.

(iv) The construction of $F = 1.5$ locus is carried out by rotating the tracing on the stereonet, so that successive great circles pass through the point N_1 and the friction cone boundary. One such great circle is shown dotted in Fig. 44 and ϕ_a in this case is 54° . Since $F=1.5 = \tan 54^\circ / \eta$, $\eta=42.5$. Successive determination of the angles η defines the $F = 1.5$ locus.

(v) For $F = 1.5$, From Fig. 44

Trend of cable anchor tension T , $\alpha_t = 205^\circ$

plunge of cable anchor tension T , $\psi_t = 18^\circ$

Angle between T and $W_e = 153^\circ$

Angle between T and $W_t = 21^\circ$

Magnitude of $W_e = 3721.43 \text{ t}$

$$\text{Since } \tan 21^\circ = \frac{W_e \sin 153^\circ}{T + W_e \cos 153^\circ}$$

$$\text{i.e. } T = 3721.43 \left[\frac{\sin 153^\circ}{\tan 21^\circ} - \cos 153^\circ \right]$$

$$= 7717.10 \text{ T}$$

(b) Determination of cable anchor tension (T') to increase the factor of safety of the slope to 1.0 in dynamic condition when the rockmass is saturated.

For F=1.0, From Fig. 45

Trend of cable anchor tension T, $\alpha_t = 205^\circ$
 plunge of cable anchor tension T, $\psi_t = 18^\circ$
 Angle between T and W_{ed} , $= 154^\circ$
 Angle between T and W_t , $= 28^\circ$
 Magnitude of W_{ed} , $= 4261.95 \text{ T}$

$$\text{Since } \tan 28^\circ = \frac{W_e \sin 154^\circ}{T + W_e \cos 154^\circ}$$

Substitution gives

$$= 7717.10 \text{ T}$$

Since the magnitude of required anchor force is maximum in normal case, when the rockmass is saturated. Hence to make the slope stable the cable anchors for 7717.10 T have to be designed. Provision of cable anchors (indicative) is shown in Fig. 46 & 47.

Tentatively the following recommendations are offered for right abutment slope.

- | | |
|---|-------------------|
| (a) Maximum length of all cable anchors | = 45.0 m |
| (b) Capacity of cable anchor | = 150.0 T |
| (c) Vertical spacing | = 2.0 m |
| (d) Horizontal spacing | = 2.0 m |
| (e) Maximum length of drainage holes | = 45.0 m |
| (f) Diameter of drainage holes | |
| with perforated pipes | = 38.0 mm |
| (g) Size of concrete pad | = 1.0 m x 1.0 m |
| (h) Total capacity of cable anchor | = 8625.00 T |
| | against 7717.10 T |

The capacity of cable anchors is governed by the critical wedge, for which only 8.0 m long anchors will be sufficient theoretically. However, many other wedges are also unstable (Figs. 34 & 43), for which longer anchors will be required. So recommended length of all anchors is 45 m. Thus a reinforced rock breast wall of width 45 m (0.4 H) will be formed which would stabilize the rock slope.

CHAPTER V
DISCUSSION OF RESULTS

5.1 LEFT ABUTMENT SLOPE

On the left abutment the slope is found stable because there is no possibility of failure by any mode.

5.2 RIGHT ABUTMENT SLOPE

On right abutment two types of rocks are found viz quartzite rock and metabasic rock. Metabasic rock is found in very small area as compared to quartzite rock.

From combined stereoplot only three wedges are found unstable in quartzite rock and six wedges in metabasic rock. Out of these wedge No.1 in quartzite rock is found most critical hence the wedge No. 1 has been analysed for suitable remedial measures.

This wedge No. 1 is formed by the intersection of discontinuity planes J_3 and J_6 . The following factor of safeties are found for different conditions as indicated below :

| | |
|--|------------------|
| Factor of safety in friction (ϕ) only condition | = 0.145 |
| Factor of safety in saturated condition | = -1.088 or 0.00 |
| Factor of safety in dynamic condition | |
| when the rockmass is dry | = 0.056 |
| when the rockmass is saturated | = -1.090 or 0.00 |

Graphical analysis of right abutment slope indicated that the slope will be unstable for all conditions.

Since the factor of safety is very less in static as well as in dynamic condition, hence this analysis brings out the importance of adopting suitable stabilization measures during the stripping of abutment under even dry condition.

The analysis also indicates that the slope is highly unstable in saturated condition, because the factor of safety is negative in saturated condition. It indicates that the wedge may float under the condition of complete saturation. However the chances of complete saturation are very rare. However the capacity of cable anchor tension may be decided on the basis of complete saturation.

The capacity of cable anchor (T) works out for wedge No. 1 is 7717.10 T, for which 8.0 m long anchors would be sufficient

theoretically. However, for other unstable wedges longer anchors would be needed, therefore, 45.0 m long anchors are recommended for stabilizing the rock slope of right abutment.

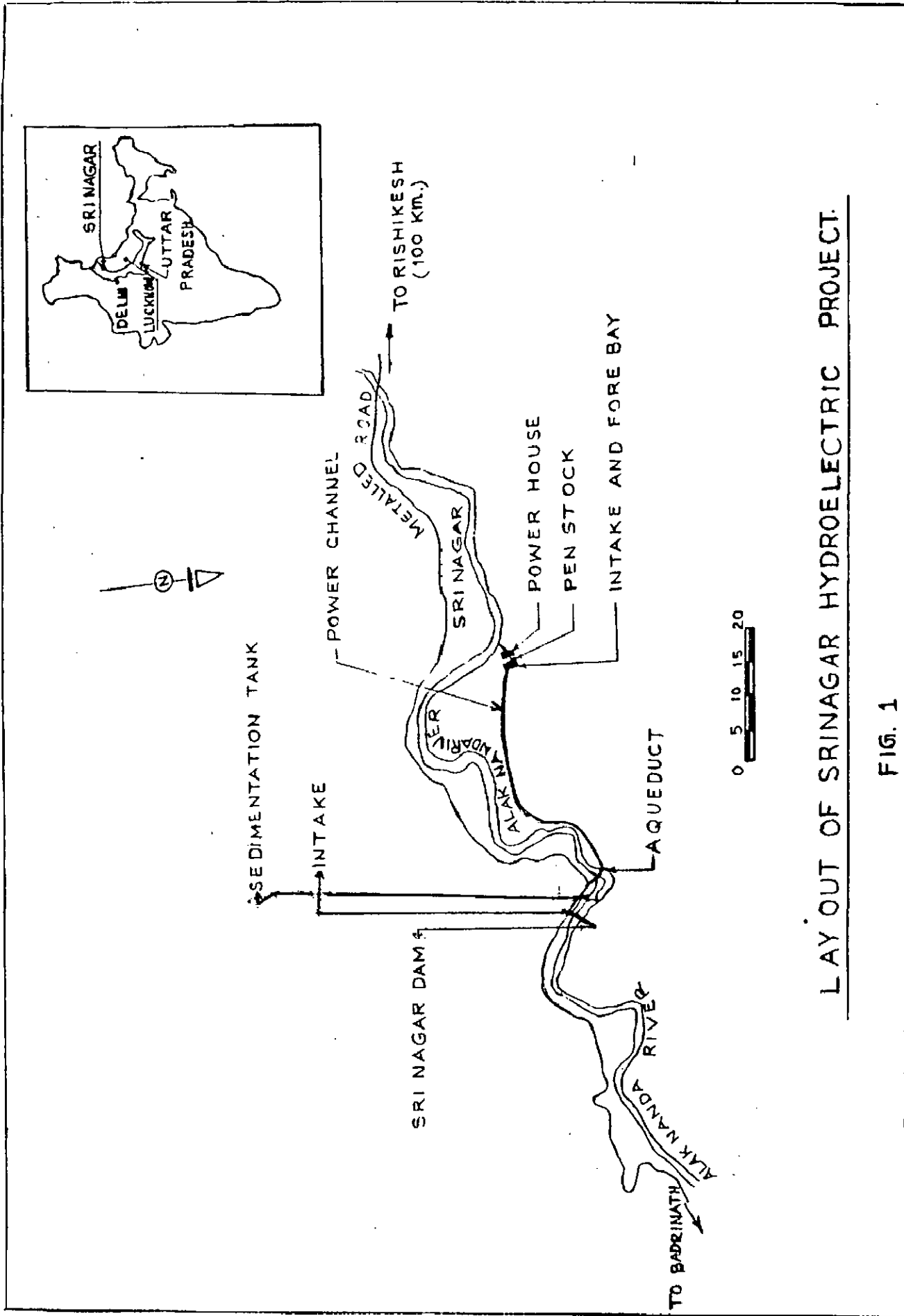
CHAPTER VI CONCLUSIONS

1. Geological investigations indicate that the proposed Srinagar dam is located in a complexly folded sheared and fractured sequence of quartzite and metabasic rocks belonging to Garhwal group.
2. The foundation rock of proposed Srinagar dam is quartzite throughout the base width. The metabasic rock is exposed at higher levels on both the abutments.
3. The overall slope for left abutment is found stable.
4. The overall slope for right abutment is unstable due to formation of wedges. The factor of safety in saturated condition is negligible, therefore it is recommended that cable anchors having a capacity of 7717.10 T in right abutment slope² have to be provided. It is also suggested that proper drainage arrangement should be made in right abutment slope so as to reduce the seepage pressure.
5. The factor of safety of slope for right abutment slope is also very less even in dry condition, hence it is suggested that stabilization measures should be followed simultaneously with the progress of excavations from higher elevation towards lower elevation.

REFERENCES

1. Hoek, E and Bray, J.(1977); "Rock Slope Engineering", 3rd Edition, The Institution of Mining and Metallurgy, London.
2. Hocking, G.(1976); "A method for distinguishing between single and double plane sliding of tetrahedral wedge", Intl, J. Rock Mechanics and Mining Sciences, Vol 13, pp 225-256.
3. Stauffer, M.R.; "An Emperical Statistical study of three dimensional fabric diagram as used in structural analysis". *Canadian Journal of Earth Science*, Vol. 3.,pp 473-497.
4. Markland, J. T.(1972); "A useful technique for estimating the stability of Rock Slopes when the rigid wedge sliding type of failure is expected", Imperical College Rock Mechanics Research Report, No. 19.
5. Panet, M.; Discussion on Graphical Stability Analysis on slopes in jointed rock by K.W. John, *Journal Soil Mechanics and Foundation Div. ASCE* Vol. 95 No. SM2, pp 685-686.
6. John, K.W.(1969); "Graphical Stability Analysis of Slopes in Jointed Rock", *Journal Soil Mechanics and Foundation division, ASCE*, Vol 94., No. SM2, pp 497-527 with discussion and closer in Vol. 95 No. SM6, pp 1541-1545.
7. Cording, E. J.(1971); "Stability of Rock Slopes", *Proceedings Thirteen Symposium on Rock Mechanics, University of Illionis, Urbana, Illinois.*
8. Sharma, Kumud and Tripathi S.K.; "A Report on Continuation of Pre Construction Stage Geological Investigators of Srinagar Hydrel Scheme, District Pauri and Tehri, U.P. (Field Seasons 1987-88 and 88-89).
9. Skempton, A.W. and Petley, D.J.(1968); "The Strength along discontinuities in stiff clays". *Proc, Geotechnical Confrence on Shear Strength propertiesof natural soils and rocks, Oslo, Vol. 2.*
10. Mehrotra, V.K.(1992); "A Ph.D. Thesis on Estimation of Engineering Parameters of Rockmass". Department of Civil Engineering, U.O.R. Roorkee.

11. Heuze, F.E. and Goodman, R.E. (1971); "A design procedure for high cuts in jointed hard rock, 3-D solutions: United States Bureau of Reclamation, Denver, Colorado.



LAY OUT OF SRINAGAR HYDROELECTRIC PROJECT.

FIG. 1

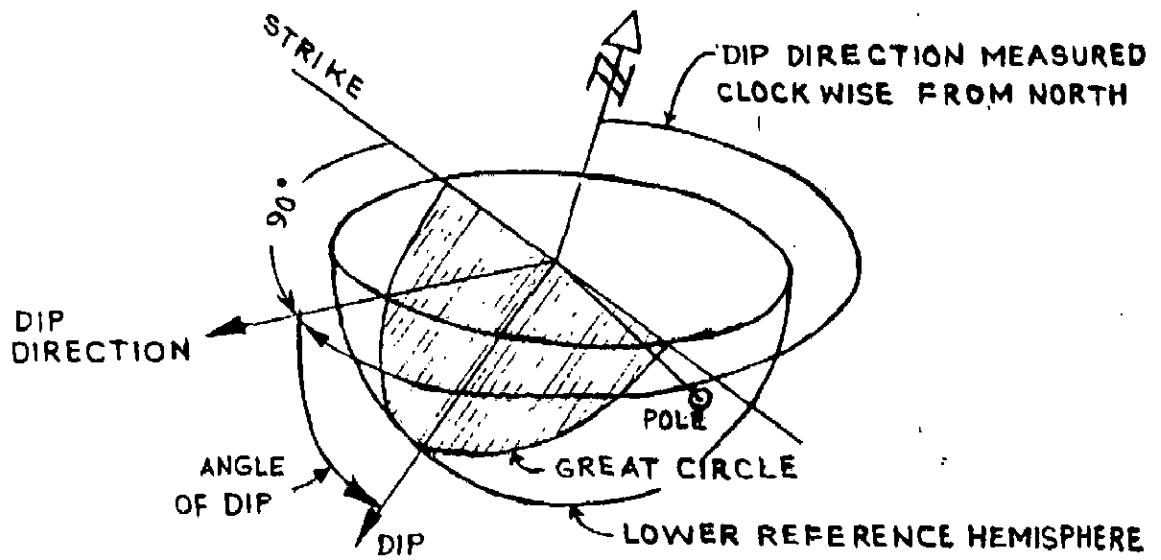


FIG.2: DEFINITION OF GEOLOGICAL TERMS.

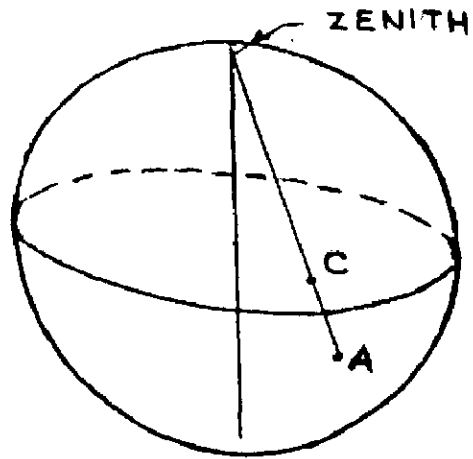


FIG.3: TECHNIQUE OF EQUAL ANGLE PROJECTION.

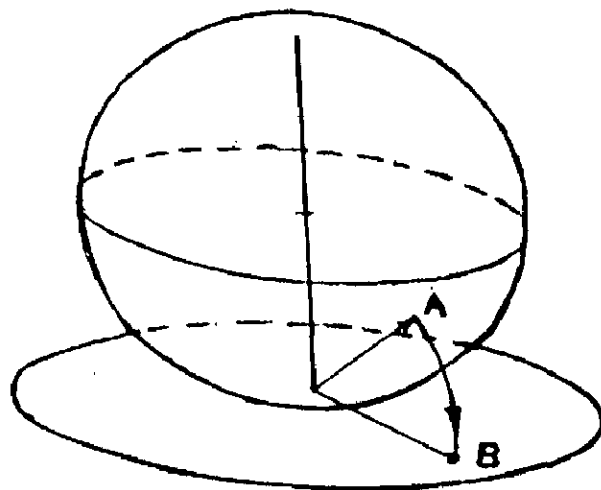


FIG.4: TECHNIQUE OF EQUAL AREA PROJECTION.

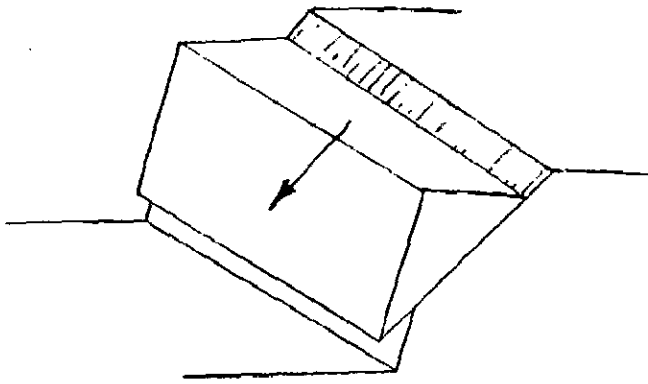


FIG. 5: PLANE FAILURE

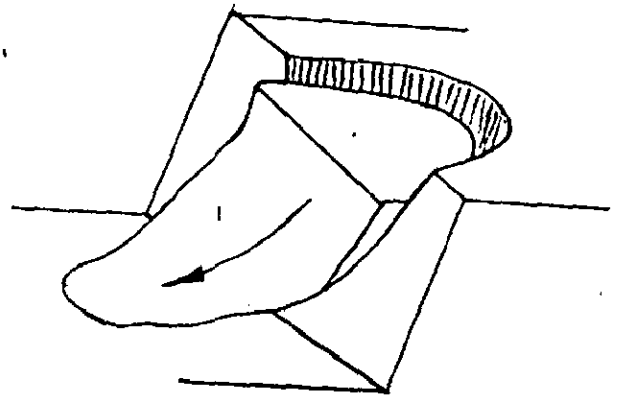


FIG. 7: CIRCULAR FAILURE

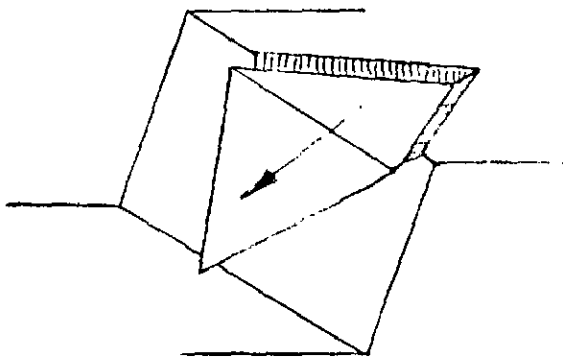


FIG. 6: WEDGE FAILURE

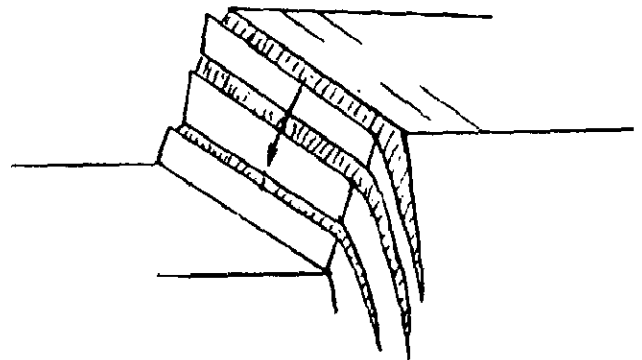


FIG. 8: TOPPLING FAILURE

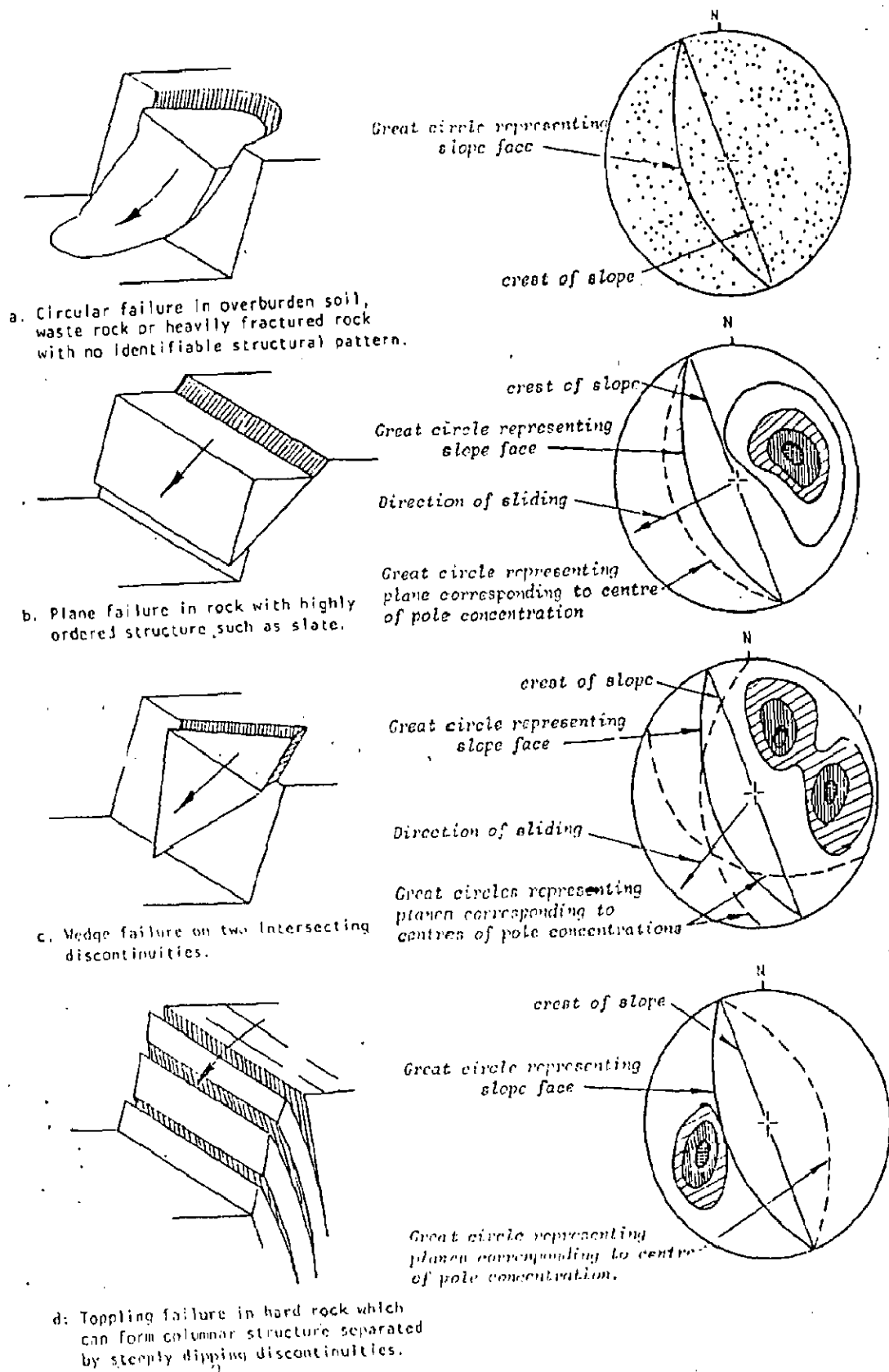
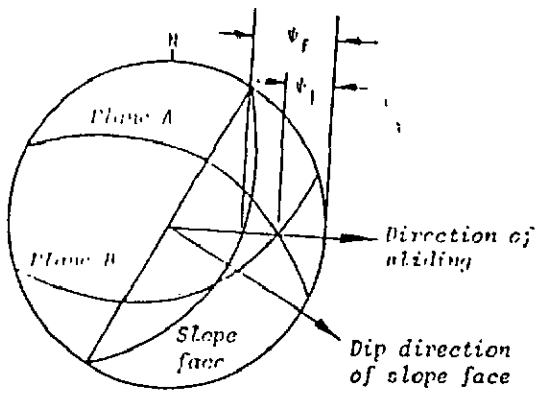
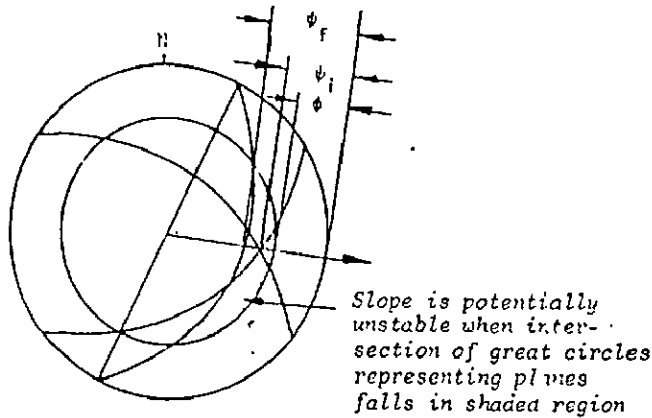


FIG. 9: MAIN TYPES OF SLOPE FAILURE AND STEREOPLOTS OF STRUCTURAL CONDITIONS LIKELY TO GIVE RISE TO THESE FAILURES. 44



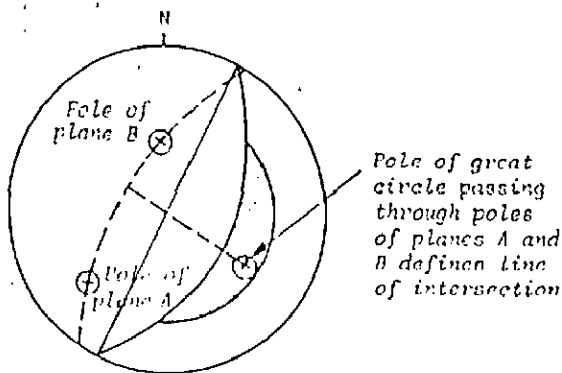
a : Sliding along the line of intersection of planes A and B is possible when the plunge of this line is less than the dip of the slope face, measured in the direction of sliding, i.e.

$$\psi_f > \psi_i$$

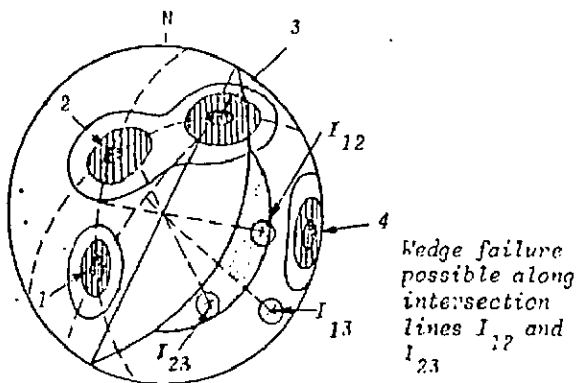


b : Sliding is assumed to occur when the plunge of the line of intersection exceeds the angle of friction, i.e.

$$\psi_f > \psi_i > \phi$$



c : Representation of planes by their poles and determination of the line of intersection of the planes by the pole of the great circle which passes through their poles.



d : Preliminary evaluation of the stability of a 50° slope in a rock mass with 4 sets of structural discontinuities.

FIG.10: VARIOUS CONDITIONS OF ROCK SLOPE FAILURE.

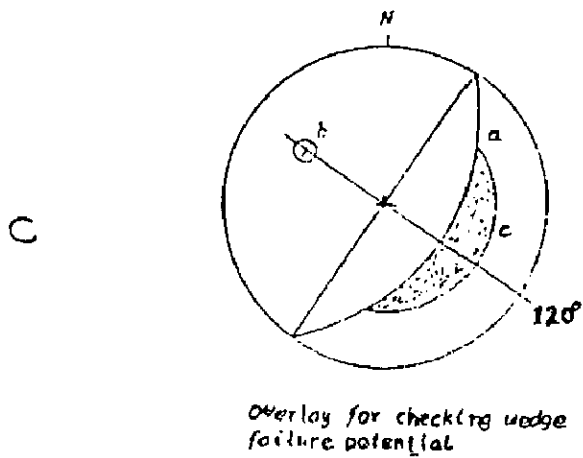
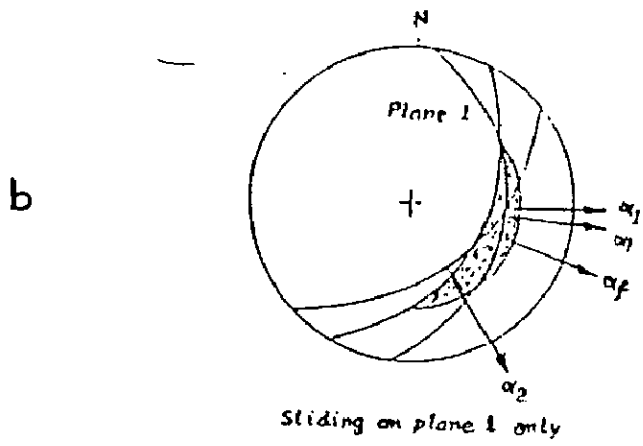
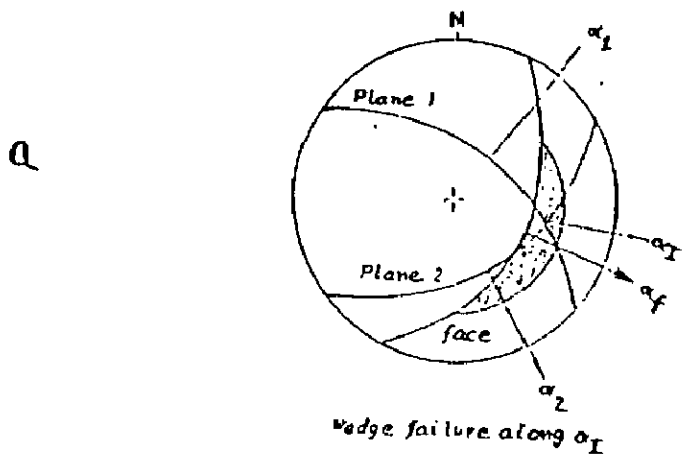


FIG. 11: VARIOUS CONDITIONS FOR SLIDING FAILURE OF A WEDGE ON A ROCK SLOPE.

FIG. 12: BLOCK SLIDING DOWN A PLANE UNDER ITS OWN WEIGHT.

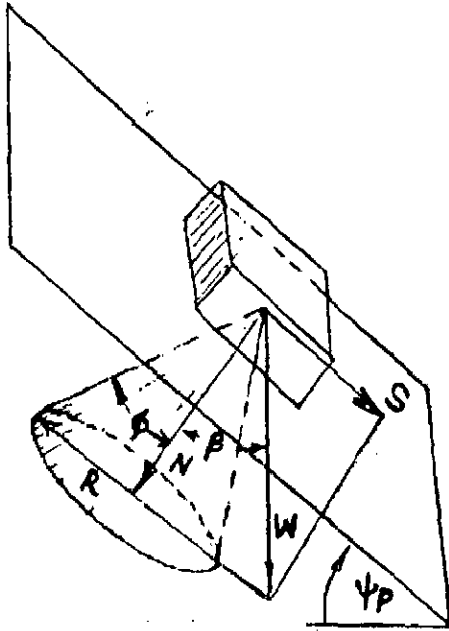
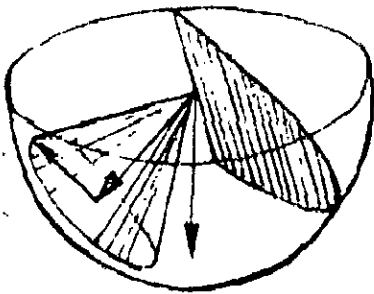
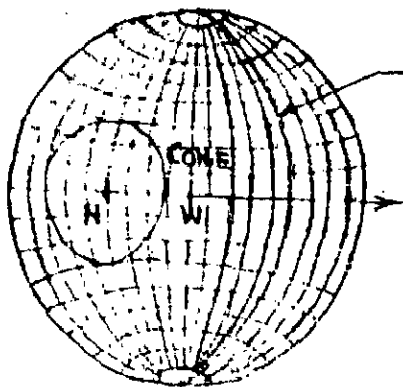


FIG. 13: PICTORIAL REPRESENTATION OF THE FRICTION CONE CONCEPT ON THE LOWER HEMISPHERE.



PLANE

FIG. 14: REPRESENTATION OF THE FRICTION CONE CONCEPT ON A STERONEET.



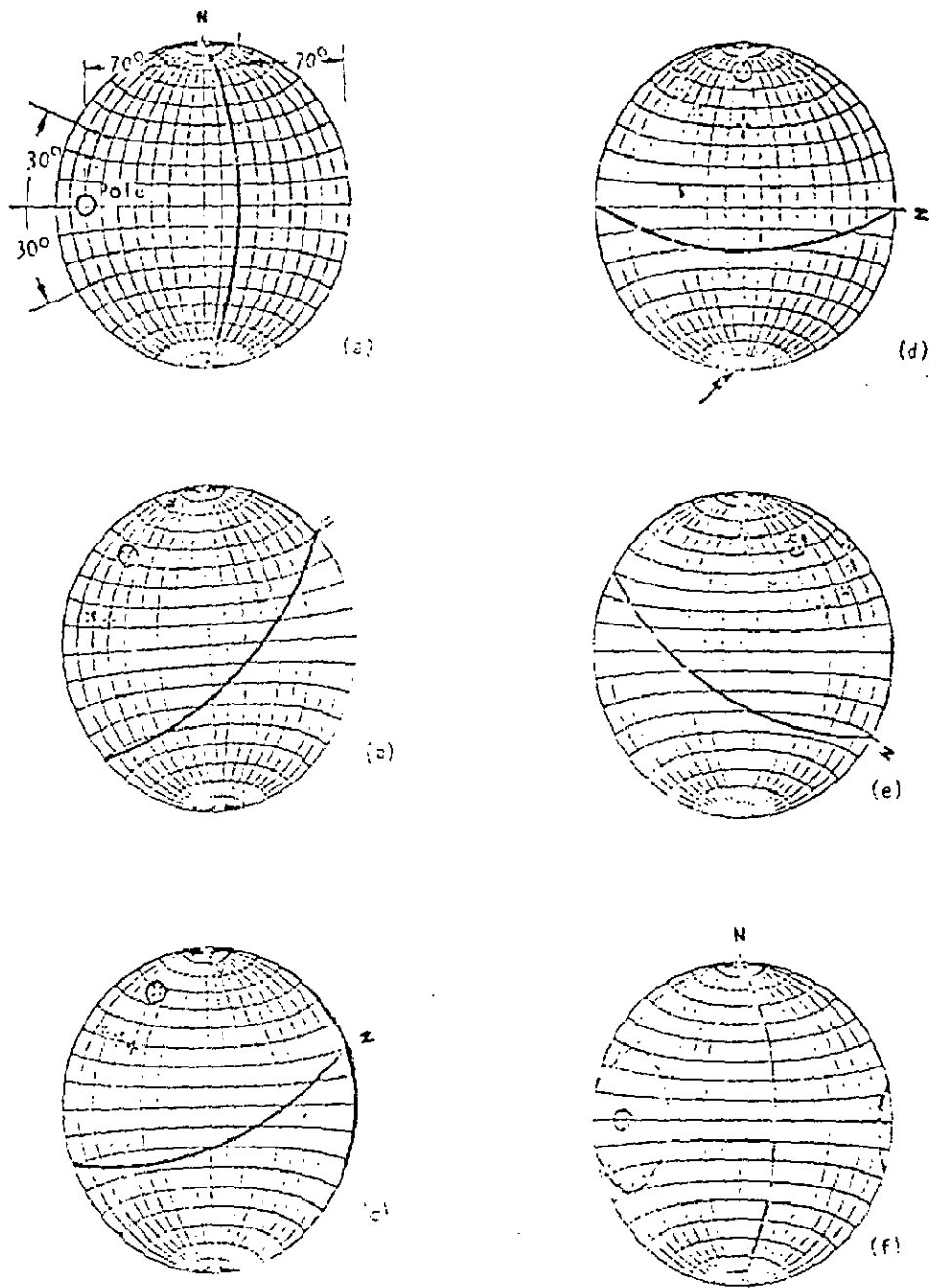


FIG.15: CONSTRUCTION OF FRICTION CONE PROJECTION

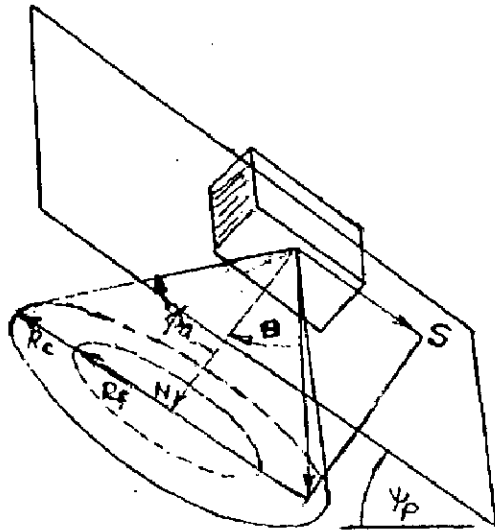


FIG. 16: APPARENT FRICTION ANGLE OBTAINED FOR RESISTANCE DUE TO BOTH FRICTION AND COHESION.

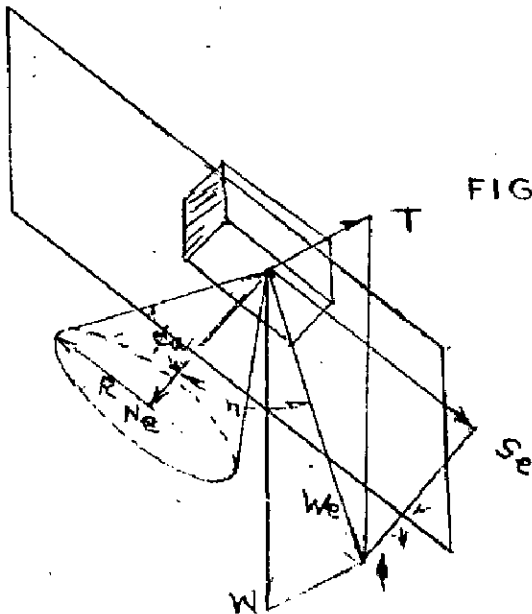
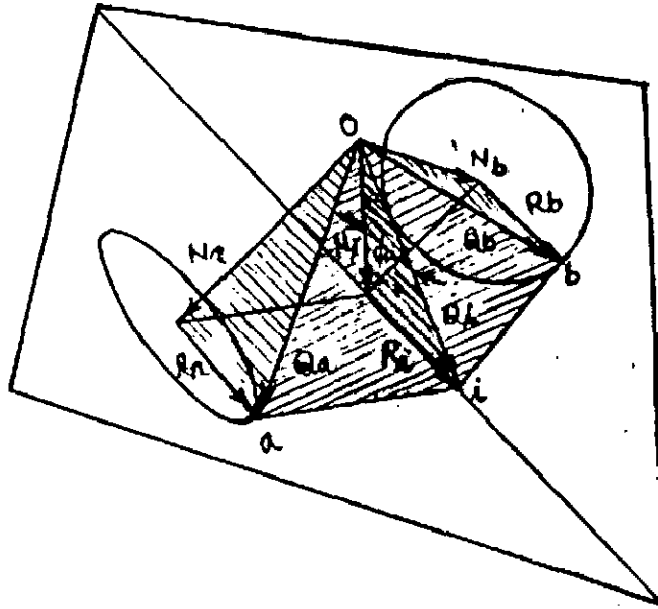
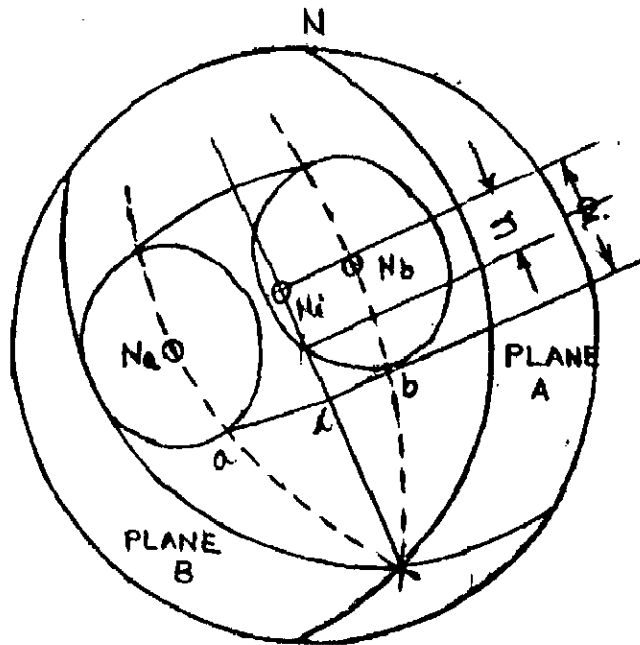


FIG. 17: INFLUENCE OF AN EXTERNAL FORCE T UPON THE STABILITY OF A BLOCK SLIDING ON AN INCLINED PLANE.



(a)

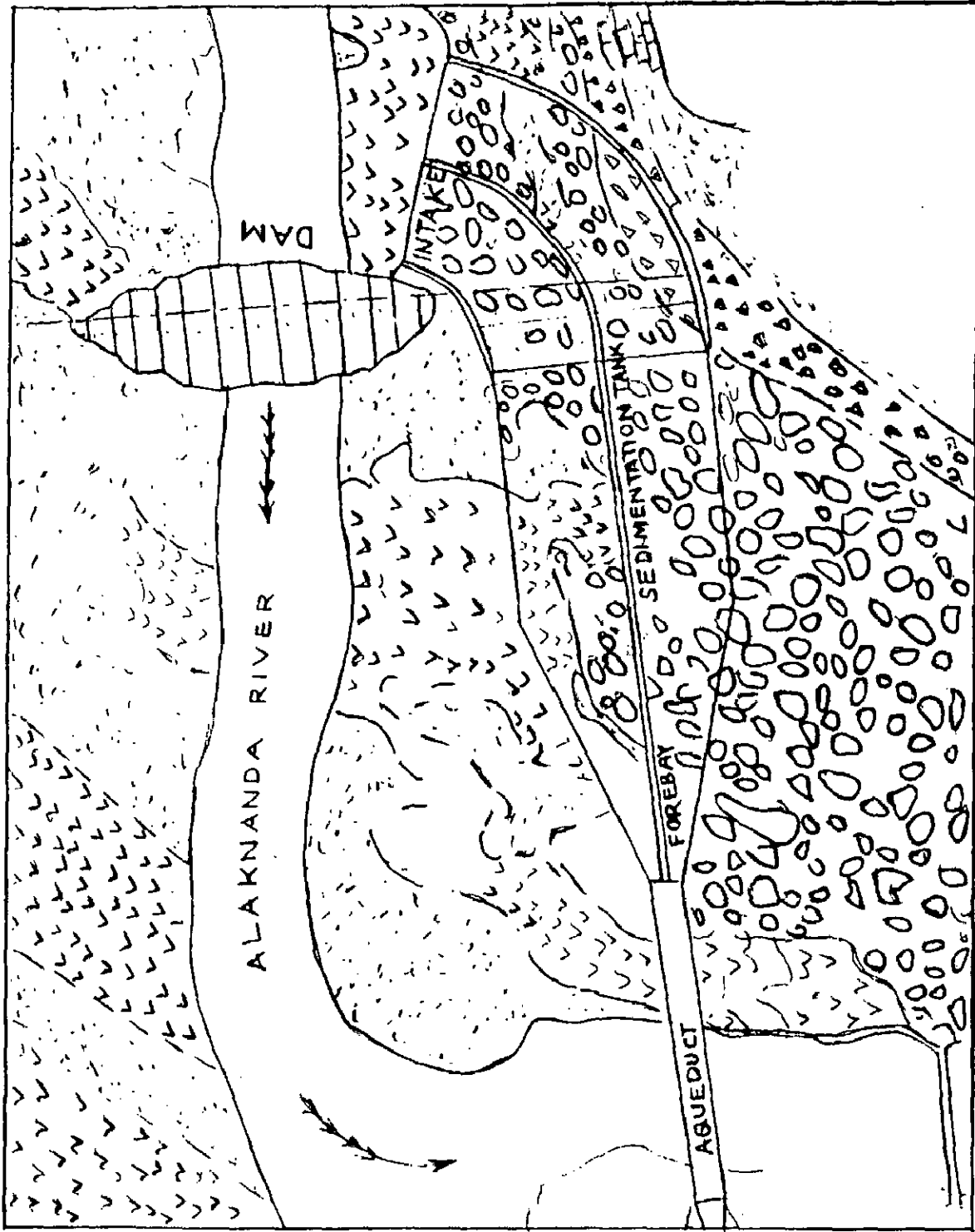


(b)

FIG. 18: PICTORIAL AND GRAPHICAL REPRESENTATION OF FRICTION CONE CONCEPT APPLIED TO SLIDING ON TWO INTERSECTING PLANES.



246491



INDEX




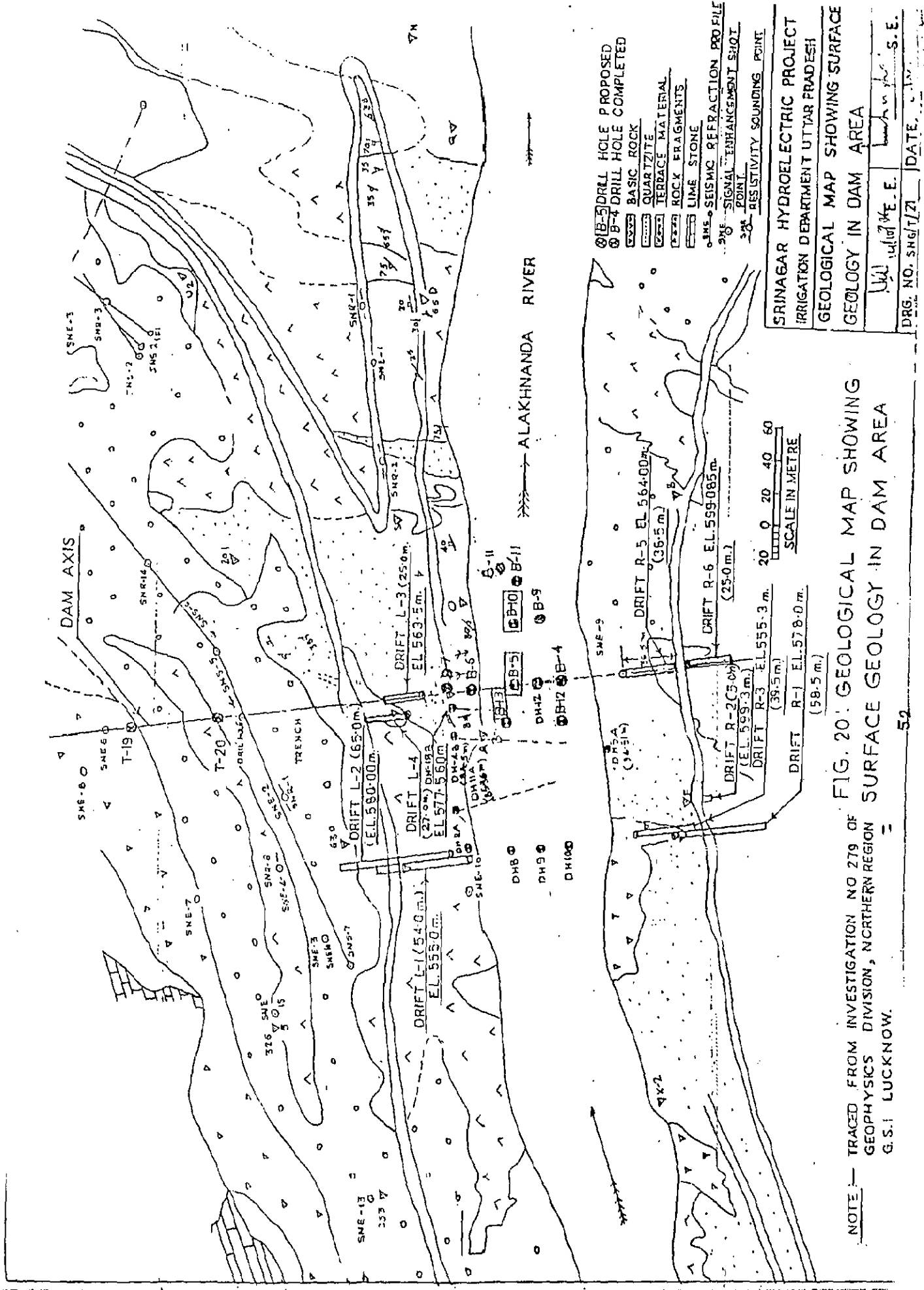
-  QUARTZITE
-  METABASIC
-  R.B.M.

FIG.19: PLAN SHOWING GEOLOGY OF DAM AREA.



NOTE — TRACED FROM INVESTIGATION NO 279 OF GEOPHYSICS DIVISION, NORTHERN REGION G.S.I LUCKNOW.

FIG. 20: GEOLOGICAL MAP SHOWING SURFACE GEOLOGY IN DAM AREA

| | |
|--|---------------------|
| SRINAGAR HYDROELECTRIC PROJECT | |
| IRRIGATION DEPARTMENT UTTAR PRADESH | |
| GEOLOGICAL MAP SHOWING SURFACE GEOLOGY IN DAM AREA | |
| DRG. NO. SHG/T/71 | DATE: 14/10/74 E.E. |
| | S.E. |

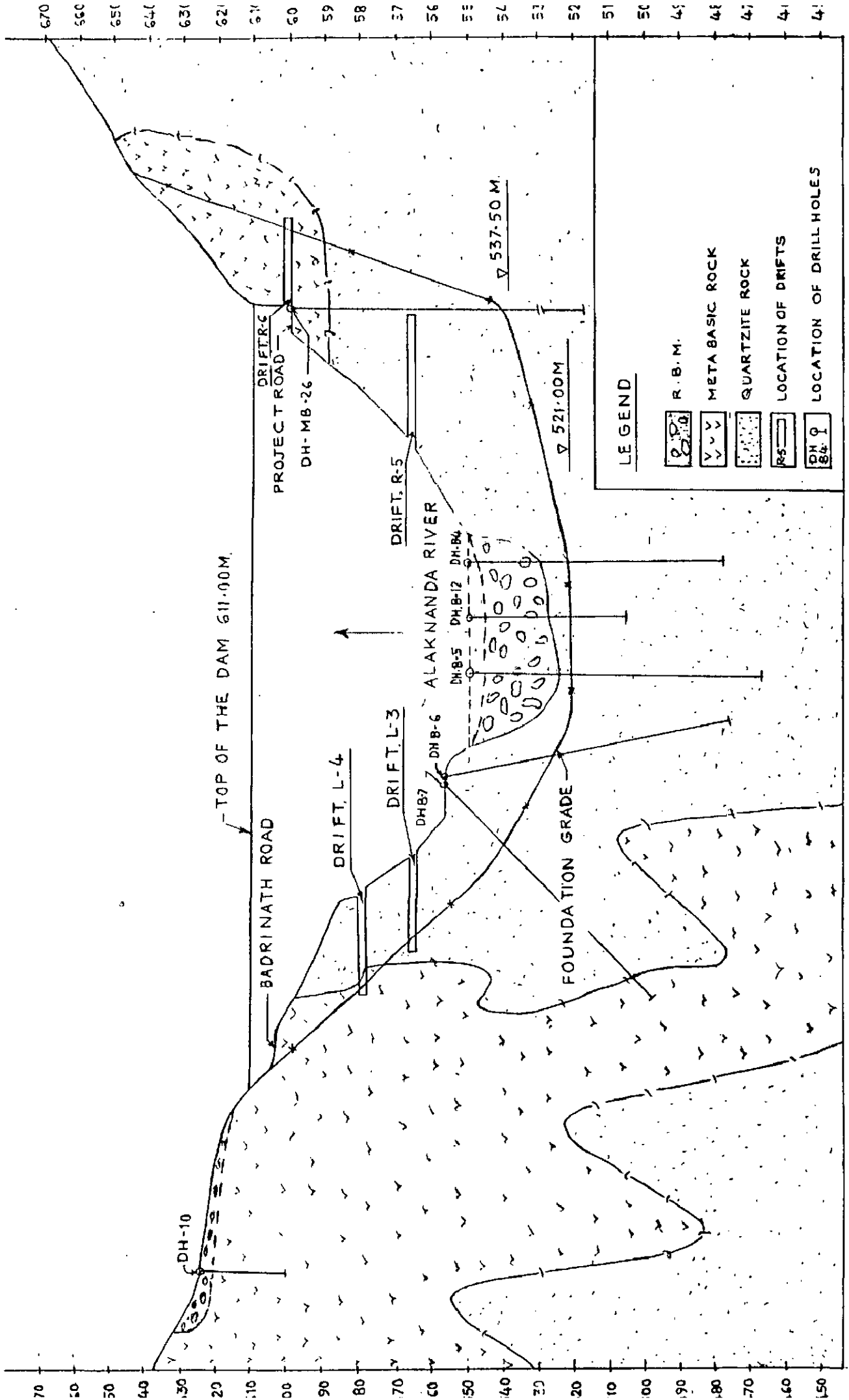


FIG.21: GEOLOGICAL SECTION ALONG DAM AXIS

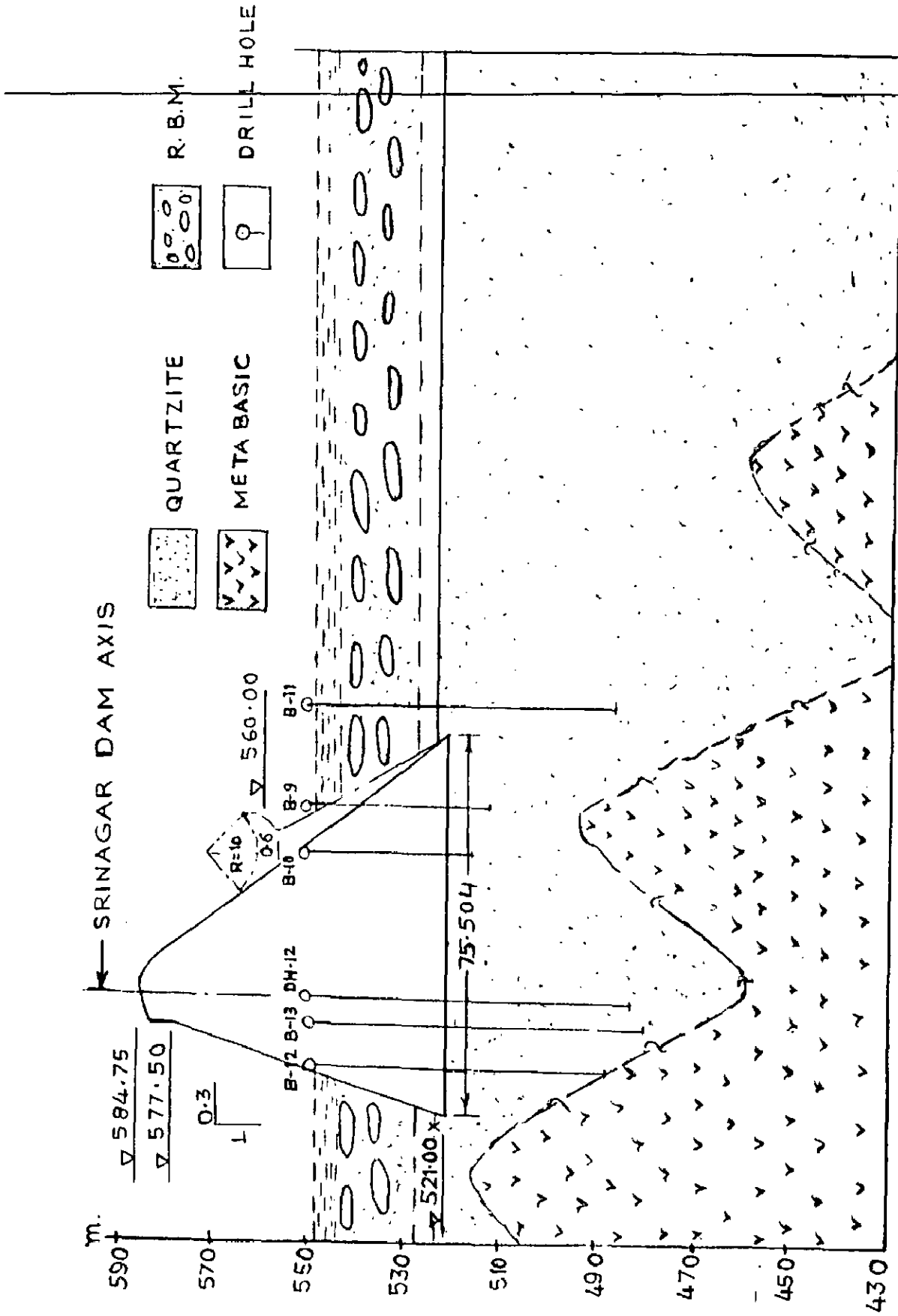
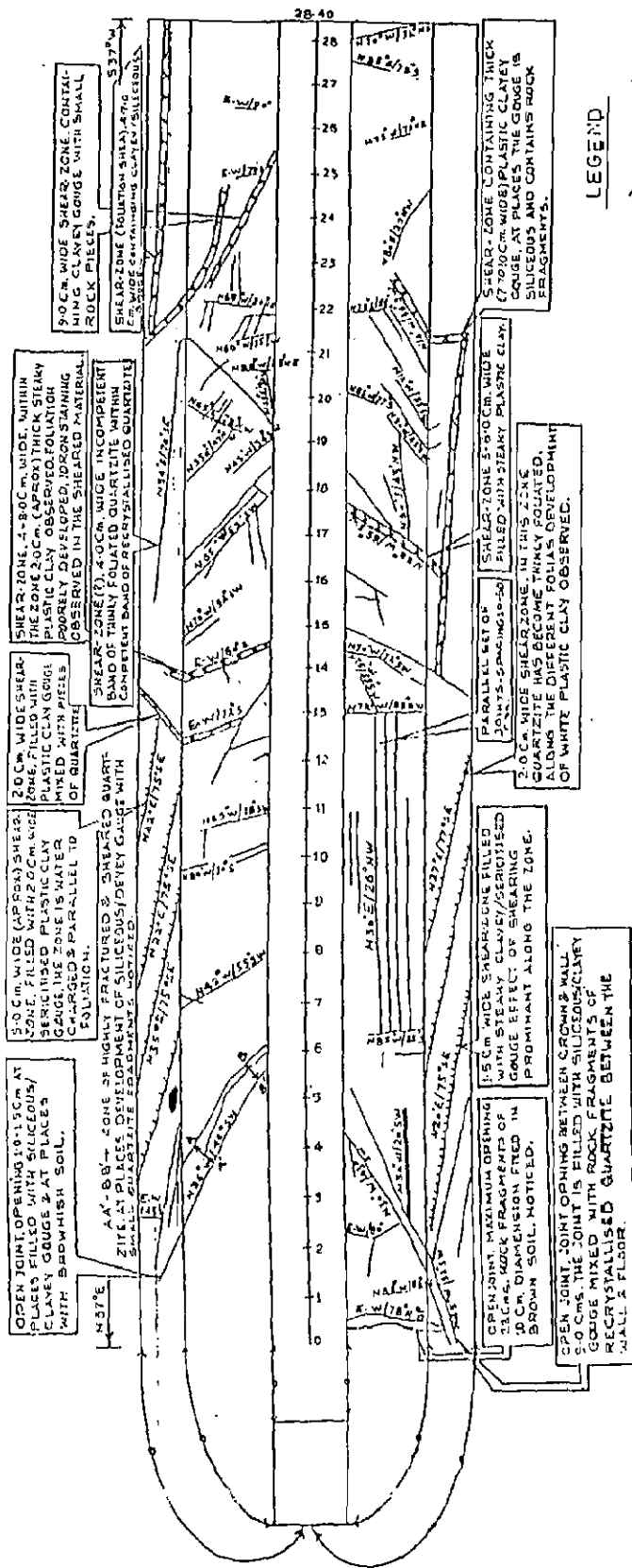


FIG. 22: CROSS SECTION OF THE DEEPEST BLOCK SHOWING FOUNDATION GEOLOGY
 IN SRINAGAR DAM



LEGEND

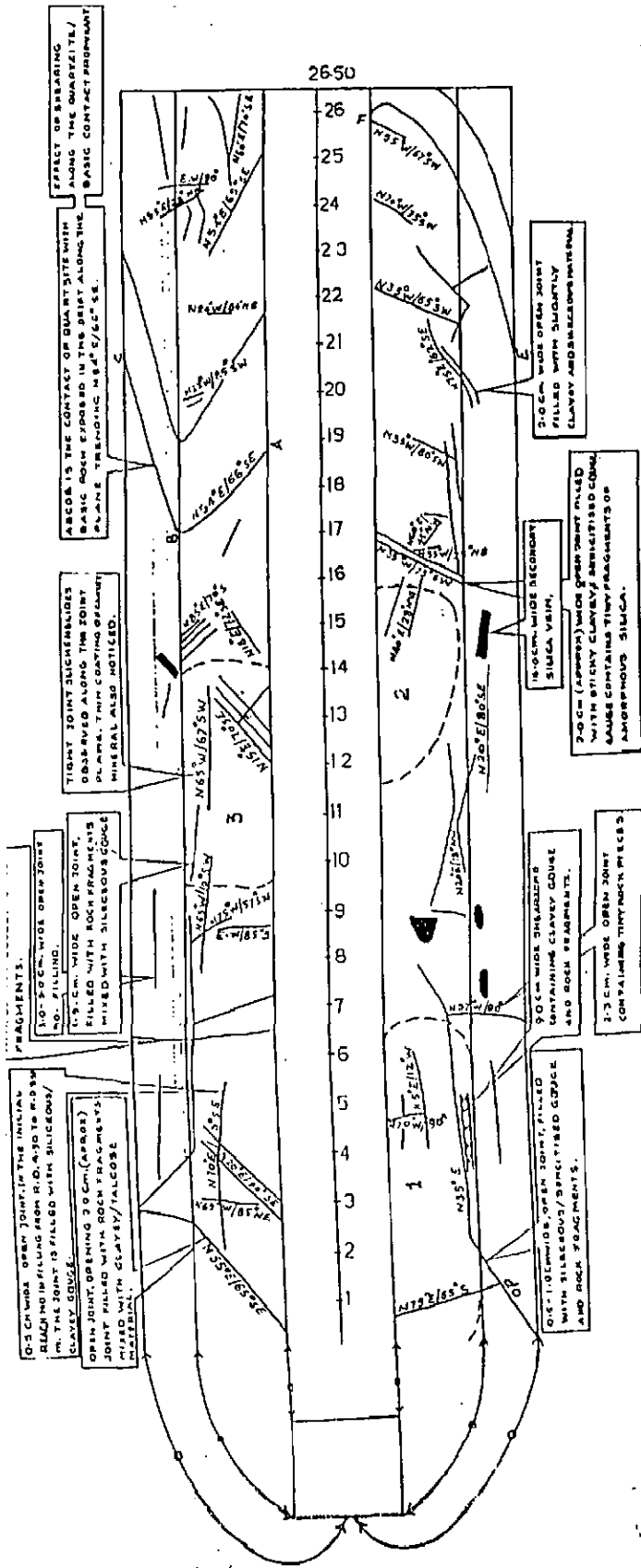
- SHEAR ZONE VARYING IN THICKNESS FROM 20CM TO 100CM.
- SHEAR ZONES LESS THAN 20CM. JOINT PLANE.
- OPEN JOINT (WITH AMOUNT OF OPENING)
- STRIKE AND DIP OF THE PLANE.
- SECONDARY SILICA VEIN

NOTES:-

- 1- THE DRIFT HAS BEEN EXCAVATED THROUGH THE RECRYSTALLISED/FOLIATED QUARTZITE. THE FOLIATION PLANE VARIES FROM 75°-80° IN 22° S 5° E.
- 2- THE DRIFT IS UNSUPPORTED FOR THE ENTIRE REACH LOGGED.
- 3- WATER DRIPPING OBSERVED FROM CROWN BETWEEN RD 40.25-50m; BETWEEN CROWN & LEFT WALL AT R.D. 62.0m AND BETWEEN CROWN & RIGHT WALL ALONG THE FOLIATION SHEAR FROM R.D. 5.20 TO 9.70m.
- 4- ROOT PENETRATION ON LEFT WALL OBSERVED AT R.D. 5.1m AND ON RIGHT WALL AT R.D. 2.80m.
- 5- OVERBREAK OF THE ORDER OF 50 TO 70 CM OBSERVED AT CROWN BETWEEN R.D. 20m & 25m.
- 6- THE FOLIATION JOINT IS EXPOSED ALONG THE RIGHT WALL BETWEEN R.D. 0.0m & 0.5m AND FROM R.D. 17.0m TILL THE FACE SIMILARLY ALONG THE LEFT WALL, THE FOLIATION JOINT IS EXPOSED BETWEEN R.D. 0.0m & 10.0m AND FROM R.D. 16m TILL THE FACE.
- 7- THE BANDS OF RECRYSTALLISED QUARTZITE VARIES IN THICKNESS FROM 5.0 CM TO 20.0 CM.
- 8- THE ROCK IS MOSTLY FRESH BEYOND R.D. 12.0 CM.
- 9- THE ELEVATION OF THE PORTAL HAS BEEN SUPPLIED BY THE PROJECT AUTHORITIES.

| |
|--|
| SRINAGAR HYDROELECTRIC PROJECT |
| IRRIGATION DEPARTMENT UTTAR PRADESH |
| 3-D GEOLOGICAL LOG OF DRIFT L-3 AT E.L. 562.50 CM ON LEFT ABUTMENT ALONG DAM AXIS (FROM 0.0m TO 28.40m R.L.) |
| DRG. NO. SNGR/12/ DATE 23.09 |
| E.E. S.E. |

FIG. 23: 3-D. GEOLOGICAL LOG OF DRIFT L-3. COPIED FROM GEOLOGICAL REPORT PREPARED BY KUMUD SHARMA



LEGEND

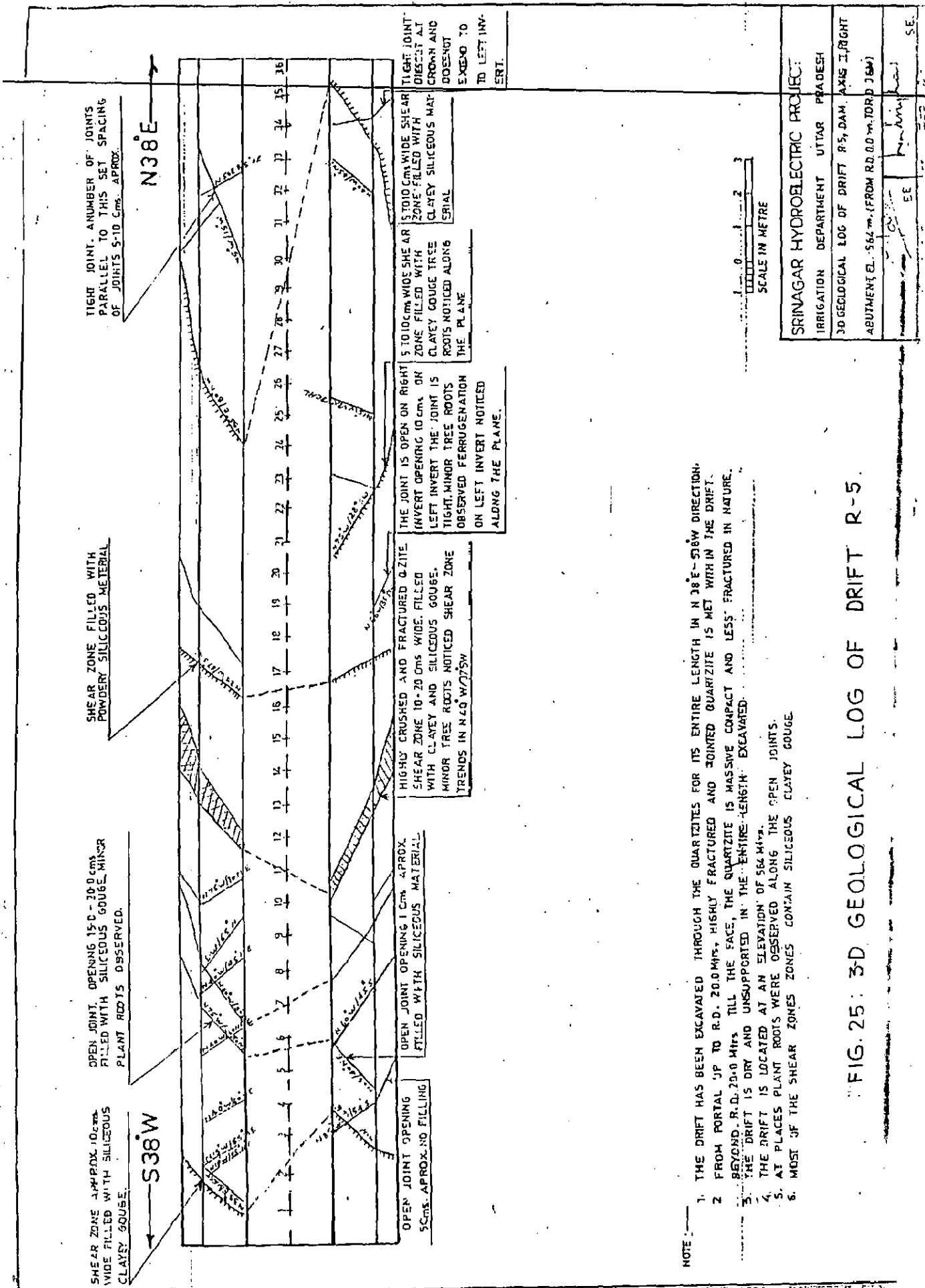
- JOINT PLANE.
- SHEAR ZONE VARYING IN THICKNESS FROM 5-00m. TO 10-00m.
- STRIKE & DIP OF THE PLANE.
- SECONDARY SILICA VEIN.
- FOLIATION JOINT EXPOSED ALONG THE WALL OF THE DRIFT.
- THIN FOLIATED BASIC ROCK.
- COARSE GRAINED MASSIVE BASIC ROCK.

| | | |
|---|--|--------------------------|
| SRINAGAR HYDROELECTRIC PROJECT. | IRRIGATION DEPARTMENT | UTTAR PRADESH |
| 3-D GEOLOGICAL LOG OF DRIFT L-4 AT EL 27.8-34 | ON LEFT ABUTMENT ALONG DAM AXIS (FROM R.D. 0.0 m TO R.D. 26.0) | |
| <i>[Signature]</i> | E. E. | <i>[Signature]</i> S. E. |
| DRG. NO. SNOIT/111 | DATE | FEB. 89 |

- NOTES**
1. THE DRIFT HAS BEEN EXCAVATED THROUGH THE QUARTZITE AND BASIC ROCK. THE QUARTZITE/ BASIC ROCK CONTACT IS EXPOSED IN THE DRIFT AT R.D. 18.60 m. THE CONTACT FOLLOWS THE PLANE TRENDING N54°E-54°W WITH 6° DIP IN SE.
 2. THE DRIFT IS UNSUPPORTED FOR THE ENTIRE REACH LOGGED.
 3. THE QUARTZITE EXPOSED IN THE DRIFT, FROM THE PORTAL UPTO R.D. 12.50, ON BOTH THE WALLS IS COMPLETELY FRESH AND STRUCTURALLY LESS DISTURBED WHILE THE ENTIRE CROWN BETWEEN THE ABOVE MENTIONED REACH IS HIGHLY FRACTURED AND SEMI-WEATHERED. THE EFFECT OF SERICITISATION/KAOLINISATION IS PROMINANT.
 4. WATER DRIPPING OBSERVED, FROM CROWN BETWEEN R.D. 17.0m. & 18.60m., BETWEEN CROWN & RIGHT WALL FROM R.D. 7.0m.-9.0m. & R.D. 15.60m. 16.80m., FROM LEFT WALL AT R.D. 16.80m. & FROM R.D. 24.40m.-26.0m.
 5. EFFECT OF SHEARING (SLICKEN SLIDES/ MINOR SCALE ROOFING) WITH IN THE QUARTZITES BETWEEN THE CROWN AND RIGHT WALL BETWEEN R.D. 15.60m.-R.D. 16.80m., WITH LESS STICKY CLAY IS WELL PRONOUNCED.
 6. THE BASIC ROCK IS FRESH THROUGHOUT, SURFICIAL WEATHERING IN FORM OF IRON - STAINING PRONOUNCED.
 7. SLICKEN SLIDES IN THE SHEETED BASIC ROCK OBSERVED BETWEEN LEFT WALL AND HALF CROWN.
 8. THE ELEVATION... OF THE PORTAL HAS BEEN SUPPLIED BY THE PROJECT AUTHORITIES.

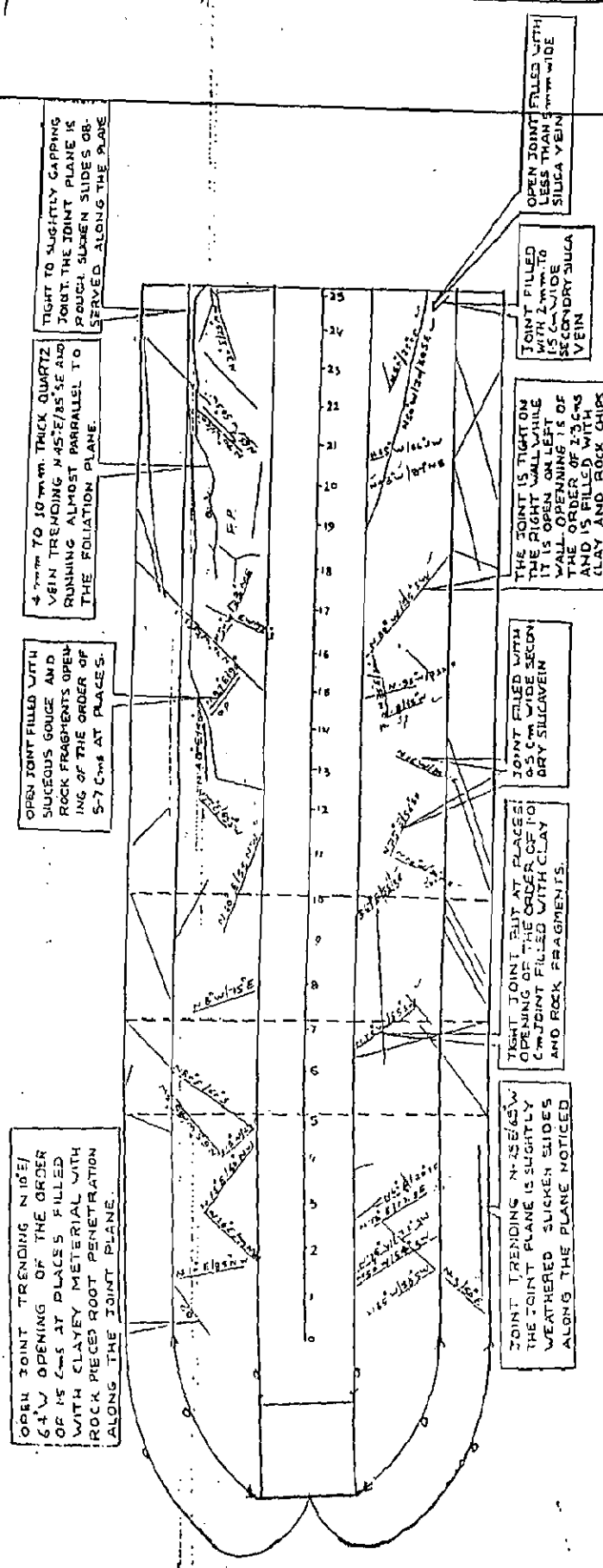
COPIED FROM GEOLOGICAL REPORT PREPARED BY KUNUD SHARMA

FIG 24: 3-D GEOLOGICAL LOG OF DRIFT L-4.



- NOTE
1. THE DRIFT HAS BEEN EXCAVATED THROUGH THE QUARTZITES FOR ITS ENTIRE LENGTH IN N 38°E-S38W DIRECTION.
 2. FROM PORTAL UP TO R.D. 20.0 MTS, HIGHLY FRACTURED AND JOINTED QUARTZITE IS MET WITH IN THE DRIFT.
 3. BEYOND R.D. 20.0 MTS TILL THE FACE, THE QUARTZITE IS MASSIVE COMPACT AND LESS FRACTURED IN NATURE.
 4. THE DRIFT IS DRY AND UNSUPPORTED IN THE ENTIRE LENGTH EXCAVATED.
 5. THE DRIFT IS LOCATED AT AN ELEVATION OF 564 MTS.
 6. AT PLACES PLANT ROOTS WERE OBSERVED ALONG THE OPEN JOINTS.
 7. MOST OF THE SHEAR ZONES CONTAIN SILICEOUS CLAYEY GOUGE.

FIG. 25: 3D GEOLOGICAL LOG OF DRIFT R-5.



LEGEND:-

- 1. JOINT PLANE
- 2. OPEN JOINT WITH AMOUNT OF OPENING
- 3. STRIKE S
- 4. DIP OF THE PLANE.
- 5. FOLLIATION JOINT PLANE
- 6. QUARTZ VEIN

NOTES

1. THE ENTIRE DRIFT HAS BEEN EXCAVATED THROUGH METABASICS. DRIFT IS RECTANGULAR IN SHAPE
2. THE DRIFT IS DRY AND UNSUPPORTED FOR THE ENTIRE LENGTH EXCAVATED.
3. OVERBREAK AT THE CROWN OBSERVED AT RD 350M-120M APPROX RD 1170-1070M & RD 1520M-300M AND AT RD 1790M-300M (APPROX)
4. ROOT PENETRATION FROM THE CROWN OBSERVED BETWEEN RD. 3-0M AND RD. 4M.
5. IN THE INITIAL REACHES FROM THE PORTAL TO RD. 50M, THE METABASIS IS COARSE GRAINED AND MASSIVE (A-TYPE), AT FACE THE ROCK IS THINLY FOLIATED (B-TYPE) AND WEATHERED ON SURFACE.
6. AT CROWN SPACING OF FOLIATION JOINT WITHIN A-TYPE METABASICS VARIES FROM 30 CM TO 60 CM.
7. AT FACE THE THINLY FOLIATED METABASICS (C-TYPE) IS TRAVERSED BY APPROX 1.5 CM THICK SECONDARY SILICA VENS. SILICA VEIN MAKES AN ANGLE OF 45-50° WITH FOLIATION OF COUNTRY ROCK. THE STRIKE EXTENSION OF SILICA VEIN IS 41 CMs & TRENDS IN NSO E DIRECTION WITH 38° DIP IN SE.
8. THE WALLS OF THE DRIFT EXPOSES. A JOINT PLANE TRENDING N40E-S40W & IS ALMOST VERTICAL.
9. THE ROCK IS MOSTLY FRESH BEYOND 10 M-RD.
10. THE ELEVATION OF THE PORTAL HAS BEEN SUPPLIED BY THE PROJECT AUTHORITIES
11. ON THE FACE HIGHLY WEATHERED & DESINTEGRATED BASIC ROCK IS EXPOSED.

SRINAGAR HYDROELECTRIC PROJECT
IRRIGATION DEPARTMENT U.P.

3-D GEOLOGICAL LOG OF DRIFT R-6 EXCAVATED AT EL. 599.08M RIGHT ABUTMENT, AXIS II (FROM R.D. 0.0 M TO R.D. 25.0 M)

EE
DRG. NO. SNG/1735 DATE 23. 89

FIG. 26: 3-D GEOLOGICAL LOG OF DRIFT R-6.

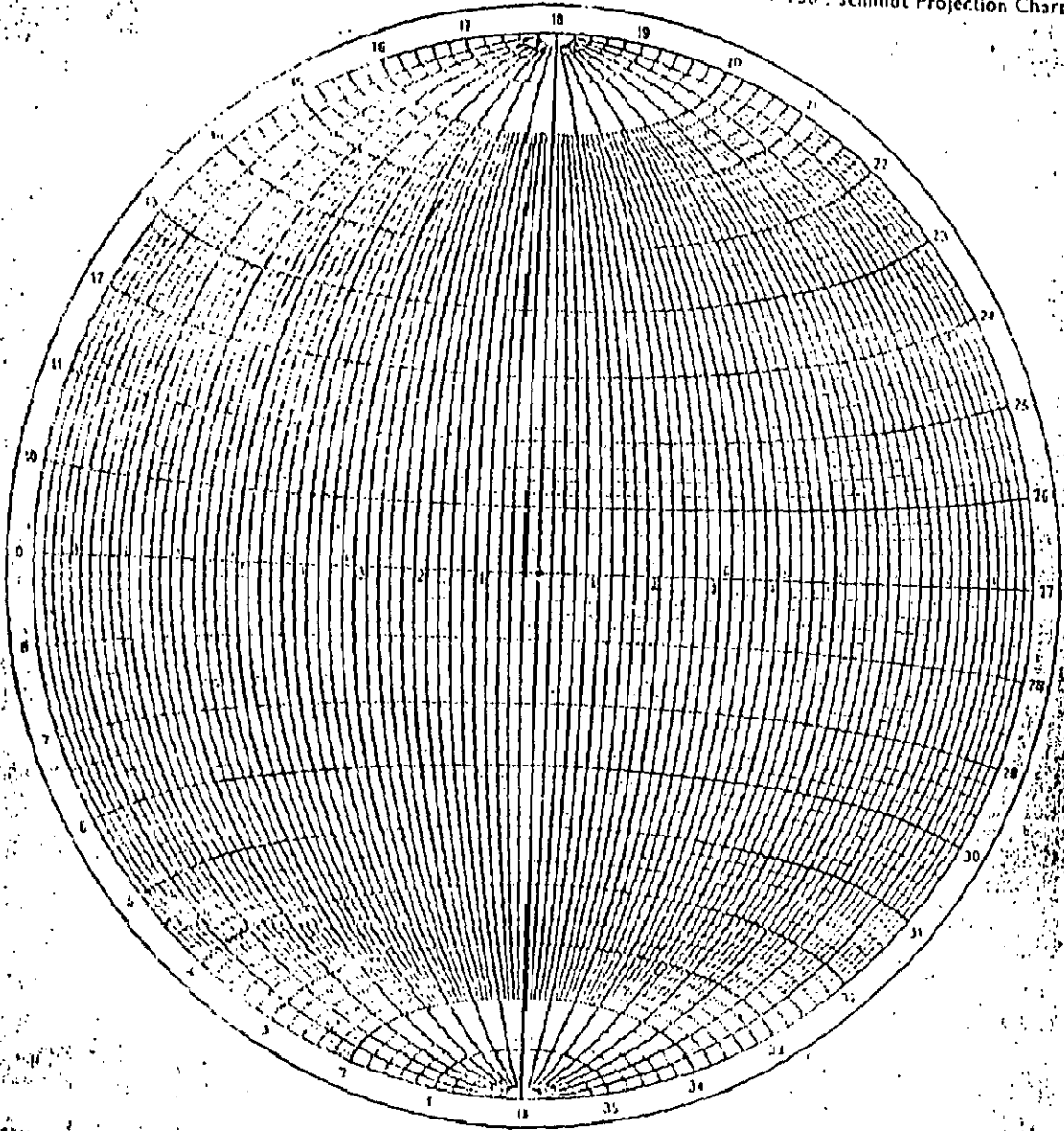
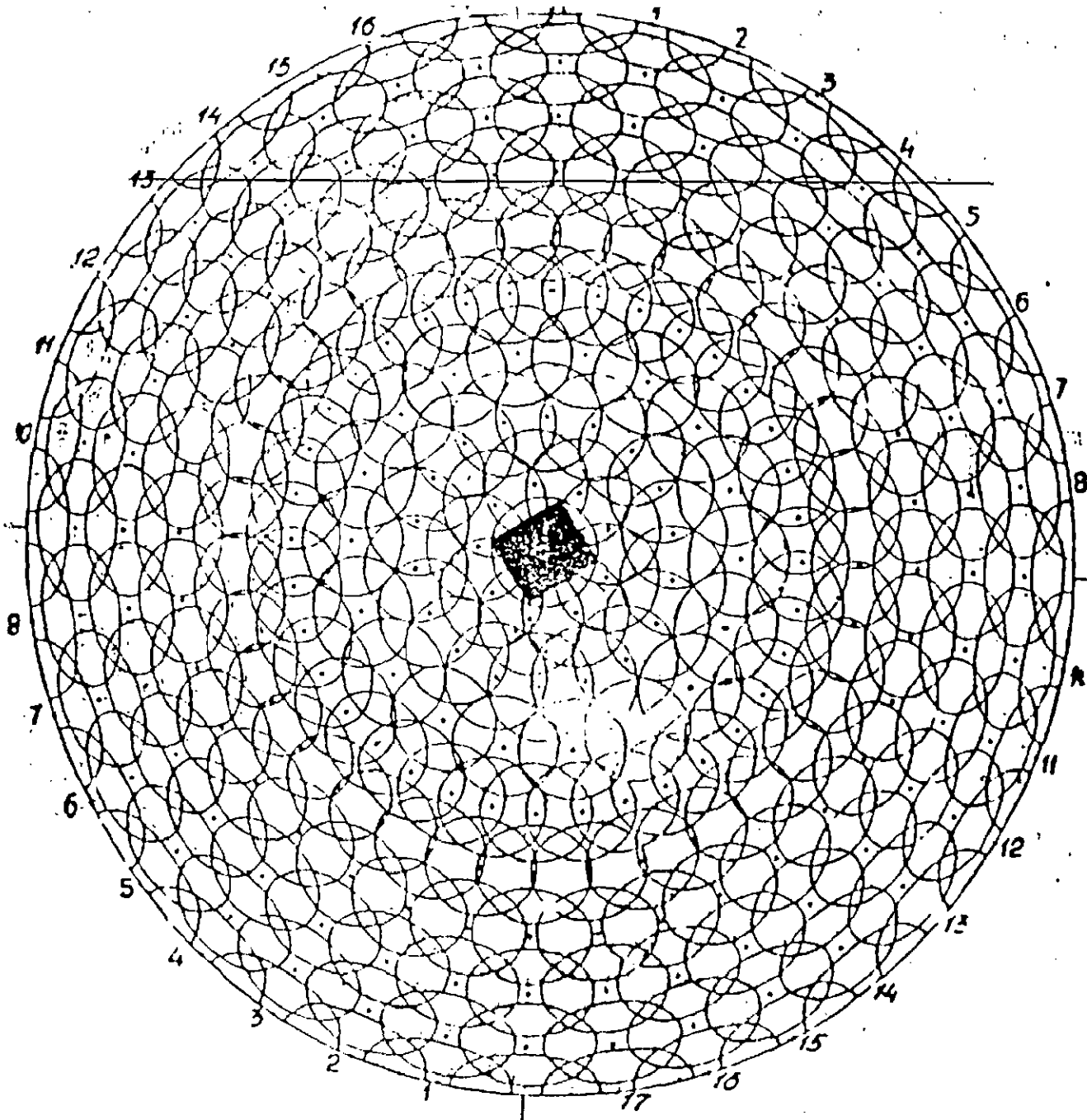


FIG. 27: SCHMIDT NET
59



Mreža sa odličarolo gestic podataka na talisastom dijagramu

FIG. 28: FLOATING CIRCLE COUNTING NET.

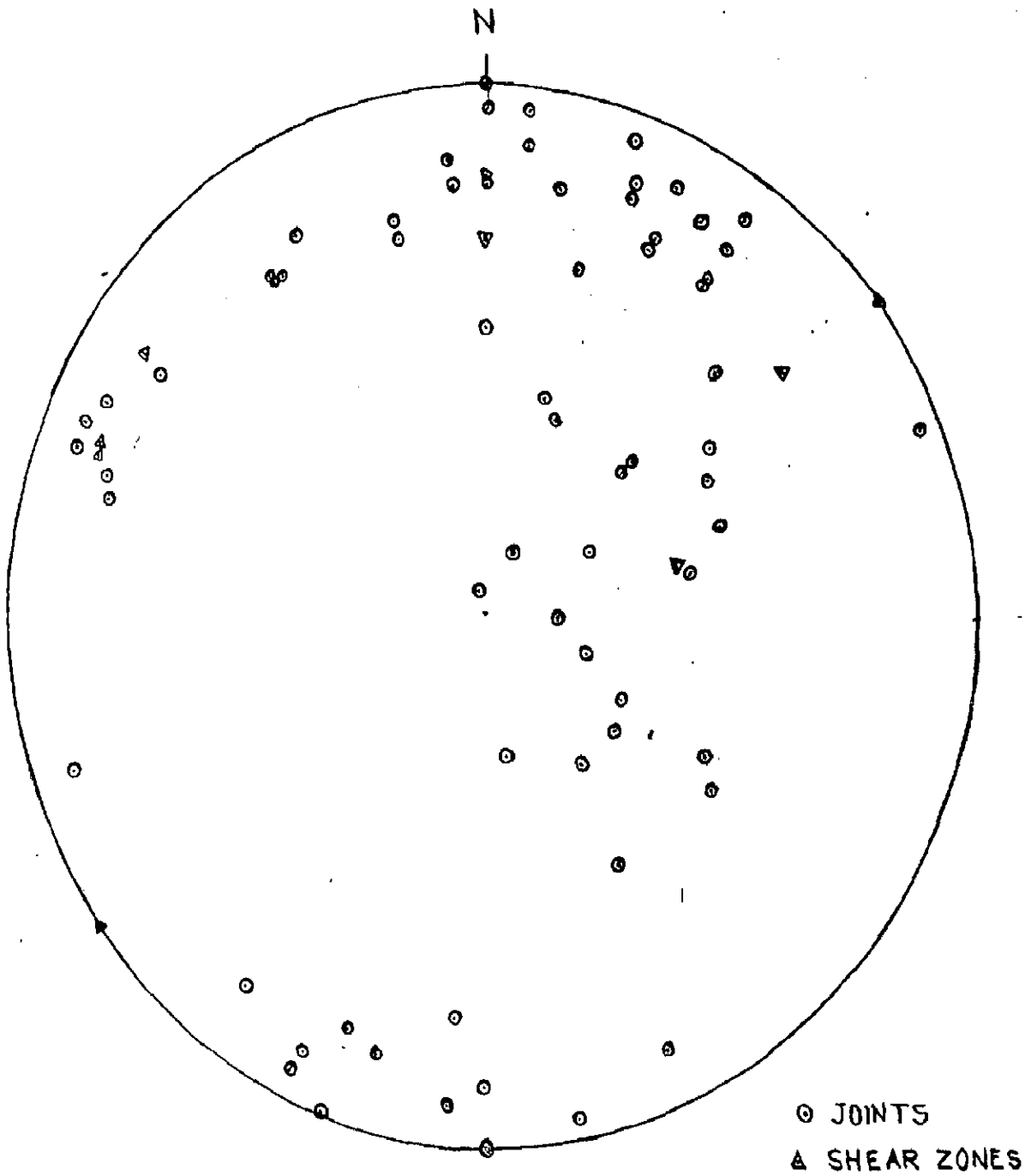


FIG. 29: PLOT OF POLES REPRESENTING
GEOLOGICAL DISCONTINUITY PLANES
IN DRIFTS, L-3 AND L-4.

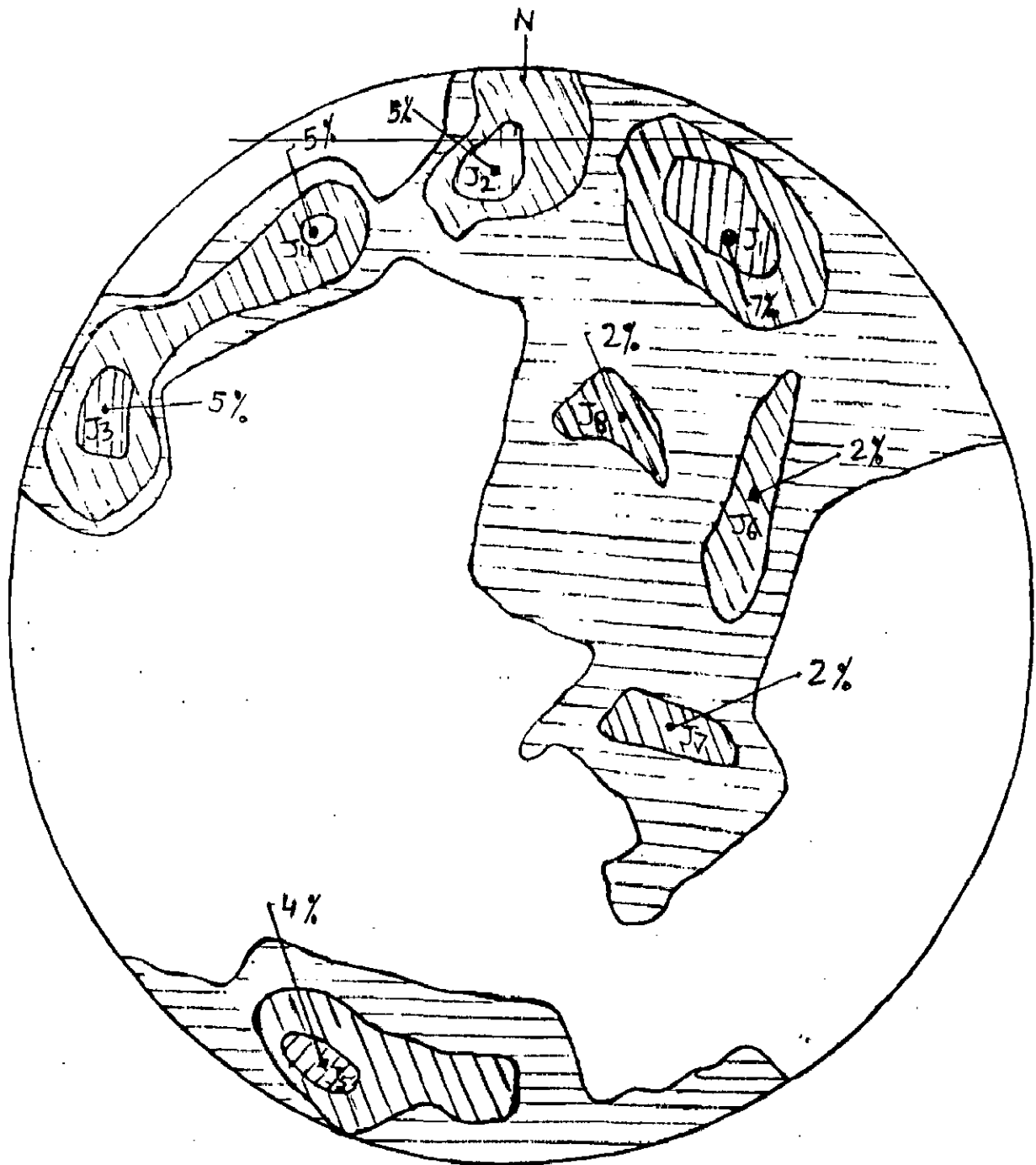


FIG. 30: STEREO PLOT DEPICTING THE VARIOUS GEOLOGICAL DISCONTINUITY PLANES IN DRIFTS, L-3 AND L-4.

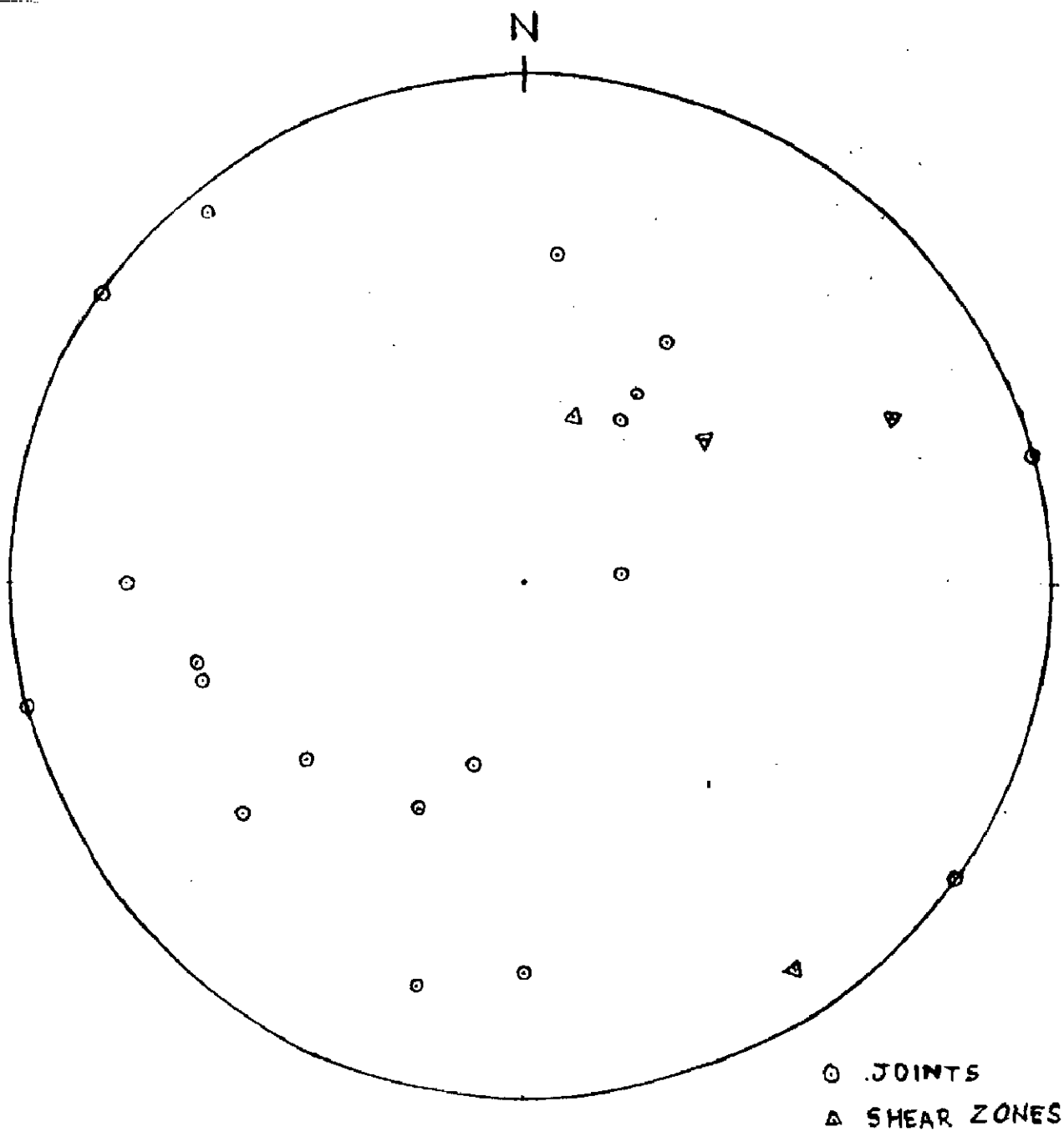


FIG. 31: PLOT OF POLES REPRESENTING
 GEOLOGICAL DISCONTINUITY PLANES
 IN DRIFT, R-5.

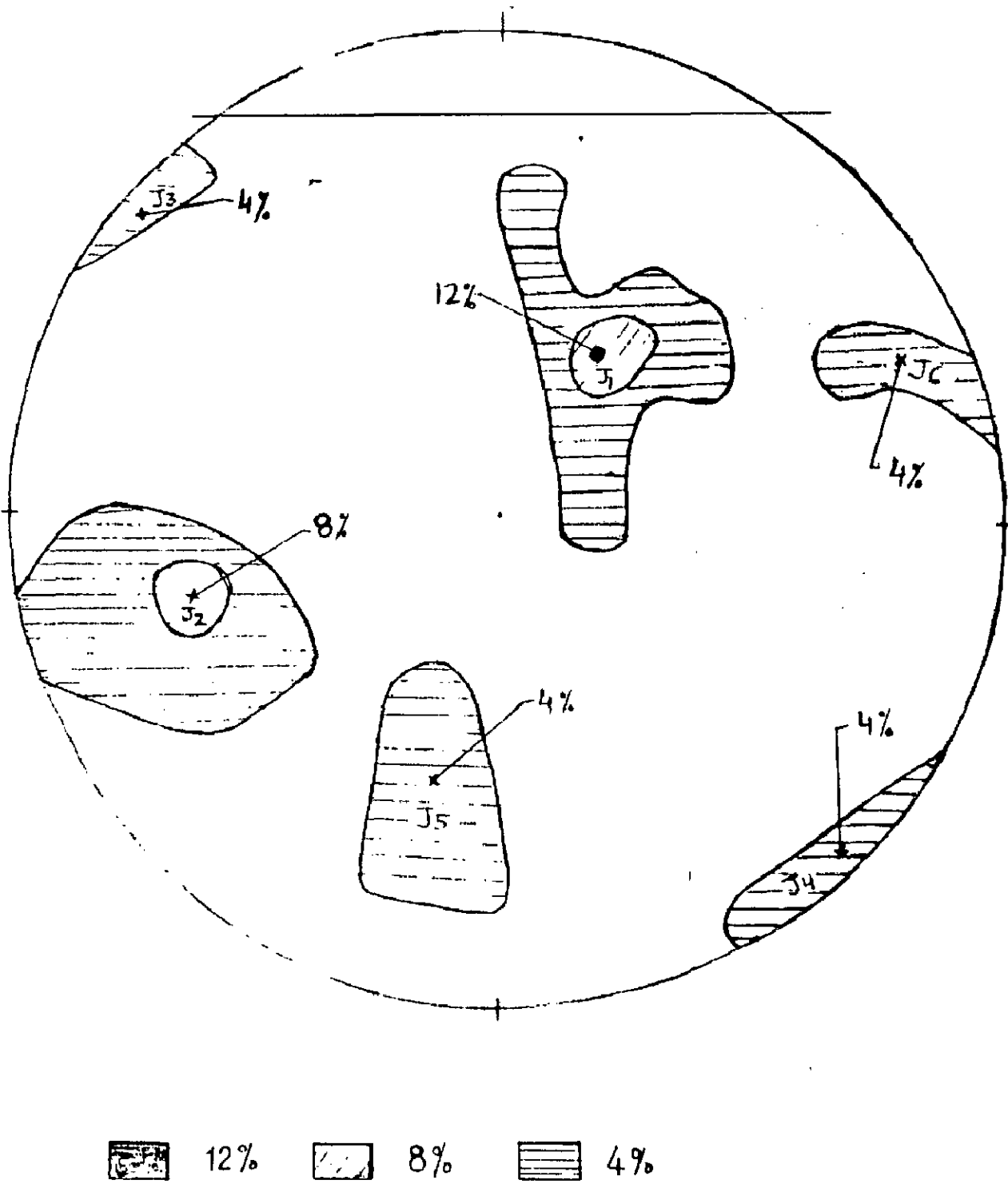


FIG. 32 : STEREO PLOT DEPICTING THE VARIOUS GEOLOGICAL DISCONTINUITY PLANES IN DRIFT, R-5.

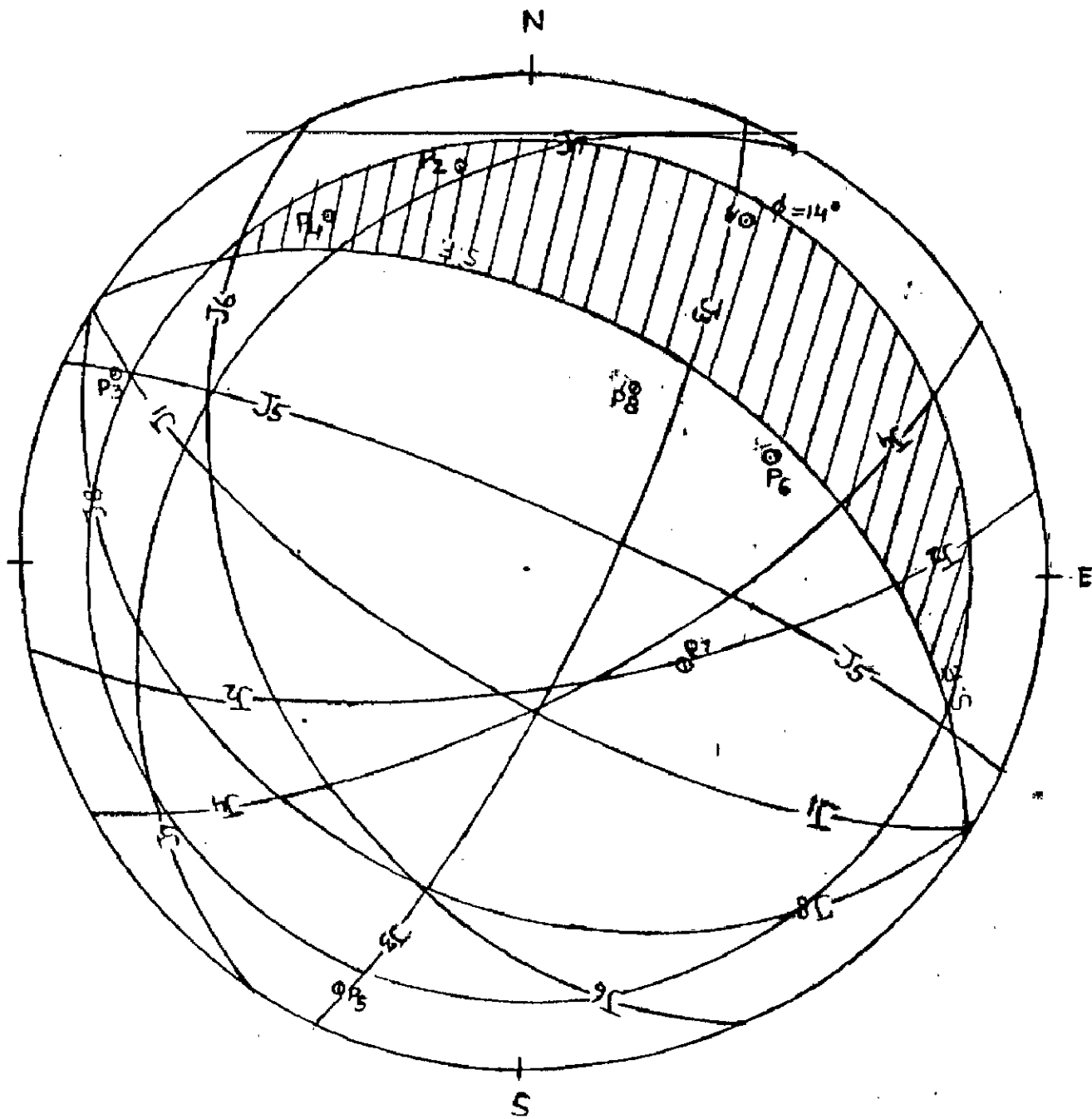


FIG. 33: COMBINED STEREO PLOT OF DISCONTINUITY PLANES (TABLE-1) FOR LEFT ABUTMENT.

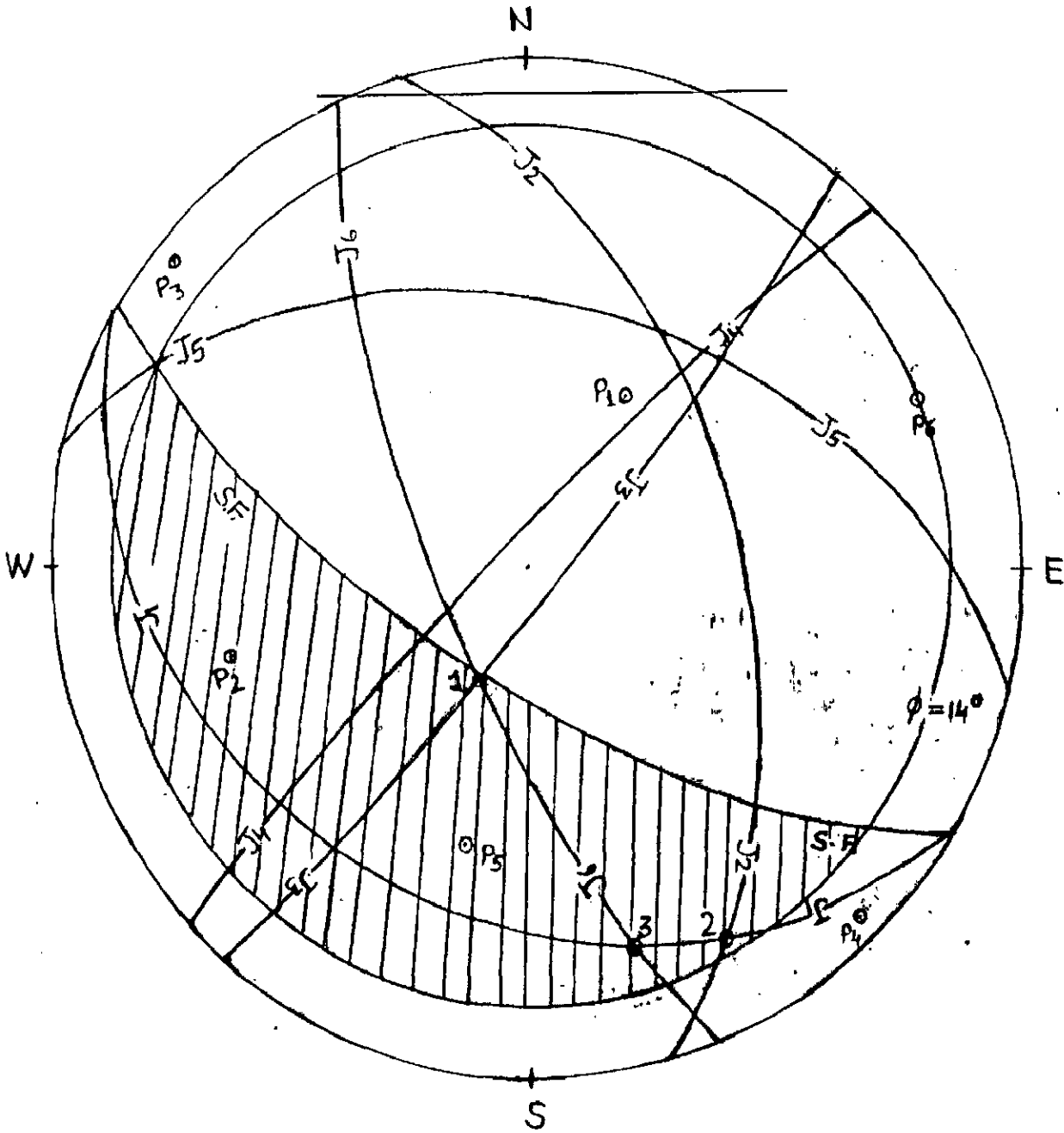


FIG. 34: COMBINED STEREO PLOT OF DISCONTINUITY PLANES (TABLE-2) FOR RIGHT ABUTMENT.

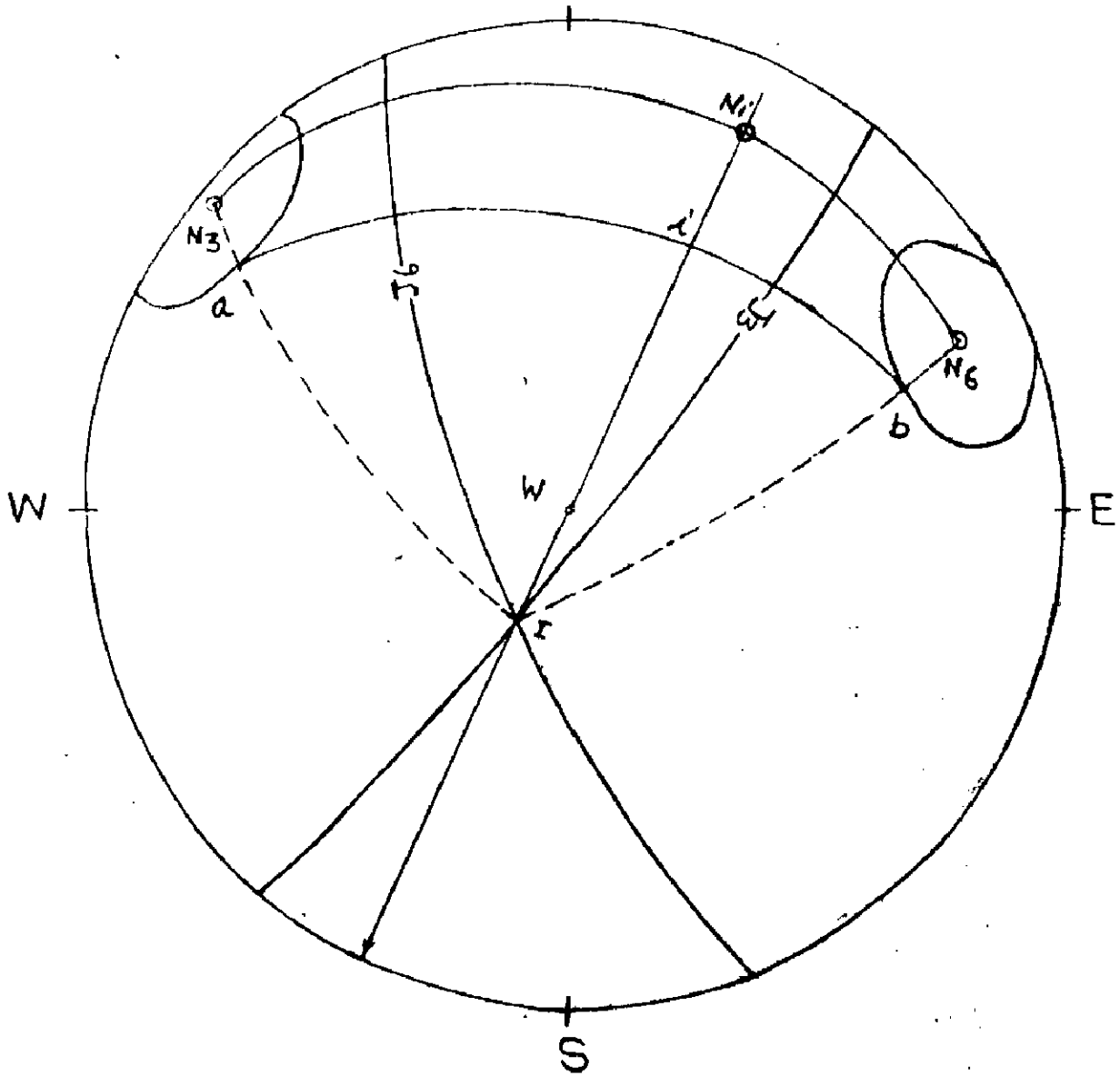


FIG. 35: F.O.S. FOR FRICTION (ϕ) ONLY CONDITION.

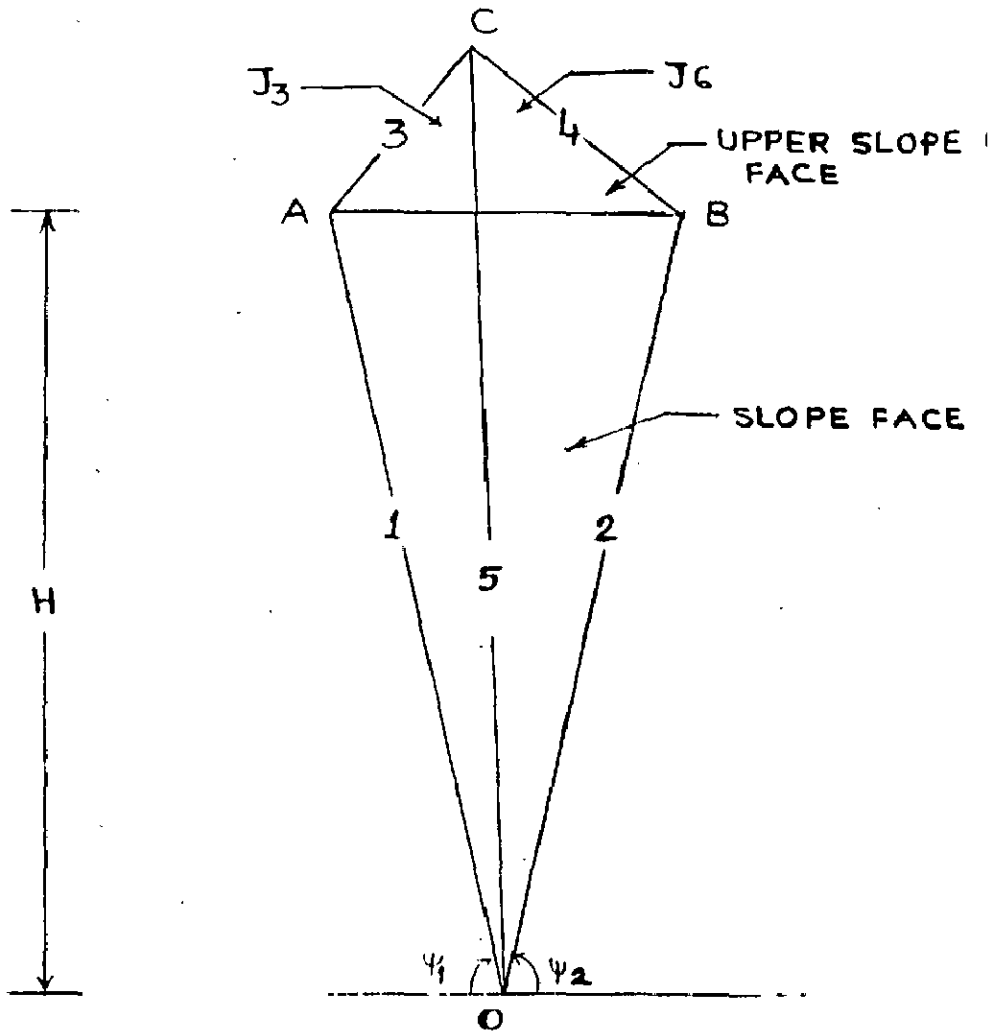


FIG. 36: PICTORIAL VIEW OF WEDGE NO-1.
(RIGHT ABUTMENT).

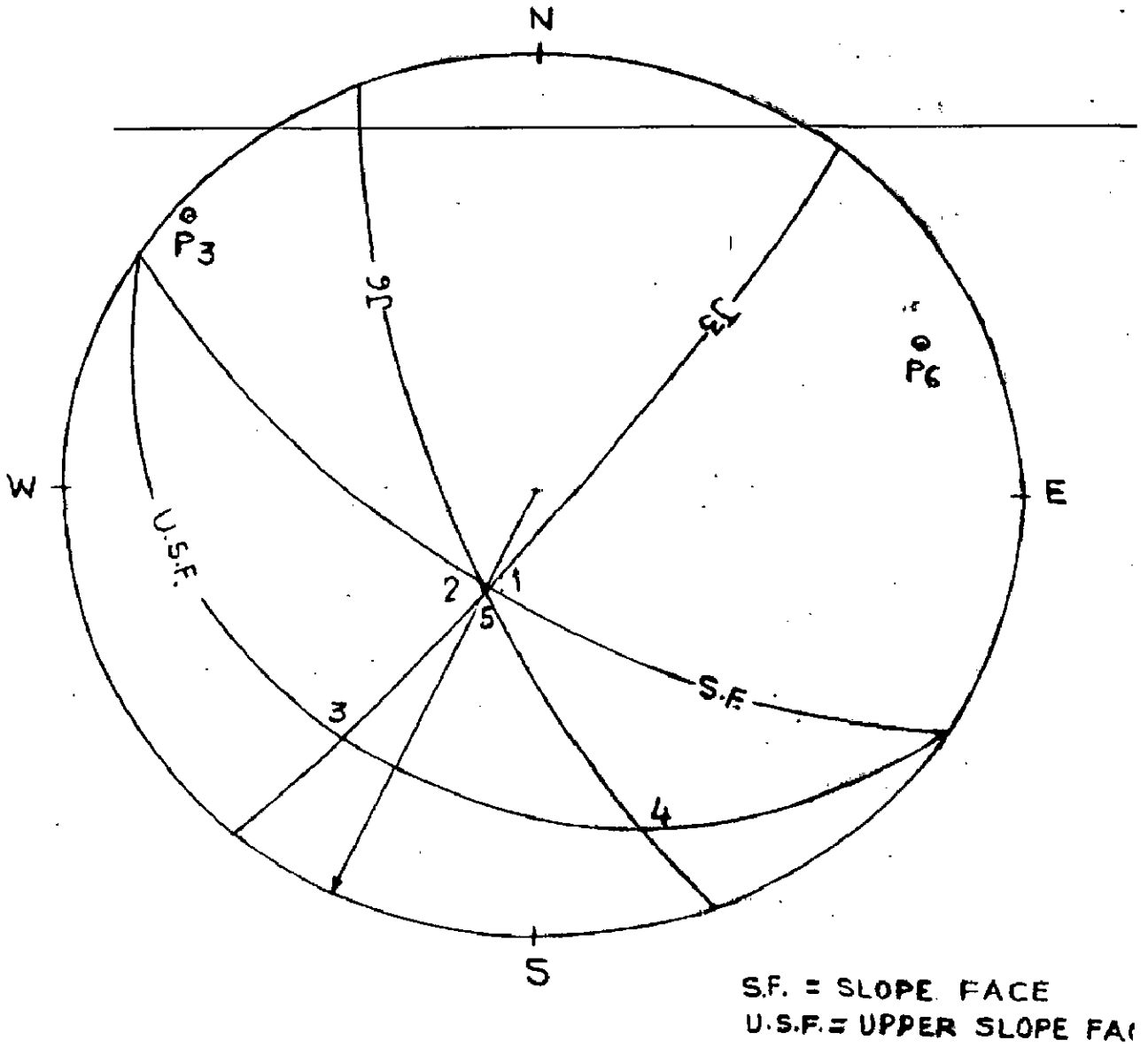


FIG. 37: STEREO PLOT FOR WEDGE NO-1
(RIGHT ABUTMENT)

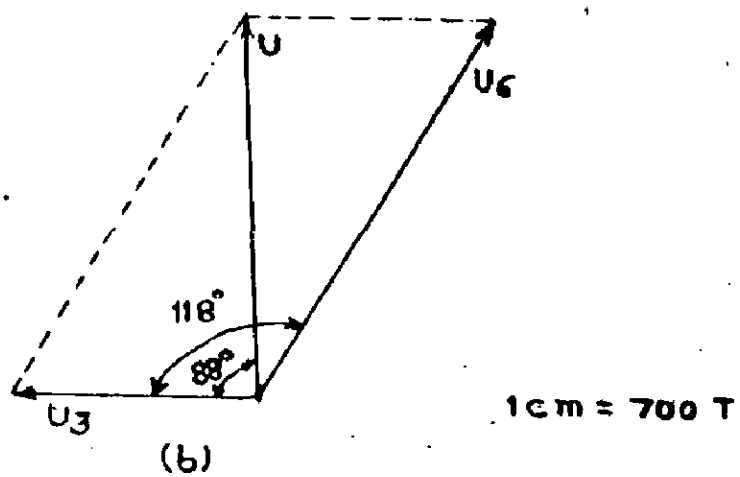
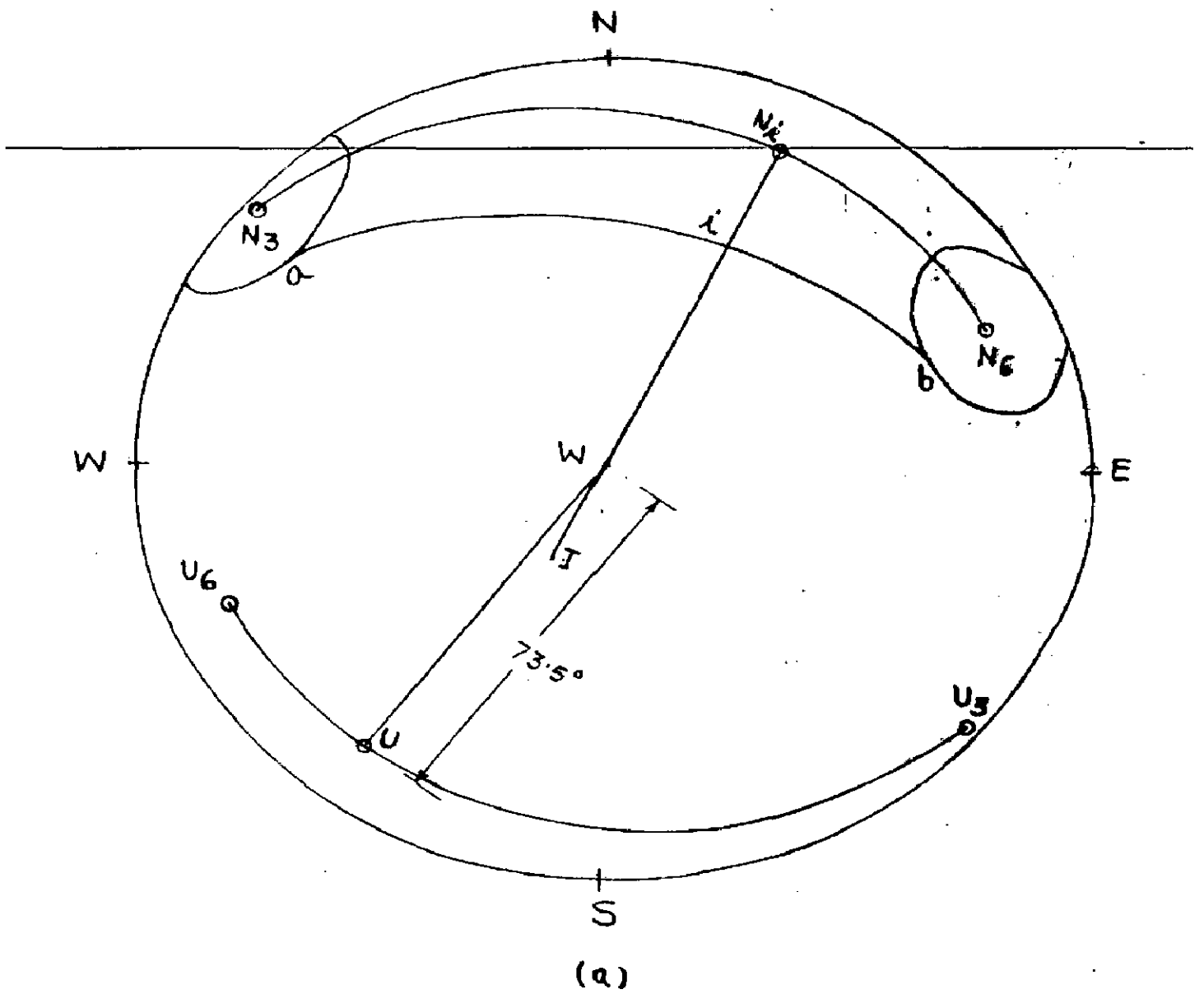


FIG. 38: STEREOPLOT FOR UPLIFT FORCES
(WEDGE NO-1, RIGHT ABUTMENT).

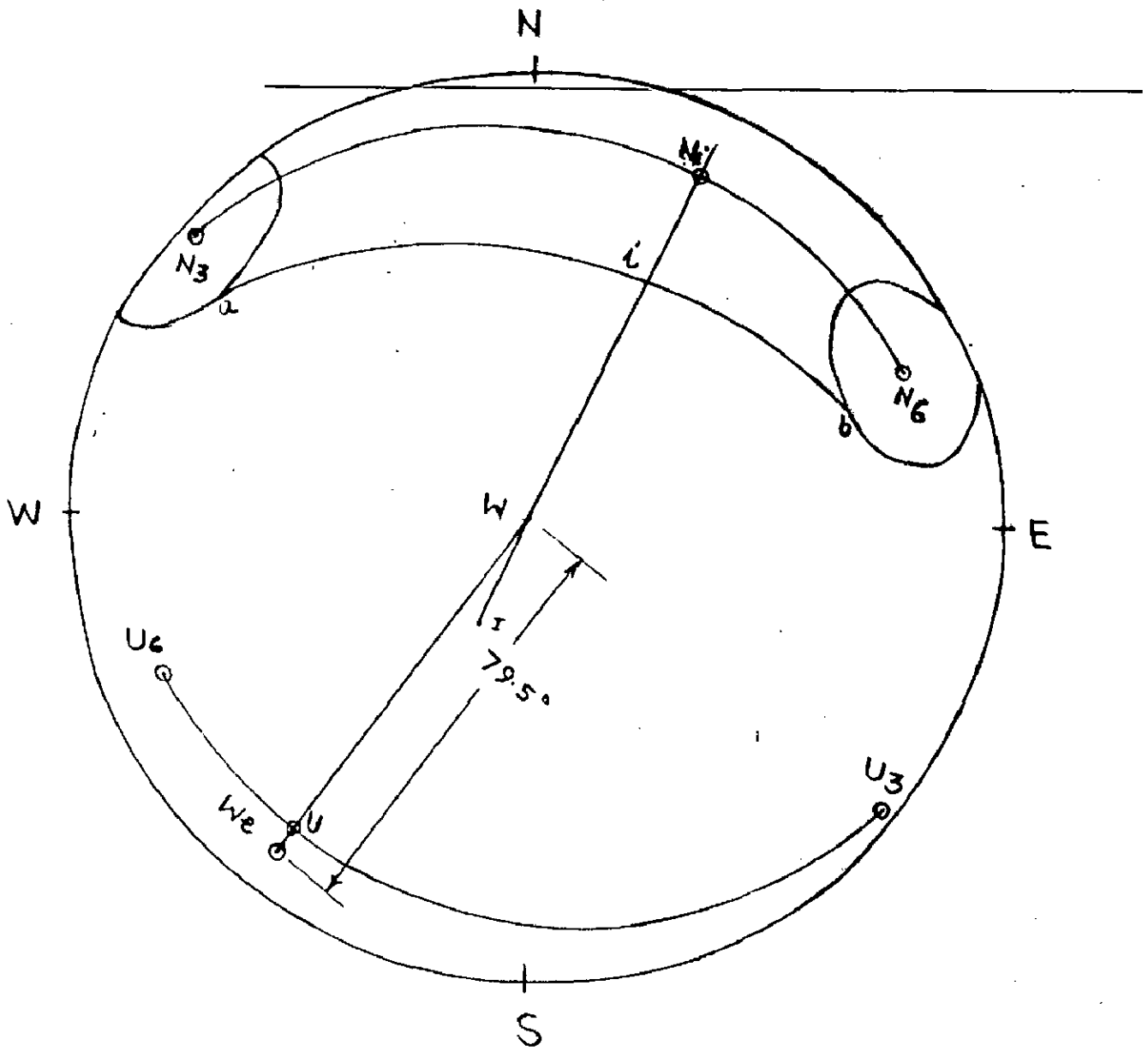


FIG. 39: STEREO PLOT FOR EFFECTIVE WEIGHT VECTOR (WEDGE NO-1, RIGHT ABUTMENT).

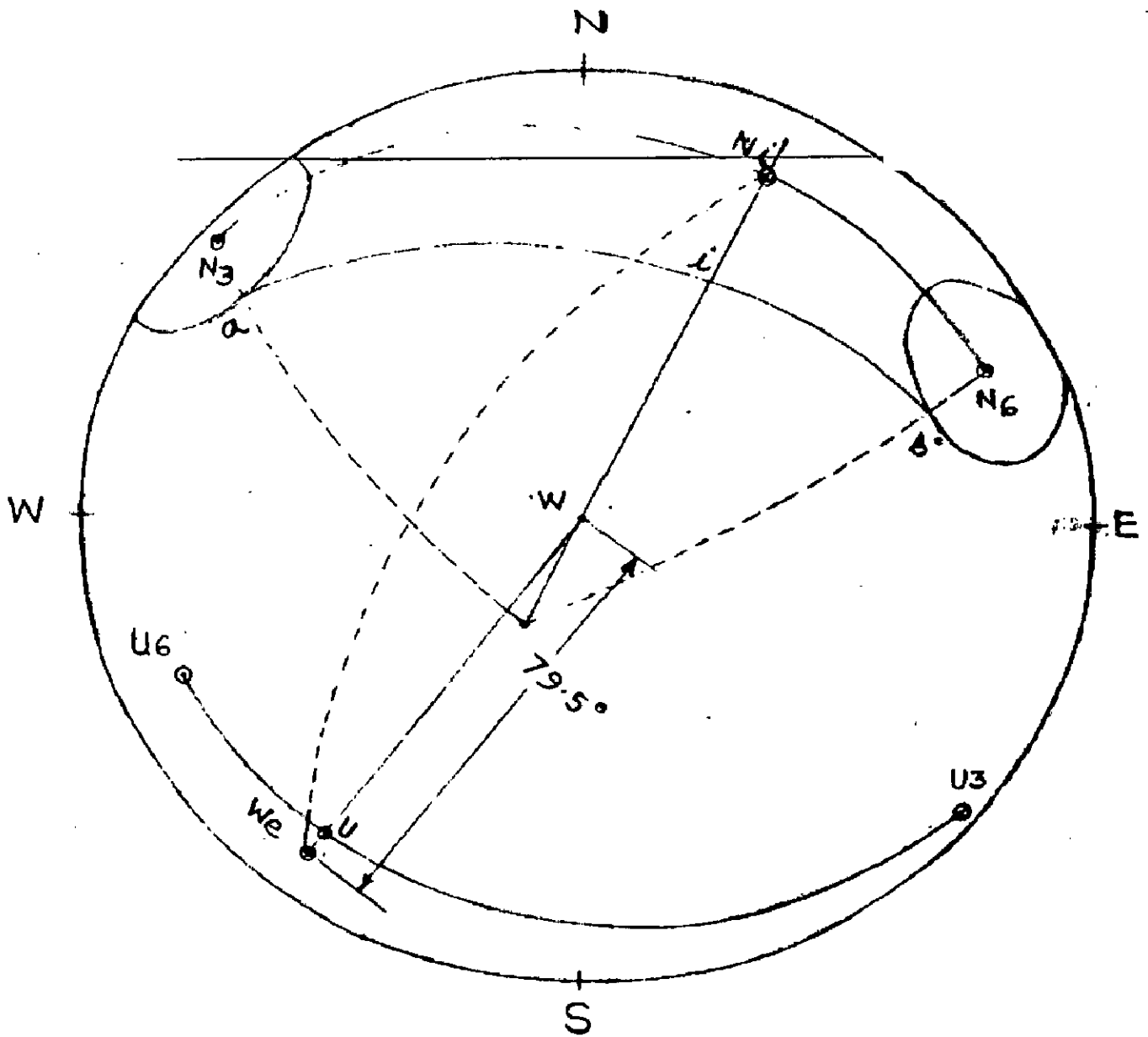


FIG.40: F.O.S. FOR SATURATED CONDITION
(WEDGE NO-1, RIGHT ABUTMENT).

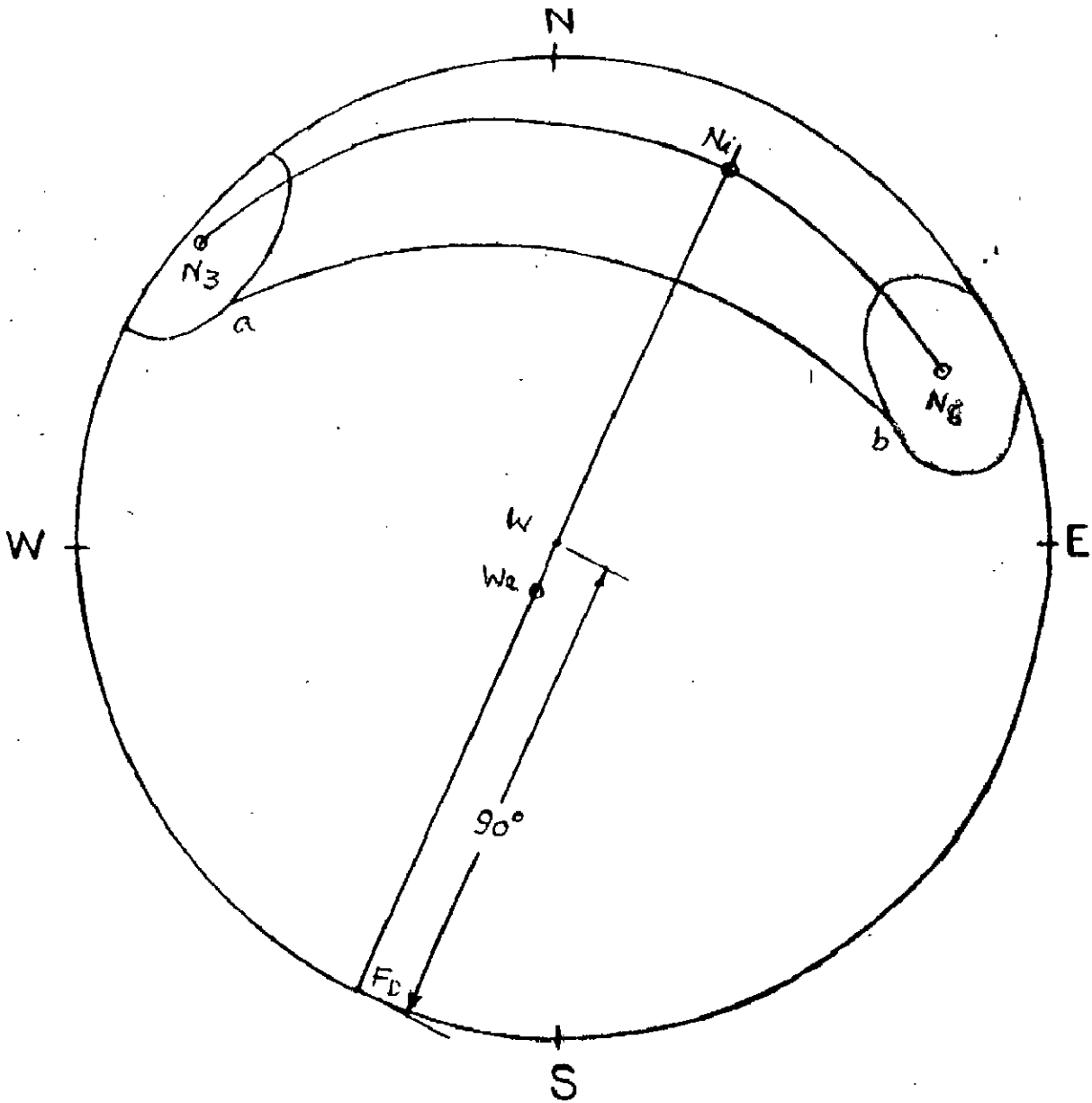
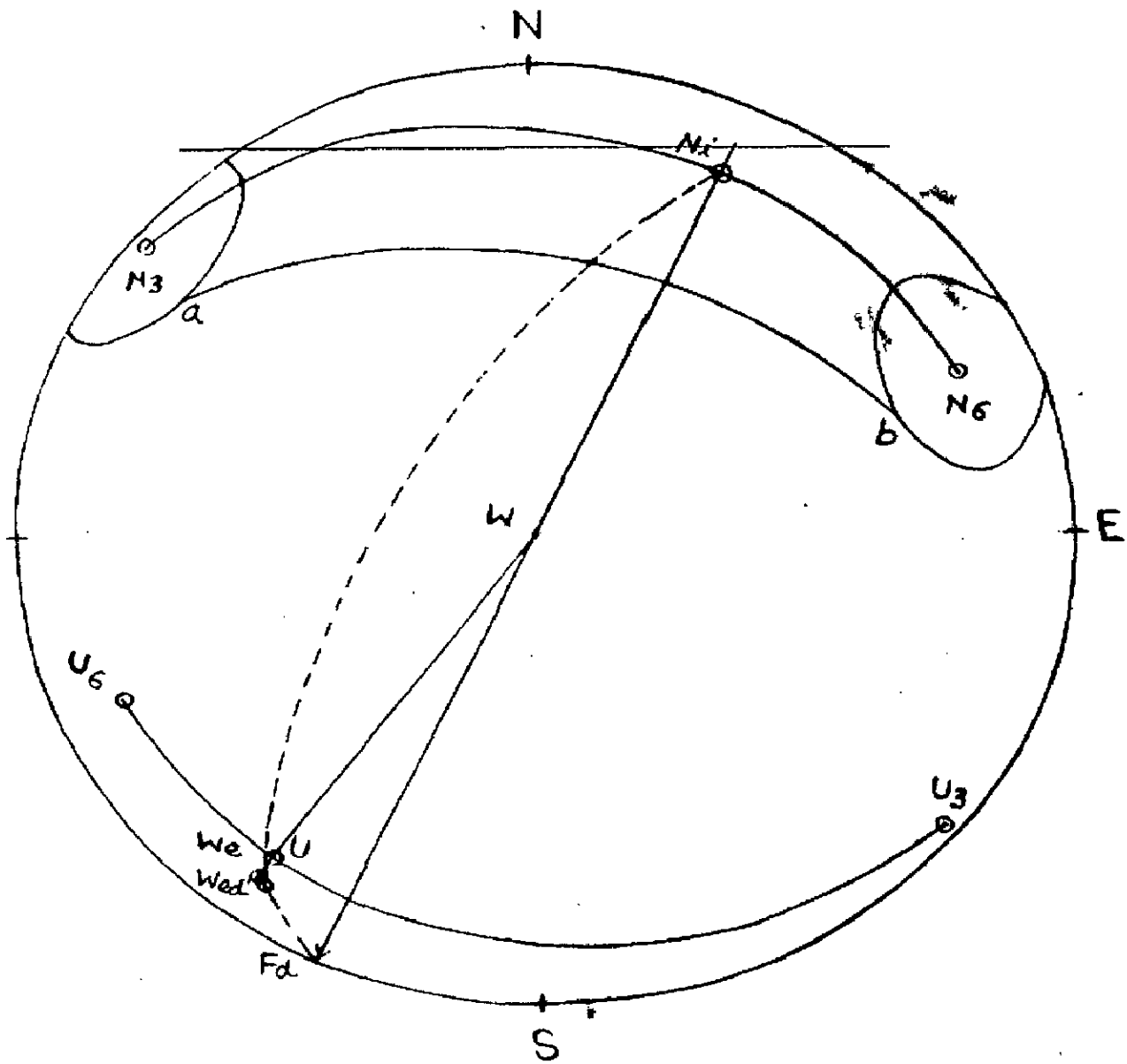


FIG. 41: F.O.S. FOR DYNAMIC CONDITION IN DRY ROCKMASS
(WEDGE NO-1, RIGHT ABUTMENT).



5.42: F.O.S. FOR DYNAMIC CONDITION IN SATURATED ROCKMASS (WEDGE NO.1, RIGHT ABUTMENT).

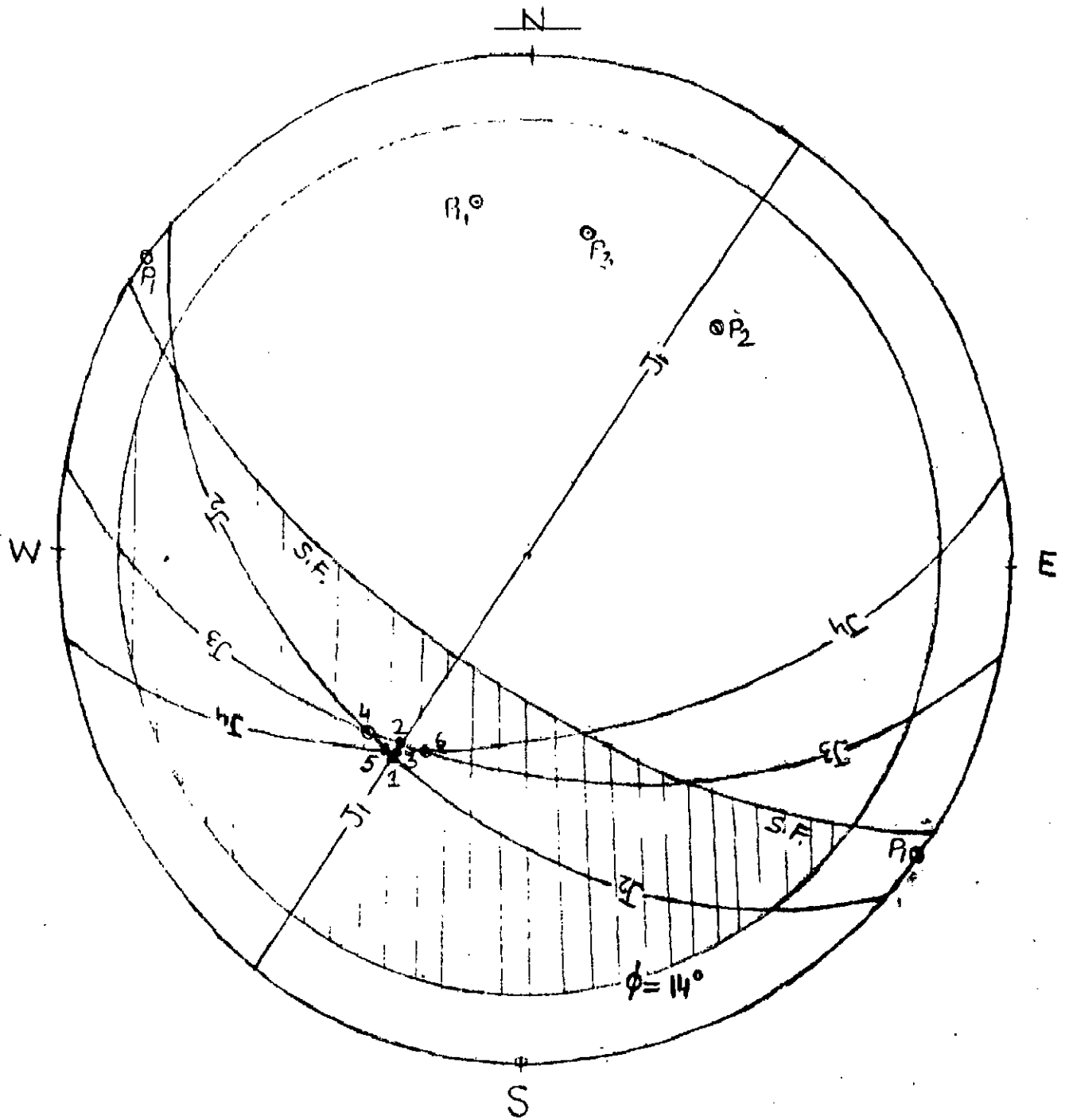


FIG. 43: COMBINED STEREO PLOT OF DISCONTINUITY PLANES (TABLE-3) FOR RIGHT ABUTMENT.

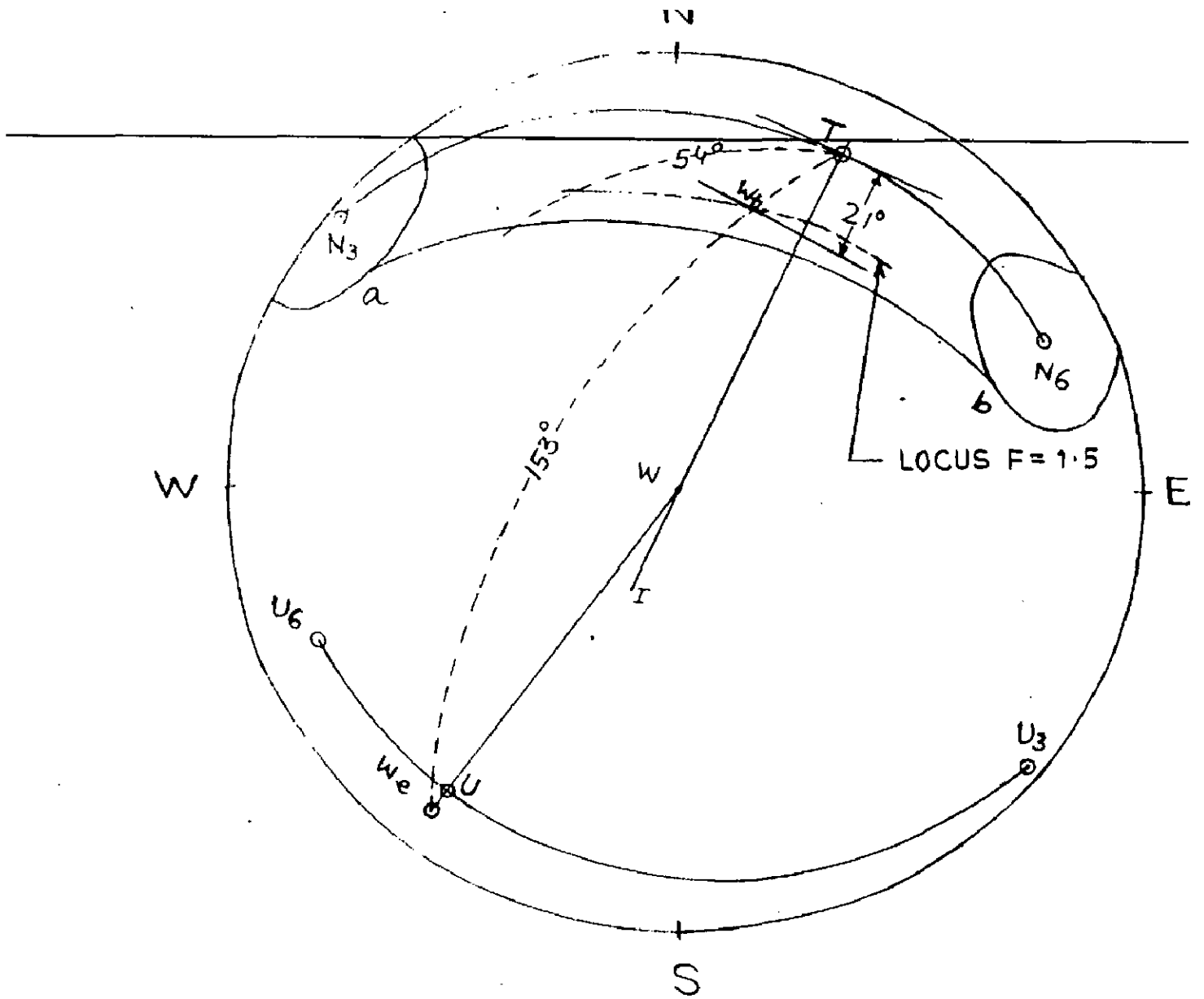


FIG. 44: DETERMINATION OF CABLE ANCHOR TENSION (T) FOR $F = 1.5$ (WEDGE NO.1, RIGHT ABUTMENT).

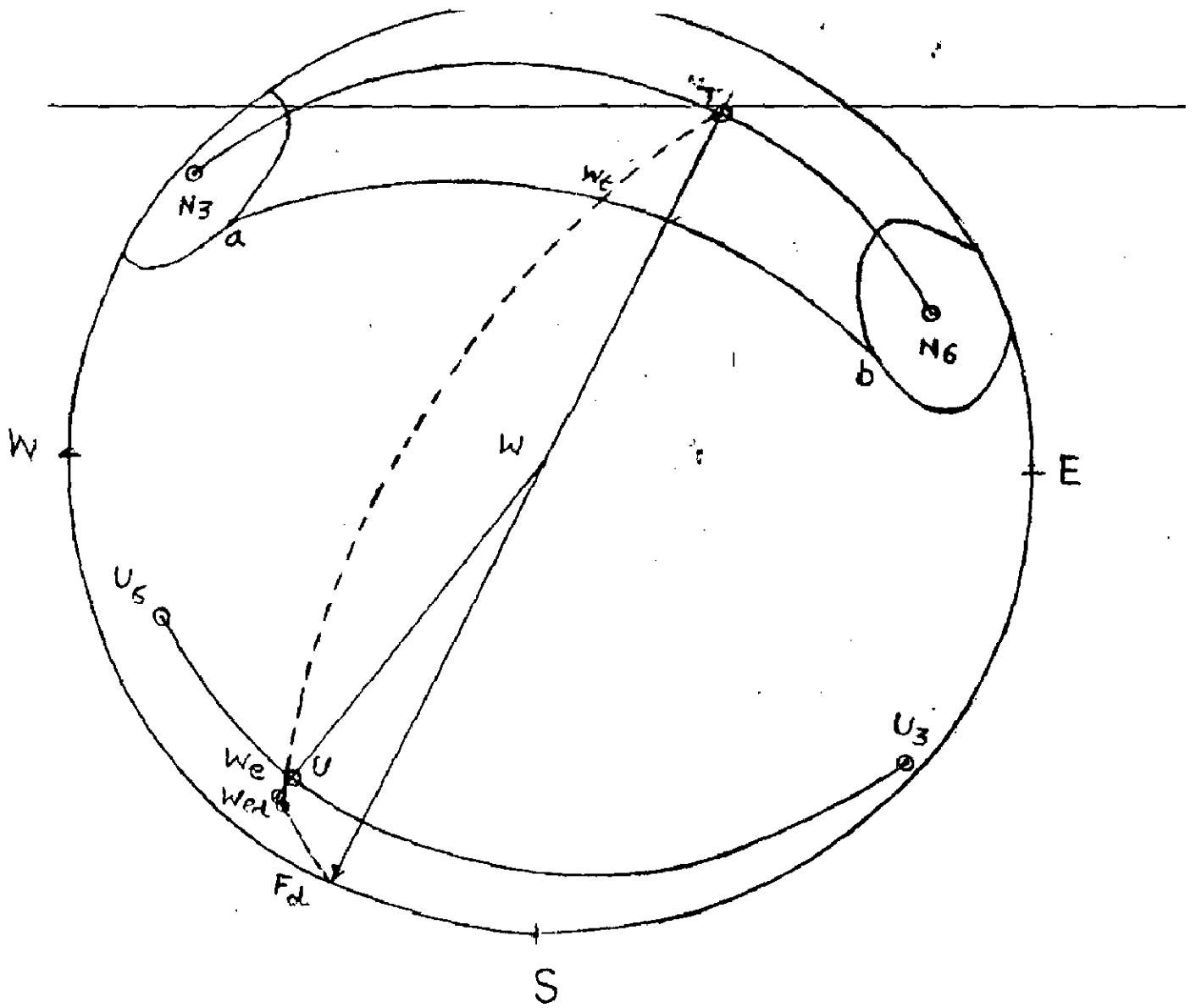


FIG. 45 : DETERMINATION OF CABLE ANCHOR TENSION (T) FOR $F=1.0$ (WEDGE NO.-1, RIGHT ABUTMENT).

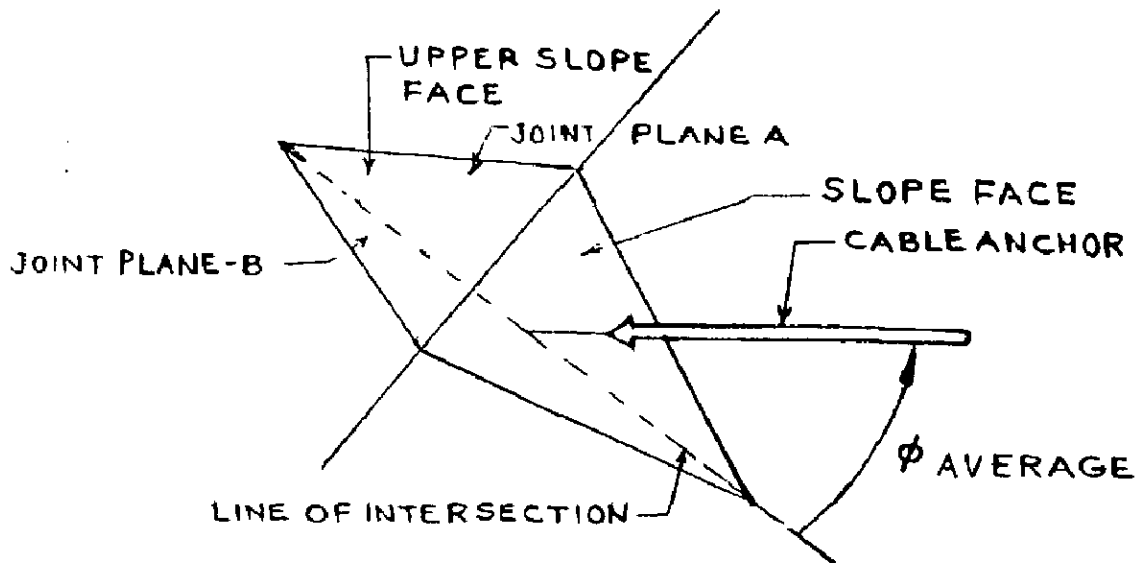


FIG. 46; OPTIMUM CABLE ANCHOR DIRECTION FOR REINFORCING A WEDGE.

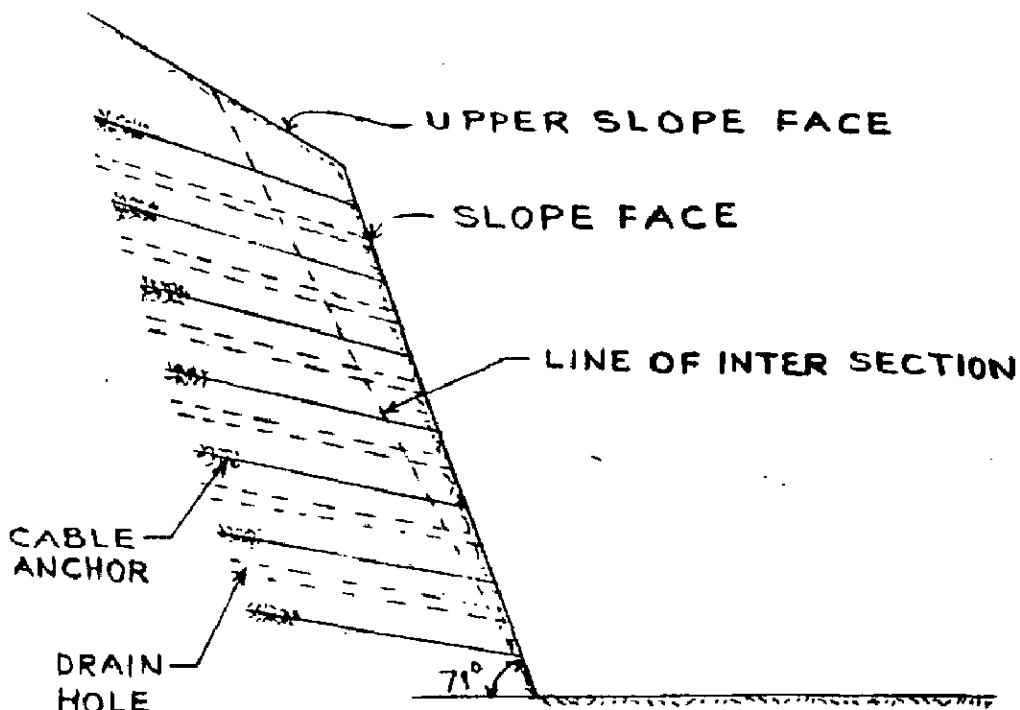


FIG. 47; PROVISION OF CABLE ANCHORS TO FORM REINFORCED ROCK BREAST WALL TO STABILIZE THE RIGHT ABUTMENT SLOPE.